Assessment of demountable steel-concrete composite flooring systems

Ioan Andrei Gîrbacea

Thesis committee:					
	prof.dr. M. Veljkovic	**TU Delft**		ir. P. Lagendijk	**TU Delft**
	ir. M.P. Nijgh	**TU Delft**		ir. M. Feijen	**FMAX ISAAC**
	dr. ir. R. Abspoel	**TU Delft**			

TU Delft Delft University of Technology

Challenge the future

Assessment of demountable steel-concrete composite flooring systems

by

Ioan Andrei Gîrbacea

in partial fulfilment of the requirements for the degree of

Master of Science
in Civil Engineering

Faculty of Civil Engineering and Geosciences
Delft University of Technology
Delft, The Netherlands

October 2018
To be defended publicly on Thursday, October 25 at 15:00.

Thesis committee:

prof.dr. M. Veljkovic	TU Delft
ir. M.P. Nijgh	TU Delft
dr. ir. R. Abspoel	TU Delft
ir. P. Lagendijk	TU Delft
ir. M. Feijen	FMAX ISAAC

TU Delft

Preface

This thesis represents the final step of my master studies at Delft University of Technology. The thesis focused on covering three main aspects of demountable steel-concrete flooring systems aiming to confirm that demountable flooring systems can be a viable solution to current traditional floorings both in terms of construction, mechanical behaviour and economical aspects.

The research was carried at the Steel and Composite Structures department under the supervision of: prof. dr. M. Veljkovic, ir. M.P. Nijgh, dr. ir. R. Abspoel, ir. P. Lagendijk from Delft University of Technology and ir. M. Feijen from FMAX ISAAC. The experimental research took place at TU Delft's Stevin II lab as part of RFCS-project REDUCE (Reuse and Demountability using Steel Structures and the Circular Economy). I would like to thank all committee members for their professional guidance, especially to prof. dr. M. Veljkovic and ir. M.P. Nijgh for all their help and support. Moreover, I would like to express my gratitude to all the laboratory staff who made all the experiments possible.

Last but not least, I would like to thank my family, girlfriend and friends for their support throughout all my studies.

Abstract

Sustainability concerns steer the construction sector towards adopting a circular economy philosophy. Steel-concrete composite beams are extensively used in multi-story buildings and bridges due to their competitive construction and efficient material use. Currently the composite action is mainly achieved by headed shear connectors welded to the top flange of the beam, obstructing the non-destructive demountability. Demountable shear connectors can be used in order to open up the composite construction for reusability. Demountable shear connectors can take the form of a bolted connection which requires a tight control of construction tolerances. This thesis is focused on studying a bolt coupler connector which is seen as a valuable alternative to the more conventional embedded bolt. The proposed shear connector consists of a bolt and coupler embedded in prefabricated concrete decks which are connected through the top flange of the steel section by an injection bolt.

Full-scale experiments have been performed to investigate the feasibility of construction of a demountable car park. The demountable flooring was obtained by large prefabricated concrete decks in combination with tapered beams. Experimental research has confirmed the possibility of assembly and disassembly of the system if construction tolerances are appropriately designed. The most influential factors were quantified based on experimental observations, measurements and finite element models. The hole clearance should be designed keeping in mind the deformability of the system during construction, the manufacturing tolerances and the speed of construction. Experiments show that resin injection can be reliably and labour efficiently used for large oversized holes which allow for higher fabrication imperfections and reduced construction while at the same time enabling composite action of the connectors under live load.

The reusability of the structure was confirmed by a set of eight four-point bending tests considering uniform and non-uniform connector arrangements. Finite element models closely match the experimental results in terms of deflection, stresses and curvature. However, the end slip is overpredicted which is in line with research performed by other authors. The efficiency of the non-uniform connector arrangements was studied experimentally and numerically to reduce the construction costs. Concentrating the shear connectors toward the supports will bring the highest benefit in terms of beam bending stiffness without the need of a large number of connectors to prevent uplift.

An extensive cost analysis was performed based on a database of 15500 beam solutions generated by a design algorithm develop as part of this thesis. The case study provides a preliminary cost assessment of two demountable steel-concrete composite floorings in order to quantify their economic viability. It was shown that the system constructed with prefabricated solid slabs is more viable compared to the demountable profiled sheeting slab. The most influential contribution to the final cost of the structure comes from the steel work and the labour intensive manufacturing.

Contents

List of figures

List of tables

1 Introduction

Environmental concerns steer the construction industry towards more sustainable designs. Steel-concrete composite beams are a popular solution in current design practice due to their efficient material use and competitive construction. However, commonly used welded connectors obstruct the non-destructive separation or require time consuming and labour intensive processes to separate the concrete slab from the steel member. Demountable shear connectors can open up the possibility of reuse in composite floorings.

1.1 Problem definition

1.1.1. Sustainability in construction.

The construction industry is responsible for 40% of the primary energy use and 36% of the energy related CO_2 emissions in industrialized countries [1]. Figures from 2009 [2] indicate a CO_2 emission on a global scale due to construction activities of 5.7 billion tons. In 2014, the waste generated by all 28 European Union member states summed up to an all-time high of 2503 million tonnes, with the construction sector contributing up to 34.6% according to [3].

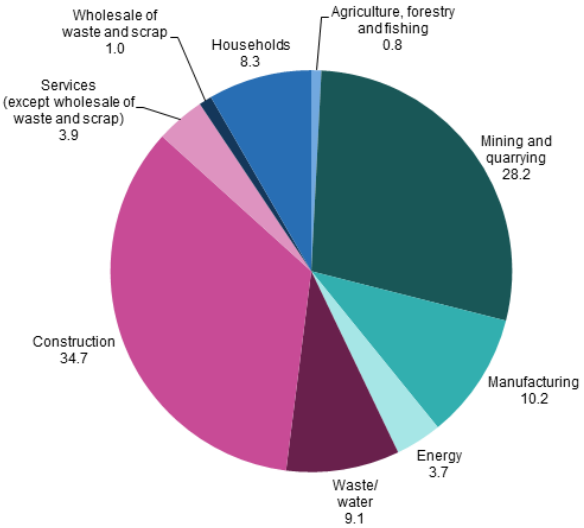

Figure 1.1 **Waste generation by economic activities and households, EU-28, 2014** [3]

In an attempt to reduce emissions and waste, many countries have introduced a carbon tax. The extra taxation will increase the costs of unsustainable buildings in order to drive the industry towards environmentally friendly solutions. The problem can be tackled by moving from a linear economy to a circular one which ensures the materials and products are reused. This will translate in a reduction of harmful emissions and waste. According to an estimate from 2002 of the European Environmental Agency [4] the recovery level of materials from the construction and demolition waste is only one quarter, with Netherlands peaking at 90 percent.

A study carried by [5] indicates that the superstructure of an concrete office building has an average footprint of 215.1kg CO_2/m^2. The study also shows that in terms of used materials, the flooring accounts for 35.2% of the CO_2 emissions followed by the external walls with a contribution of 35%. Further, the study investigates different approaches to reduce the carbon footprint and concludes that reusing the existing beams and columns has the highest influence compared to other structural parts.

Applying circular economy in the case of buildings is best illustrated in Figure 1.2 by the virtuous circle of design for deconstruction and reuse presented by [6]. A circular economy building system requires an ability to closely couple the recovery and reuse of products from end-of-life buildings to stock replacement and maintenance [7]. The design process should focus on the future reuse by integrating the building in a closed-loop cycle. Up to 81.3% of the embodied energy of the initial steel building can be saved by reusing the main steel structure of the prefabricated modules and other components in another new building [8].

Three requirements are presented by [9] based on [6] which must be fulfilled by a building in order to be reused. The structure:

- is not worn-out
- is not out-dated
- can still cooperate with other structural components.

Additionally, another requirement should be considered to make a reusable building viable:

- The structure should be in the first cycle, as cost-effective and competitive as a traditional solution.

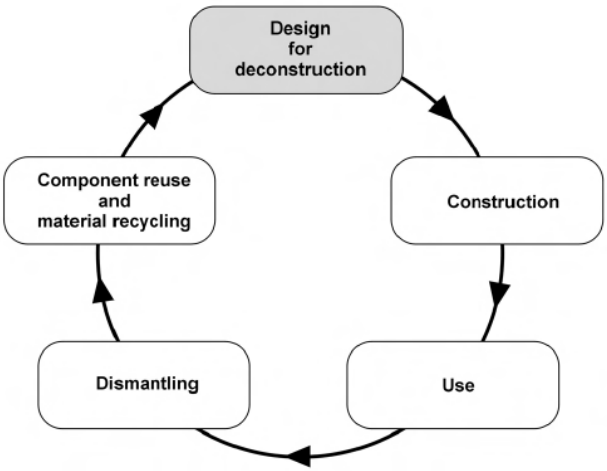

Figure 1.2 **The virtuous circle: Design for deconstruction and reuse** [6]

1.1.2. Demountable composite construction

Steel-concrete composite structures are a popular solution in current design practice. The development of the shear studs in the 1950s [10] marked a turning point from a design perspective. Embedding the welded headed studs in concrete ensures interaction between the steel beam and concrete slab. The composite behaviour between the slab and the steel section leads to a cost-effective flooring system, which is widely used both in buildings and bridges.

The advantage gained by the development of the shear studs now raises serious environmental issues. Welding the studs on the top flange will permanently obstruct the separation between the concrete and steel part. In order to achieve a sustainable flooring system, the non-destructive disassembly between the two components must be possible. At this moment, there are multiple solutions in terms of connectors suitable for disassembly, but still this is a new field of research.

This master thesis focuses on demountable resin injected bolt coupler systems as means to obtain composite action. The shear connector consists of an embedded bolt and coupler connected by an exterior injection bolt through the top flange. The demountable flooring is constructed from large prefabricated concrete decks in a combination with tapered steel beams. The assembly and disassembly of such systems is investigated through full-scale experiments and finite element models. Due to manufacturing tolerances and deformations of the structure during construction there is a need for large oversized holes in the top flange of the steel beam. However, due to the increased hole clearance the composite action can be enabled by resin injecting the formed gap or prestressing the bolts. The resin injection is investigated in terms of its reliability of filling the void and required labour. Through four point bending tests the relationship between applied load and deflection is established.

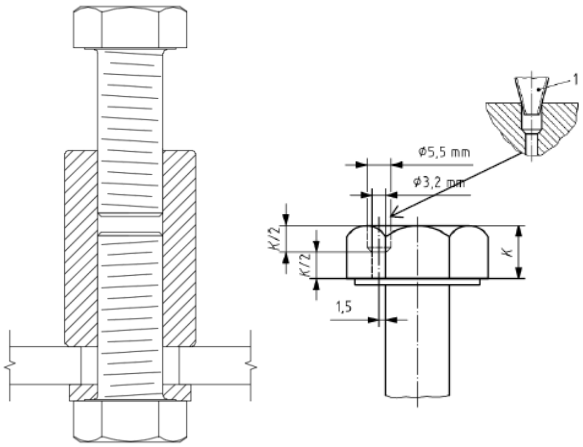

Figure 1.3 **Bolt coupler conector and resin injection head according to** [11]

A study by [12] concludes that through prefabrication, the waste reduction is on average about 52%, mainly due to minimising of cut-off. Apart from the environmental aspects, demountable prefabricated systems come with numerous potential benefits such as:

- increased construction speed,
- fast deconstruction,
- reduced in-situ labour,
- safer working environment,
- increased quality control.

In terms of the economics of demountable steel-concrete composite flooring systems, a preliminary assessment has been carried out in [13]. Based only on material costs, two solutions of demountable composite beams were compared to a traditional in-situ casted trapezoidal sheeting slab. The cost breakdown concluded that the demountable connector has a significant contribution to the final material cost. Due to the novelty of these connectors, their unit price is up to 15 times compared to a simple headed stud. For this reason, the connector arrangement needs to be optimized to keep material costs low. The previous assessment will be extended as part of this thesis in order to obtain a more realistic estimation because the construction costs contribute significantly to the final cost of such systems.

A great economical advantage brought by demountable structures is the flexibility against rental demand fluctuation. Retail spaces demand has recorded a downfall as illustrated through Figure 1.4 in UK and reported by [14] in the USA due to the shift in consumer habits towards online shopping [15]. However, the initial investment can become again profitable if the flexibility in terms of location and functionality is inherent in the building design.

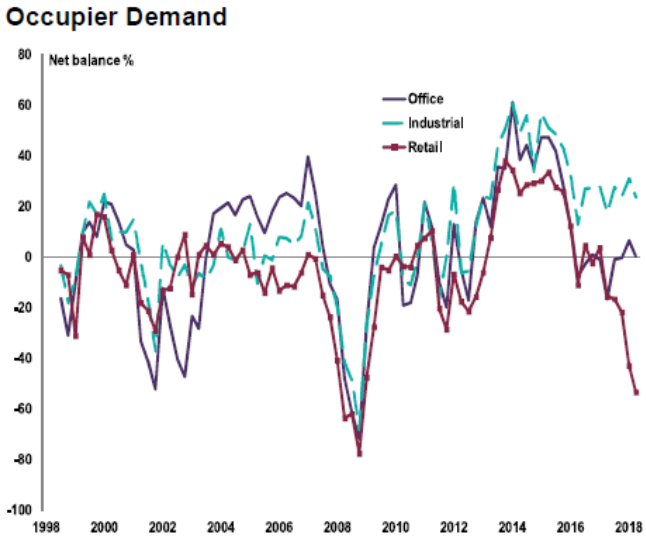

Figure 1.4 **Occupier demand - sector breakdown** [16]

1.2 Main objectives

The main objectives of this thesis are to:

i. Asses and confirm the feasibility of construction of demountable composite flooring systems,
ii. Investigate the load-deflection behaviour of demountable composite beams,
iii. Study the benefits in terms of beam stiffness of non-uniform connector arrangements,
iv. Provide an initial cost estimation per m^2 and study the economic viability of demountable composite floorings.

1.3 Research questions

To fulfil the main objectives of the thesis the following research questions have to be answered:

- **Feasibility of construction:**
  - Which are the influencing factors for assembly and disassembly of demountable systems?
  - Can resin injection be used reliably and labour efficiently for demountable buildings?

- **Mechanical behaviour of demountable composite beams**
  - What is the load-deflection behaviour of resin injected demountable composite beams?
  - Which is the optimal connector arrangement to achieve an economical design?

- **Cost assessment**
  - Which are the most influential cost contributions to the final price of demountable composite floorings?
  - To what extent a demountable flooring system will increase the initial cost per m^2 compared to a traditional solution?

1.4 Thesis outline

The thesis has been structured in three main parts. The structure of the thesis is detailed in Figure 1.5.

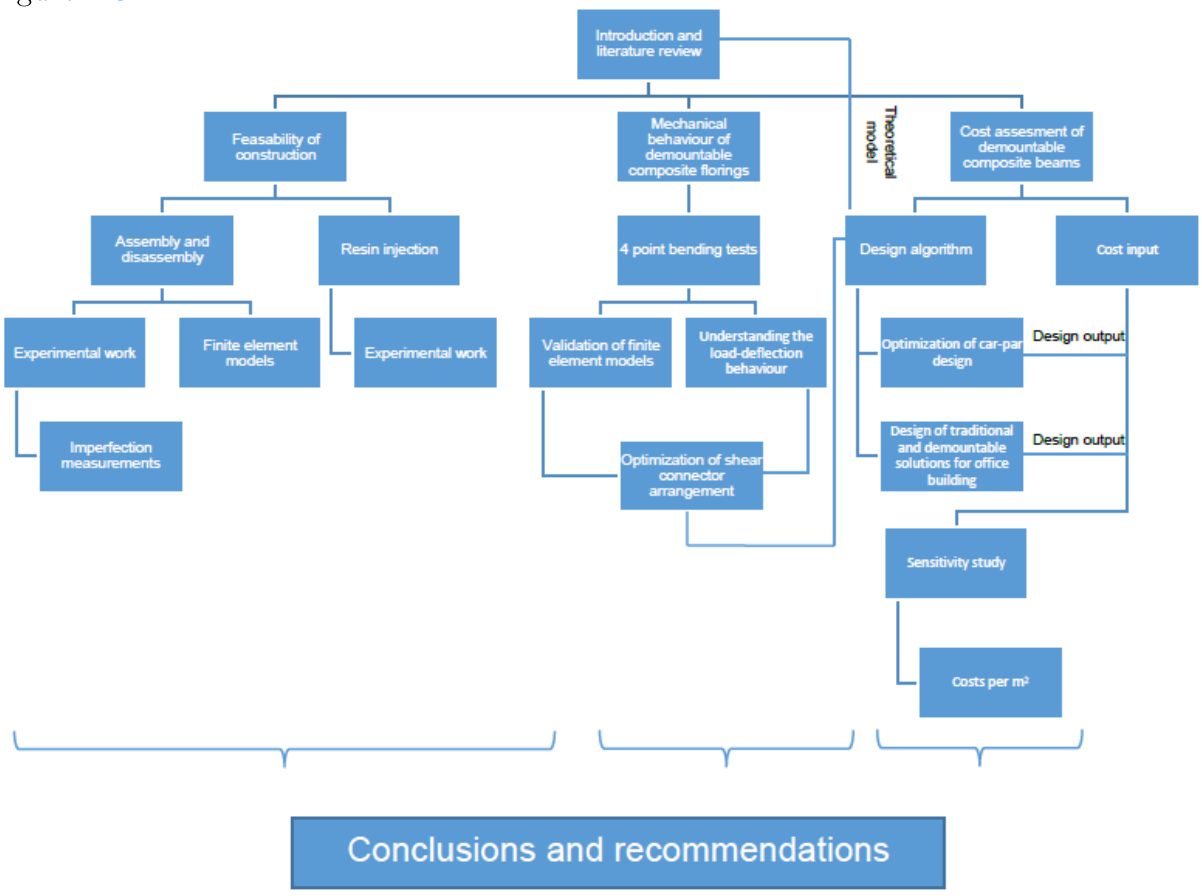

Figure 1.5 **Thesis structure**

2 Literature review

2.1 Theoretical background on composite beams

Obtaining the composite behaviour between the concrete slab and the steel beam is advantageous both in terms of stiffness and resistance. The mechanical connectors will transfer the longitudinal shear force generated at the interface and will also ensure that the curvature of the two parts is the same [17].

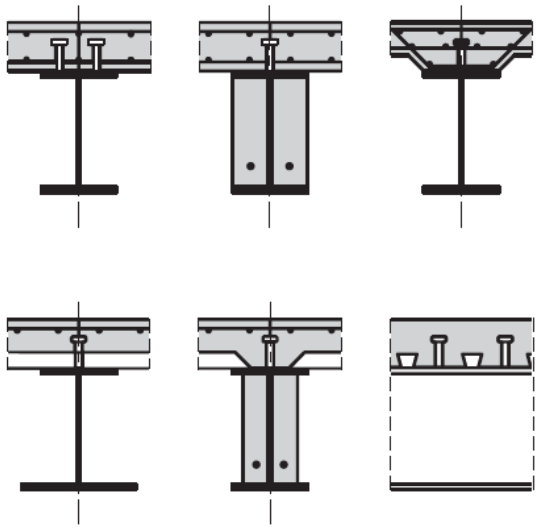

Figure 2.1 **Different composite cross-sections** [18]

In Figure 2.2 the same beam will be considered having three different degrees of composite action. The degree of connection is defined by [18] and by [19] in a more general manner:

$$\eta = \frac{N_c}{N_{c,f}} = \frac{P_{sh}}{(P_{sh})_{fsc}}$$

The notations given by [19] are as follows:

- N_c or P_{sh} - force taken by the mechanical connectors in one half-span
- $N_{c,f}$ or $(P_{sh)fsc}$- resistance corresponding to full connection, given either by the steel section or the concrete flange.

The limit case of no connection is shown in Figure 2.2 (a). Because there is no interface interaction and the bending stiffness of each component is different, the strain profile is be bilinear. The difference in strains at the interface, known as the slip strain is equal to:

$$\frac{ds}{dx} = \varepsilon_c - \varepsilon_s$$

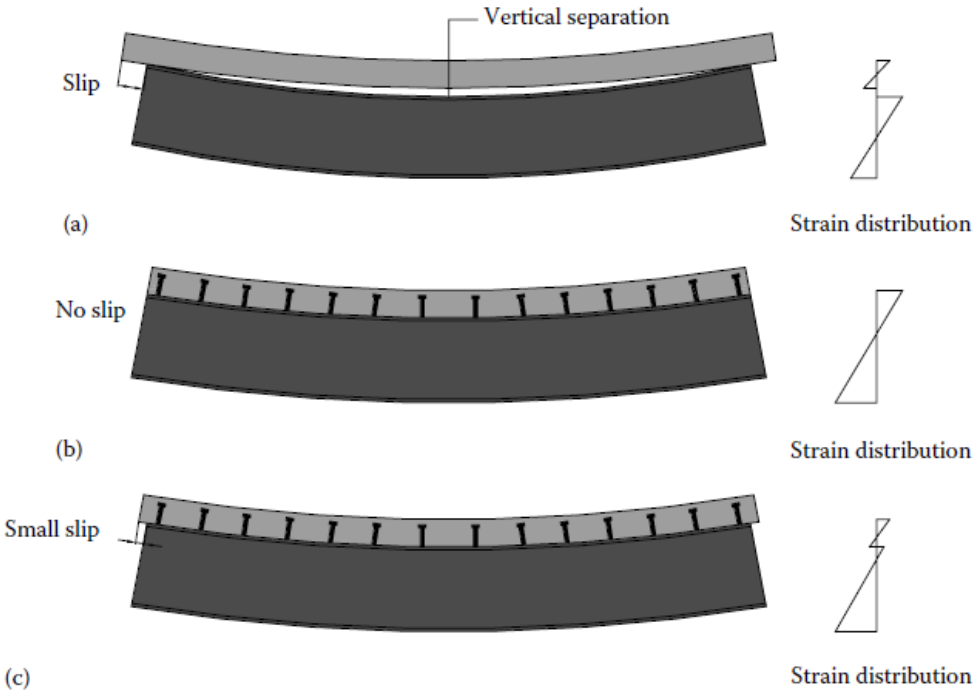

Figure 2.2 **Effect of shear connection on the behaviour of composite beams: (a) no shear connection, (b) complete shear connection and (c) partial shear connection.** [20]

Similar to the strain, which is defined as the rate of change of deformation, the slip strain is the rate of change of slip. Therefore, the integral of the slip strain is the slip at the interface. Moreover, due to this the difference in deformation there will be a vertical separation, also called uplift. Research carried by [21] shows that vertical separation is limited during the elastic range.

$$s = u_c - u_s$$

$$s = \int_0^L \varepsilon_c dx - \int_0^L \varepsilon_s dx$$

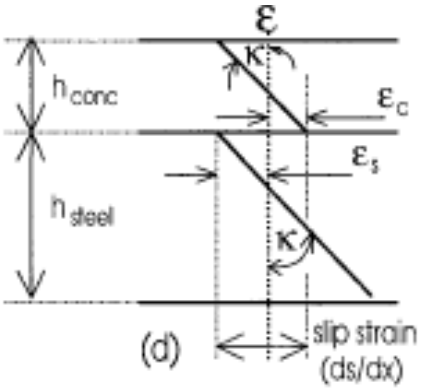

Figure 2.3 **Slip strain** [17]

Moving further to the second limit case the composite beam having full shear connection is shown in Figure 2.2 (b). This form of interface condition is only theoretical as it requires infinite shear, bending and axial stiffness. The interface is treated as an infinitely rigid connection which leads to a linear strain distribution over the depth of the cross-section. The slip and uplift between the surfaces are no longer present due to the continuity ensured by the infinitely rigid interface.

The two theoretical situations can be compared in terms of their elastic bending stiffness and resistance of the cross-sections. Assuming the slab and the steel beam are two rectangular blocks of same dimensions and material, the following section properties are obtained:

$$I_{\text{no interaction}} = 2\frac{1}{12}bh^3 = \frac{1}{6}bh^3$$

$$W_{\text{no connection}} = 2\frac{1}{6}bh^2 = \frac{1}{3}bh^2$$

$$I_{\text{full interaction}} = \frac{1}{12}b(2h)^3 = \frac{2}{3}bh^3$$

$$W_{\text{full connection}} = \frac{1}{6}b(2h)^2 = \frac{2}{3}bh^2$$

The benefits of composite beams are seen when the two situations are compared:

$$\frac{I_{\text{full interaction}}}{I_{\text{no interaction}}} = 4$$

$$\frac{W_{\text{full connection}}}{W_{\text{no connection}}} = 2$$

In between these two theoretical situations, lies the partial shear connection which represent the real behaviour of composite beams.

2.2 Shear connectors

The mechanical shear connectors are characterized by load-slip curves. The load-slip curve shows the relationship between the applied shear force per connector at a certain interface slip. The curves are obtained based on standardized push-out test specimens. EN 1994-1-1 [18] gives specifications on the dimensions of these specimens and the loading procedure.

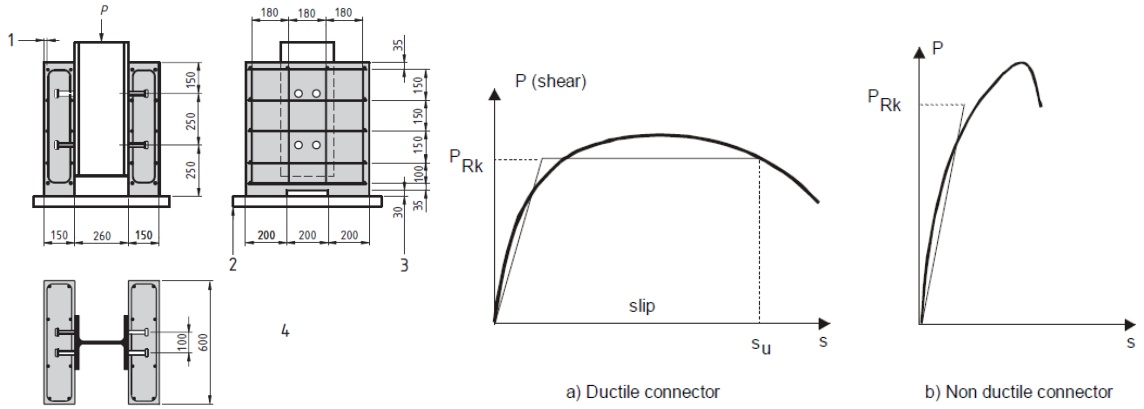

Figure 2.4 **Standardized push-out test [18] and load-slip curves [22]**

Based on the load-slip curve, the shear connectors can be characterized as ductile or non-ductile if the slip at failure is less than 6mm as defined by [18]. The slip distribution peaks at supports but is not constant along the length of the beam. For this reason, ductility is required in order for the redistribution of forces between connectors to take place. As seen from Figure 2.4 a ductile connector is characterized by an yield plateau with a high ultimate slip capacity. On the other hand, non-ductile shear connectors are very stiff with a low ultimate slip capacity. In terms of resistance, the ductile connectors have a lower capacity mainly because the failure is governed by the concrete slab.

If it is assumed that the rigidly connected composite beam behaves elastically, then the shear flow, T (shear force per unit length), between the concrete slab and the steel section may be calculated from: [22]

$$\tau = \frac{VS}{I}$$

Where: V -vertical shear
S - first moment of area
I - second moment of area

The relation above shows that the longitudinal forces which must resisted by the connection depend on the vertical shear force.

Apart from the longitudinal shear forces the connection must resist tensile stresses generated by vertical separation of the two parts. This is ensured by anchoring the head of the connector into concrete.

2.3 Effective width

The in-plane shear strain in the concrete slab of a composite section under bending causes the longitudinal displacements in the parts of the slab remote from the steel web to lag behind those near the web [20].This phenomenon is called shear lag effect and is referred in design guidelines as the effective width. The distribution of elastic bending stresses, peaks at point D and reduces with distance from the connection. The effective width b is obtained by assuming a constant stress distribution described by GHJK, which is equal to the sum of stresses below the curve ACDEF.

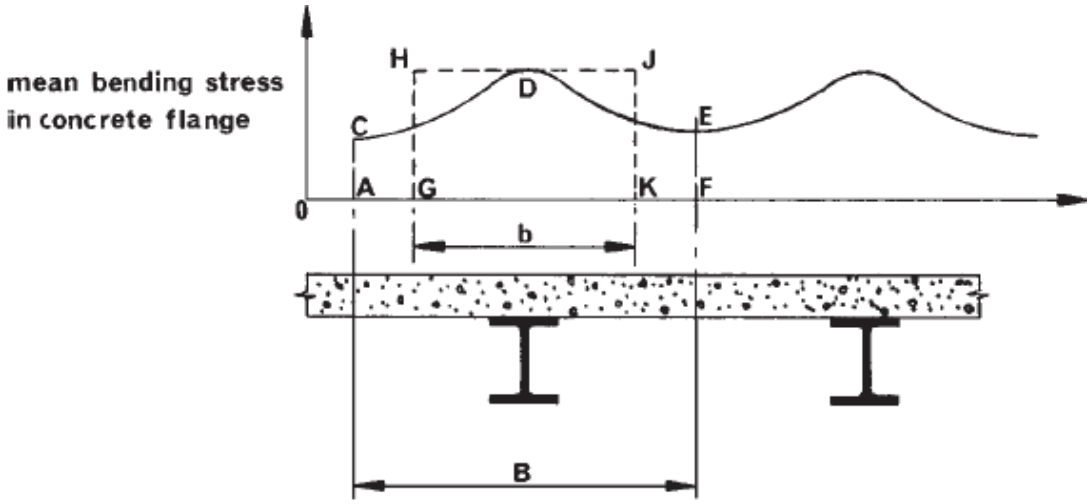

Figure 2.5 **Shear lag effect** [10]

2.4 Bending moment resistance of composite beams

The bending moment resistance of composite beams depends on the degree of shear connection and on the cross-section class. The theory presented will be used in the parametric study.

2.4.1. Full shear connection

Assuming that cross-section classes 1 or 2 are used, the bending moment resistance can be determined based on the plastic stress distribution in case of partial shear connection. When the concrete slab including the sheeting is subjected to bending, their tension resistance is ignored. Moreover, due to its low contribution the compression, reinforcement is generally not be taken into account

The resistance of the two materials is defined by [18] as follows:

$$f_{\mathrm{yd}} = \frac{f_{\mathrm{y,k}}}{\gamma_{\mathrm{a}}} \quad \text{where} \quad \gamma_{\mathrm{a}} = 1.0$$

$$f_{\mathrm{cd}} = \frac{f_{\mathrm{c,k}}}{\gamma_{\mathrm{c}}} \quad \text{where} \quad \gamma_{\mathrm{a}} = 1.5$$

The concrete design resistance is further reduced by a factor of 0.85 which accounts for the differences in the stress distribution between the cylinder test and the real structure and its assumed block stress distribution. These include the longer duration of loading in the structure, the presence of a stress gradient across the section considered, and the differences in the boundary conditions of the concrete [10].

EN 1994-1-1 [18] does not provide explicit expressions to determine the bending moment resistance of the composite section therefore, through longitudinal equilibrium the bending moment resistance can be expressed. Three cases are identified:

1. Neutral axis in the concrete slab
2. Neutral axis in the flange of the steel beam
3. Neutral axis in the web of the steel beam

The notations used in following sections are in line with EN 1994-1-1 [18] and to differentiate the steel part the subscript $_{a}$ is used.

Neutral axis in the concrete slab

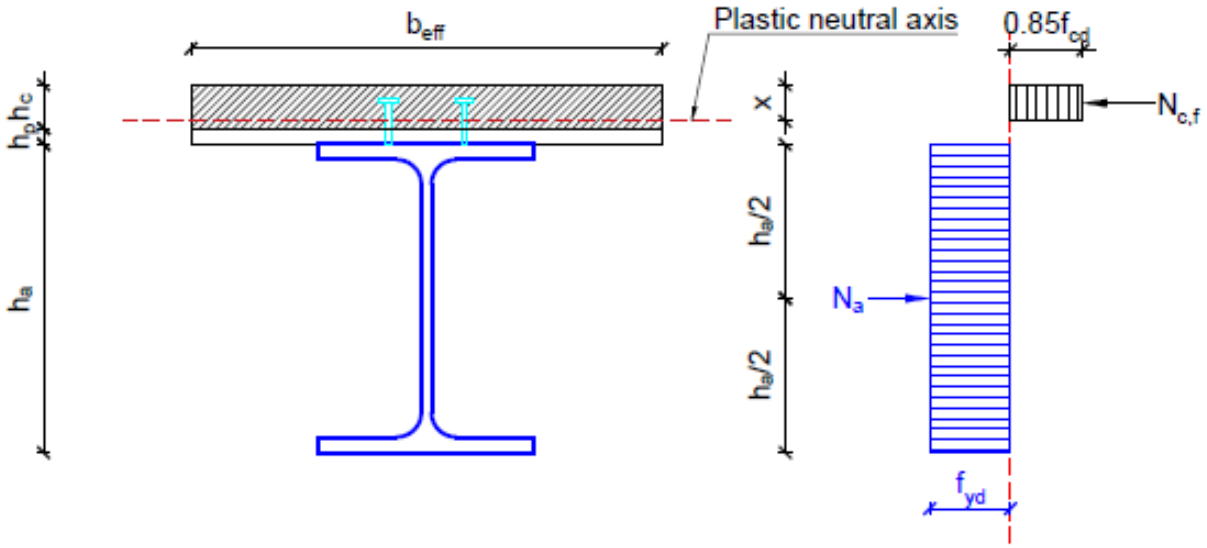

Figure 2.6 **Neutral axis in the concrete slab** [13]

The resulting axial forces of the concrete flange and steel member are expressed as follows:

$$N_{\mathrm{a}} = A_{\mathrm{a}} f_{\mathrm{yd}}$$

$$N_{\mathrm{c,f}} = 0.85 h_{\mathrm{c}} b_{\mathrm{eff}} f_{\mathrm{cd}}$$

Where the subscript $_{\mathrm{f}}$ stands for full shear connection

The position of the neutral axis can be obtain by setting equilibrium:

$$x = \frac{N_{\mathrm{a}}}{0.85 b_{\mathrm{eff}} f_{\mathrm{cd}}} < h_{\mathrm{c}}$$

The bending moment resistance determined by taking moment about the steel or the concrete resultant force:

$$M_{\mathrm{pl,Rd}} = N_{\mathrm{c}}(\frac{h_{\mathrm{a}}}{2} + h_{\mathrm{c}} + h_{\mathrm{p}} - \frac{x}{2})$$

$$M_{\mathrm{pl,Rd}} = N_{\mathrm{a}}(\frac{h_{\mathrm{a}}}{2} + h_{\mathrm{c}} + h_{\mathrm{p}} - \frac{x}{2}).$$

Neutral axis in the flange of the steel beam

If the steel axial resistance is higher compared to the concrete one, the plastic neutral axis will lie below the concrete slab. In order to verify whether the plastic neutral axis is situated in the top flange, the condition below must be satisfied:

$$N_{\mathrm{a}} > \mathrm{N_{c,f}} = 0.85 b_{\mathrm{eff}} h_{\mathrm{c}} f_{\mathrm{cd}} > h_{\mathrm{w}} t_{\mathrm{w}} \mathrm{f_{yd}}$$

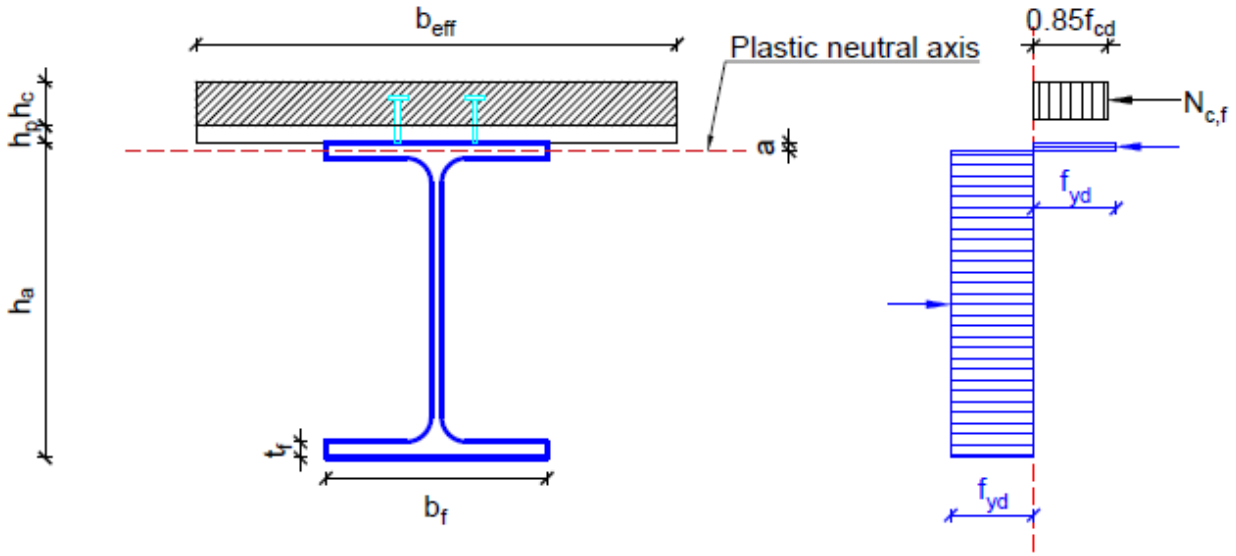

Figure 2.7 **Neutral axis in the flange of the steel beam** [13]

The stress distribution in the steel member can be simplified by a superposition of two distributions. The compression resultant force will have a counteracting part in the bottom flange with a depth equal to a.

$$a = \frac{N_{\mathrm{a}} - \mathrm{N_{c,f}}}{2 b_{\mathrm{f}} f_{\mathrm{yd}}}$$

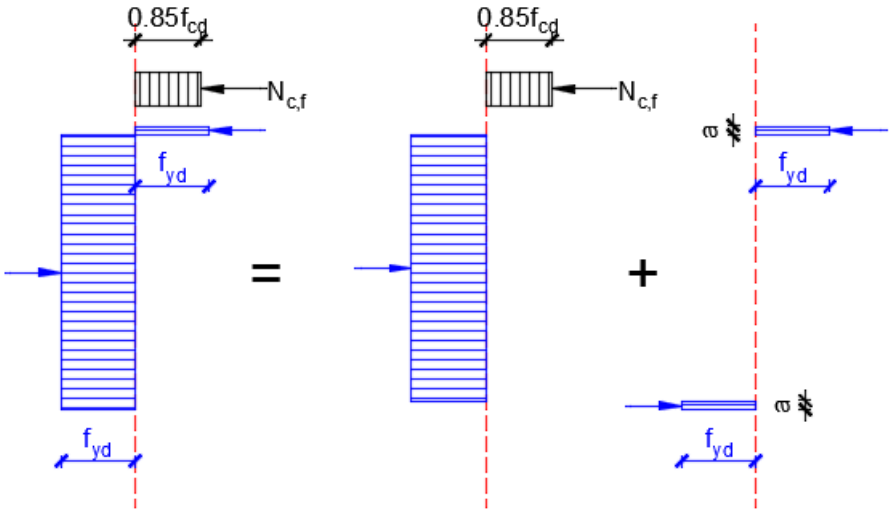

Figure 2.8 **Stress decomposition - n.a. in top flange** [13]

The bending moment resistance can be obtained by summing up the moments arround the concrete resultant force and the moment generated by the couple.

$$M_{\mathrm{pl,Rd}} = N_{\mathrm{c,f}}(\frac{1}{2}h_{\mathrm{a}} + h_{\mathrm{p}} + \frac{1}{2}h_{\mathrm{c}}) + \frac{N_{\mathrm{a}} - N_{\mathrm{c,f}}}{2}(h_{\mathrm{a}} - a).$$

Neutral axis in the flange of the steel beam

To verify whether the plastic neutral axis lies in the web, the following requirement must be satisfied:

$$0.85h_{\mathrm{c}}b_{\mathrm{eff}}f_{\mathrm{cd}} < h_{\mathrm{w}}t_{\mathrm{w}}f_{\mathrm{yd}}.$$

In similar as before, the stress distribution from the figure below is decomposed to ease the derivation of the bending moment resistance expression.

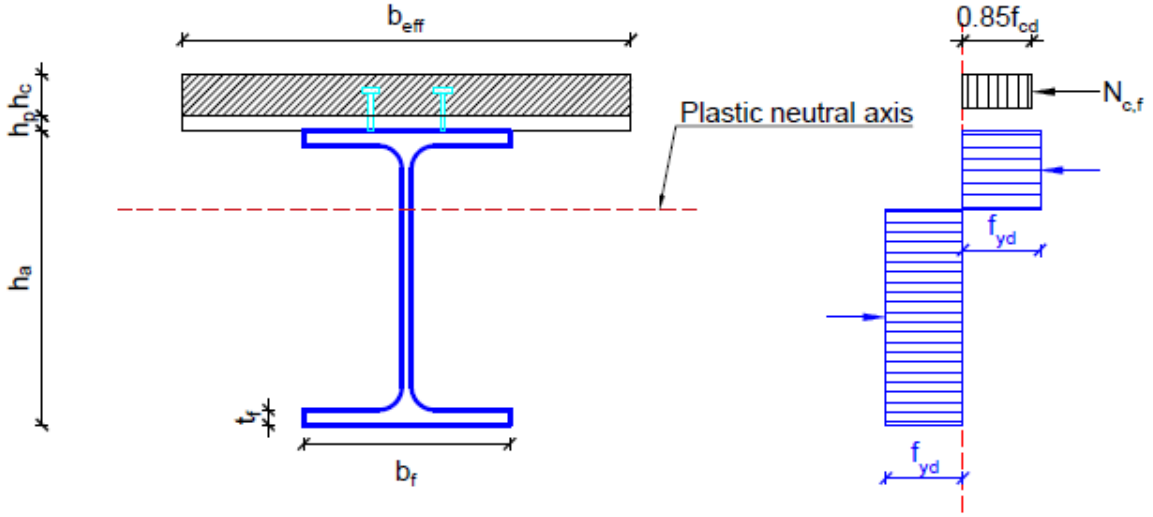

Figure 2.9 **Neutral axis in the flange of the steel beam** [13]

The bending moment resistance is given by the following expression:

$$M_{\mathrm{pl,Rd}} = N_{\mathrm{c,f}}(\frac{1}{2}h_{\mathrm{a}} + h_{\mathrm{p}} + \frac{1}{2}h_{\mathrm{c}}) + W_{\mathrm{a,pl}}\mathrm{f}_{\mathrm{yd}} - \frac{1}{4}(\frac{N_{\mathrm{c,f}}}{t_{\mathrm{w}}f_{\mathrm{yd}}})^2 f_{\mathrm{yd}}.$$

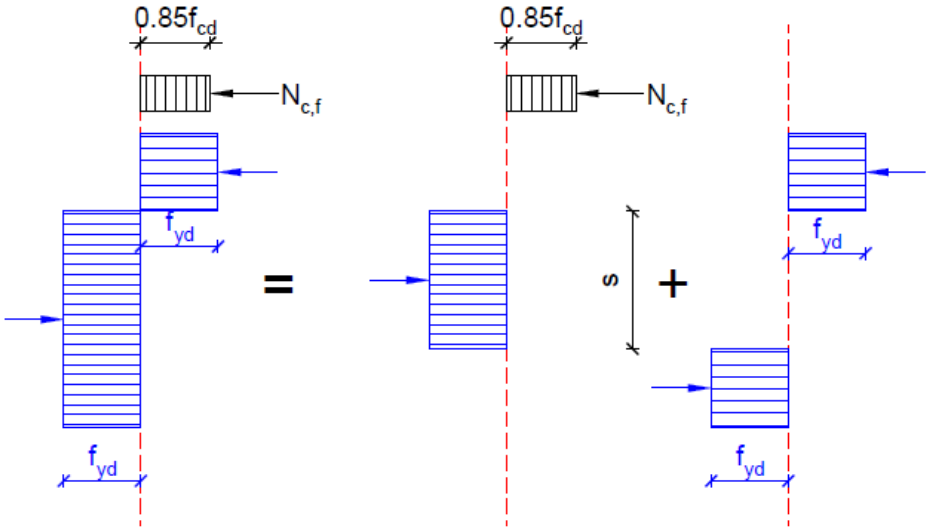

Figure 2.10 **Stress decomposition** [13]

The number of shear connectors can be determined afterwards such that the sum of the shear resistance of all the shear connectors in one half of the steel beam is equal of higher than the lowest axial resistance of the concrete or steel member.

$$n_{\mathrm{req}} = \frac{\min(N_{\mathrm{c}}, N_{\mathrm{a}})}{P_{\mathrm{Rd}}}.$$

2.4.2. Partial shear connection

From case to case, the designer might decide to choose for a partial shear connection because the steel section is dimensioned by the construction phase. This translates into a shear connection weaker than the lowest axial resistance of the concrete flange or steel member. For this reason, the stress distribution will change, and a second neutral axis will appear as already mentioned in 2.1.

EN 1994-1-1 [18] provides a provides a simplified linear relationship between the ratio $\frac{\mathrm{M_{Rd}}}{\mathrm{M_{pl,Rd}}}$ and η for section class 1 and 2.

$$M_{\mathrm{Rd}} = M_{\mathrm{pl,a,Rd}} + (M_{\mathrm{pl,Rd}} - M_{\mathrm{pl,a,Rd}})\eta.$$

Where:

$$\eta = \frac{N_{\mathrm{c}}}{N_{\mathrm{c,f}}}.$$

$\mathrm{M_{pl,a,Rd}}$ - the plastic bending moment resistance of the steel section

$M_{pl,Rd}$ - the plastic bending moment resistance of the composite section with full interaction
N_c - the resistance of the shear connectors
$N_{c,f}$ - the full interaction force in the concrete.

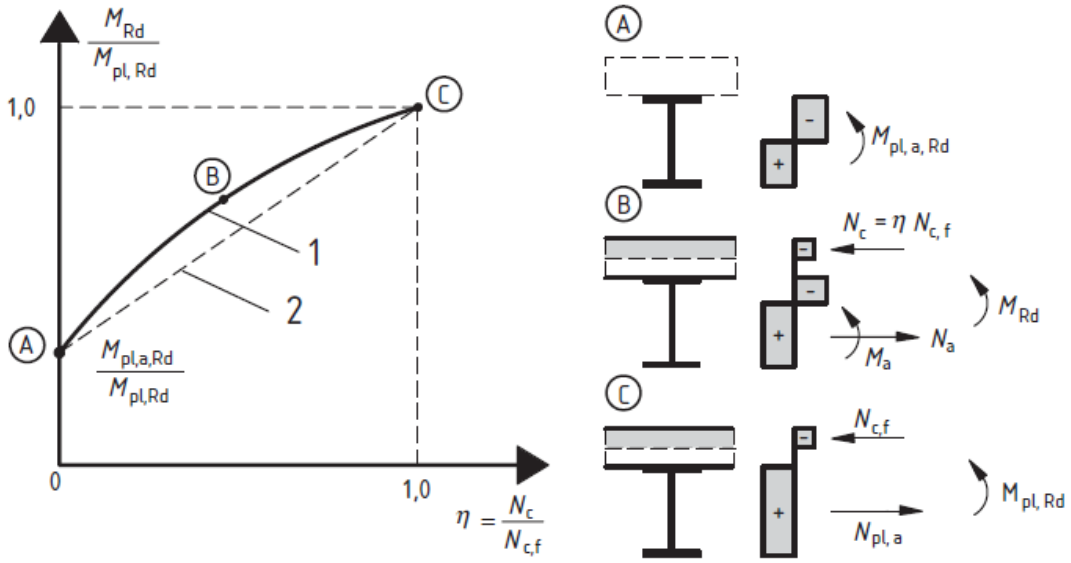

Figure 2.11 **Relation between M_{Rd} and N_c** [18]

Apart from the linear simplication, the bending moment resistance of the composite section can be obtained by determining the exact value of point B on the convex curve using longitudinal equilibrium. Two cases need to be accounted for in the derivation:

1. Neutral axis in the flange of the steel section
2. Neutral axis in the web of the steel section.
3. **Neutral axis in the flange of the steel section**

To verify whether the neutral axis lies in the top flange of the steel section, the following requirement must be checked:

$$nP_{Rd} > h_w t_w f_{yd}.$$

Where n is the number of applied shear connectors in one halfspan.

The bending moment resistance of the composite section is obtained by replacing the concrete resultant force with the cumulated resistance of the connectors.

$$M_{red,Rd} = nP_{Rd}(\frac{1}{2}h_a + h_p + \frac{1}{2}\frac{nP_{Rd}}{0.85b_{eff}f_{cd}}) + \frac{N_a - nP_{Rd}}{2}(h_a - \frac{N_a - nP_{Rd}}{2b_f f_{yd}}).$$

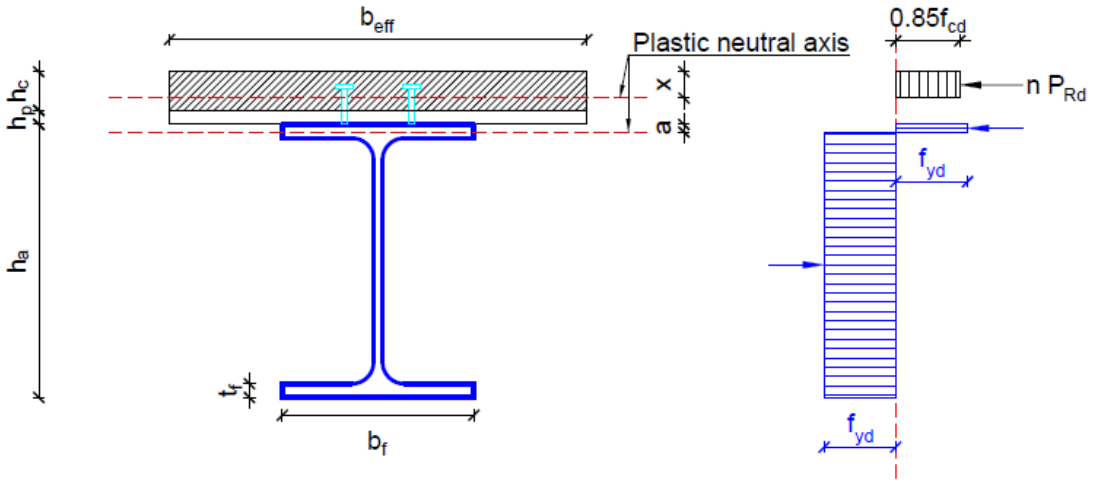

Figure 2.12 **Neutral axis in the flange - partial shear connection** [13]

Neutral axis in the web of the steel section

To verify whether the neutral axis lies in the web of the steel section, the following requirement must be checked:

$$nP_{Rd} < h_w t_w f_{yd}.$$

Using longitudinal equilibrium, the bending moment expression is obtained:

$$M_{red,Rd} = nP_{Rd}(\frac{1}{2}h_a + h_p + \frac{1}{2}\frac{nP_{Rd}}{0.85b_{eff}f_{cd}}) + Wa, plf_y - \frac{(nP_{Rd})^2}{4t_w f_{yd}}.$$

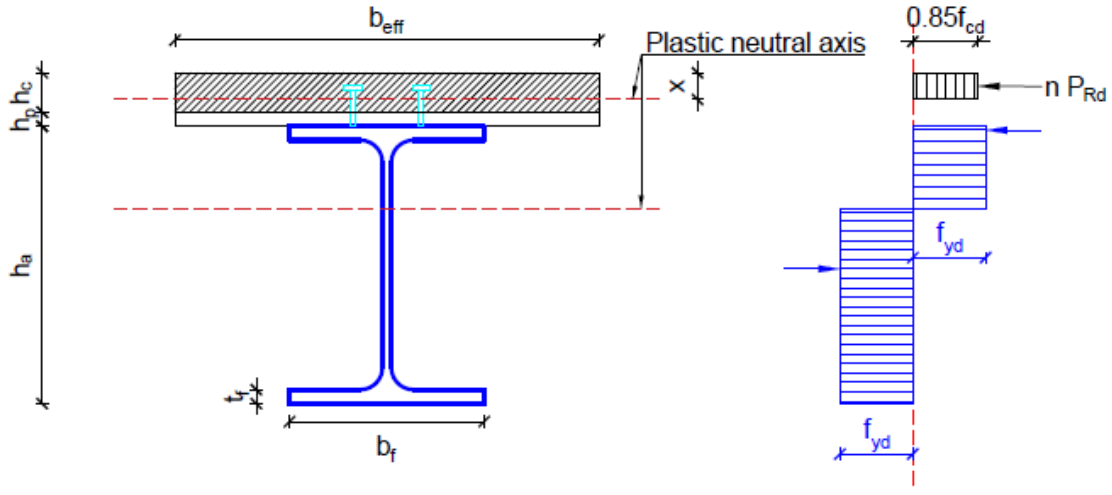

Figure 2.13 **Neutral axis in the web - partial shear connection** [13]

2.5 Vertical shear

The contribution of the slab to the vertical shear resistance is influenced by whether it is continuous across the end support, by how much it is cracked, and by local details of the shear connection [10]. To simplify the design verification the shear force is assumed to be resisted only by the steel beam. According to EN 1993-1-1 [23],the shear capacity of the steel section is determined as follows:

$$V_{pl,a,Rd} = \frac{A_v f_{yd}}{\sqrt{3}}$$

For cross section class 1 and 2

$$A_v = A_a - 2b_f t_f + (t_w + 2r)t_f \quad \text{or} \quad A_v = \eta h_w t_w \quad \eta = 1$$

In order to neglect shear buckling effects, the following requirement must be satisfied:

$$\frac{h_w}{t_w} \leq 72\varepsilon \quad \text{where} \quad \varepsilon = \sqrt{\frac{235}{f_{yd}}}$$

If the shear force is higher than one half of the steel section shear resistance, the yield strength of the web must be reduced by $1 - \rho$ as seen in Figure 2.14.

$$\rho = (\frac{2V_{Ed}}{V_{Rd}} - 1)^2$$

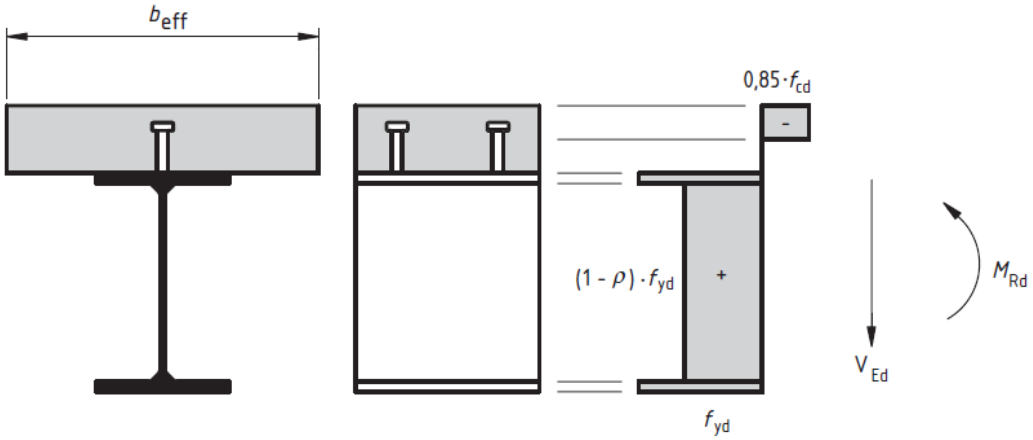

Figure 2.14 **Plastic stress distribution modified by the effect of vertical shear** [18]

2.6 Serviceability limit state

Serviceability limit state covers a wide range of checks such as deflections, vibrations or stresses. The design guide [24] can be used to check in a simplified manner, the vibrations of composite beams. Numerical examples studying the vibrations of demountable composite beams can be found in [13] and [9].

2.7 Deflection - code approach

In case of full shear connection the bending stiffness of the composite beam can be determined without accounting for the flexibility of the connectors. To simplify the calculation the modular ratio is introduced while also taking into account long term effects of concrete based on [18] or [25].

$$n = \frac{E_a}{E_{c,eff}}$$

Using the modular ratio the section is adapted by transforming the concrete slab into a steel part, as seen in Figure 2.15. Afterwards, the neutral axis is determined followed by the second moment of area. Having determined the section properties, the deflection of a simply supported beam can be obtained using simple structural mechanics relations:

$$\delta = \frac{5}{384}\frac{ql^4}{E_a I_{composite}}$$

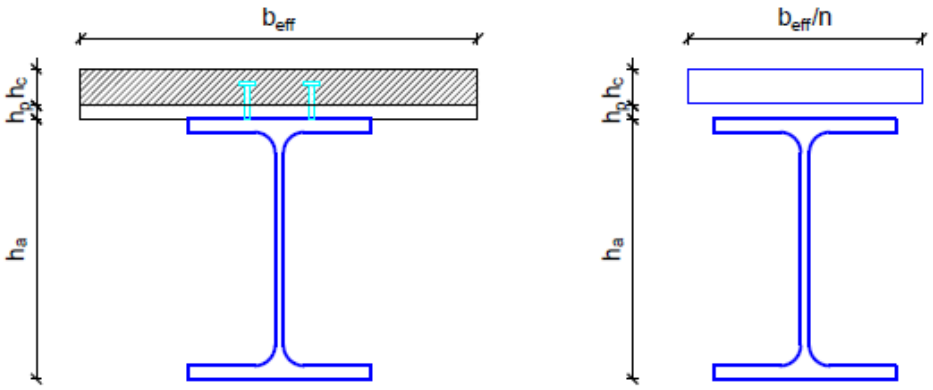

Figure 2.15 **Transformation of the cross-section** [13]

In order to account for partial shear connection interaction, the Dutch National Annex [26] provides a formulation for the deflection only if the requirements of section 7.3.1 of [26] are satisfied.

$$\delta = \delta_c(1 + k(1 - \eta)(\frac{I_c}{I_a} - 1))$$

Where:

δ is the final corrected deflection

δ_c is the deflection considering the composite section,

η is the degree of shear connection

k accounts for the construction method with values of 0.5 for propped and 0.3 for unpropped construction.

Similar formulations can be found in [27] and [28]. The comparison of the additional deflections due to partial shear connection between the tests and the former BS 5950 [27] and the AISC Code [28] were found to be reasonably accurate for the shorter span beams, but conservative by about 20% for the 11m span asymmetric beam test with 33% shear connection [29].

2.8 Deflection - analytical approach

The formulations provided by guidelines are limited for the following cases:

- Only applicable to uniformly distributed connector arrangements
- Not applicable to other types of connectors with different initial stiffness compared to headed studs.

An analytical solution to determine the deflection of composite beams while accounting for the flexibility of the connectors have been developed by [30] and further developed and investigated by [31-35]. A formulation based on an assumed slip distribution in the form of a cosine was proposed by [29]. Uplift effects were included in a formulation presented by [21]. All these analytical solutions are limited to uniformly distributed connector arrangement and prismatic beams. The deflection of tapered beams can be obtained using an analytical model developed by [36].

The flexibility of the connectors, the non-uniform connector arrangement and the shape of the beam are accounted in the formulation of [37]. The formulation was validated based on the beam tests presented in this thesis. Even though the formulation can be considered complete, its complexity requires to be implemented in a numerical calculation software. The theoretical background of the formulation is briefly described.

2.8.1. Theoretical background analytical formulation

Starting from the derivation presented by [32] for uniformly distributed connectors, the differential equation describing the behaviour of a composite beam is the following:

$$\frac{d^6w}{dx^6} - \propto^2 \frac{d^4w}{dx^4} = -\frac{\propto^2}{EI_\infty} q + \frac{1}{EI_0}\frac{d^2q}{dx^2}$$

Where:

$$\propto = \sqrt{\frac{Kr^2}{EI_0(1-\frac{EI_0}{EI_\infty})}}$$

$$K = \frac{n_{sc} k_{sc}}{\frac{L}{2}}$$
$$EI_0 = E_a I_a + E_c I_c$$
$$EI_\infty = EI_0 + \frac{EA_p r^2}{EA_0}$$
$$EA_0 = E_a A_a + E_c A_c$$
$$EA_p = E_a A_a \times E_c A_c$$

K - slip modulus of shear connection

r - the distance between the centroids of the two pars, eg. concrete slab and steel member

n_{sc}- number of shear connectors in one half-span

k_{sc}- initial stiffness of a connector

The solution to the sixth order differential equation is described by the superposition of the general and the particular solution:

$$w = a_1 \sinh \propto x \ + a_2 \cosh \propto x \ + a_3 x^3 + a_4 x^4 + a_5 x^5 + a_a + w_{particular}$$

The moment, shear force and compression force in the concrete are expressed according to [73] as follows:

$$M = \frac{EI_\infty}{\propto^2} \left(-\frac{d^4 w}{dx^4} + \propto^2 \frac{d^2 w}{dx^2} + \frac{q}{EI_0} \right)$$
$$V = \frac{-dM}{dx} = \frac{EI_\infty}{\propto^2} (-\frac{d^5 w}{dx^5} + \propto^2 \frac{d^3 w}{dx^3} - \frac{1}{EI_0} \frac{dq}{dx})$$
$$N_c = \frac{EI_\infty}{\propto^2 r} \left(-\frac{d^4 w}{dx^4} + \propto^2 \left(1 - \frac{EI_0}{EI_\infty} \right) \frac{d^2 w}{dx^2} + \frac{q}{EI_0} \right)$$

The slip can be expressed as the ratio between the shear flow and slip modulus of the shear connection. The shear flow represents the rate of change in the concrete compression force therefore, the interface slip is defined as follows:

$$s = \frac{dN_c}{dx} \frac{1}{K}$$

In case of uniformly distributed loads differentiating q in eq. ?? with respect to x is reduce the solution of the differential equation only to the general part. Boundary conditions for different static schemes are presented in [32].

In order to generalize the analytical formulation for non-uniform connector arrangement and non-prismatic steel beams, [37] proposed the discretization of the beam in segments to describe the overall behaviour. Each segment will be governed by a sixth order

differential equation which will account for the connection stiffness. For this reason, the discretization has to be done in segments with equal length as the connector spacing in order to capture the non-uniform arrangement (see Figure 2.16). The formulation showed close match with finite element models and the experiments presented in this thesis.

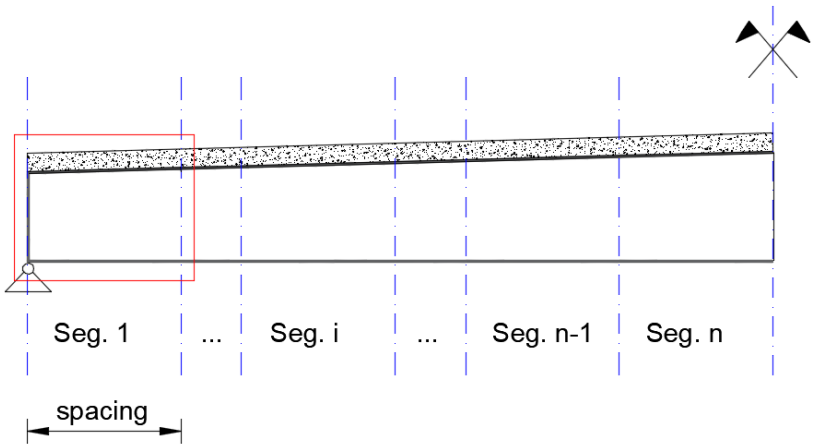

Figure 2.16 **Discretization in segments of a tapered beam**

Non-prismatic beams can be described by the average section properties of the segment as shown in Figure 2.17.

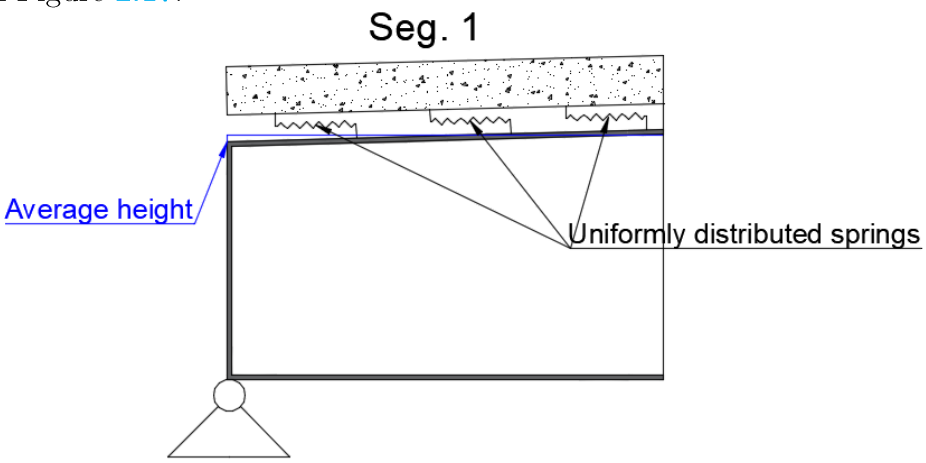

Figure 2.17 **Segment properties**

The set of n differential equations will lead to 6 x n unknowns. The number of unknowns can be reduced by considering only one half of the simply supported beam. To solve the unknowns 3 boundary conditions will be applied at each end of the beam and 6x(n-2) interface conditions will be used to describe the continuity between the segments.

Boundary conditions:

- $x = 0$

$$w = 0$$
$$M = 0$$
$$\frac{ds}{dx} = 0$$

- $x = L/2$

$$\frac{dw}{dx} = 0$$
$$V = 0$$
$$s = 0$$

Interface conditions:

i. Continuity of displacement
ii. Continuity of rotation
iii. Continuity of moment
iv. Continuity of shear force
v. Continuity of axial force
vi. Continuity of slip

Due to the large number of unknowns the solution can be obtained numerically using specialized software.

2.9 State of the art

2.10 Non-demountable shear connectors

This section summarizes the common solutions for non-demountable shear connectors. Starting with the welded and moving to the un-welded solutions the summary will describe the features of each type of connectors.

2.11 Welded connectors

2.11.1. Welded headed studs

Headed studs are the most popular solution in terms of mechanical shear connectors. Due to their extensive use, this connector was thoroughly researched and standardized. Large scale experimental research led to the development of empirical solutions for the load-slip curves. Their load-slip behaviour and failure modes are well known for both solid and trapezoidal slabs. The shear force is resisted in bearing against the concrete, by the shank and the weld collar. In order to resist uplift forces the head diameter dimensions are imposed by [18] for a good anchorage. The advantage is the combination of a relatively large stiffness with a very large deformation capacity [22].

Headed studs are installed by electrically spot welding with microchip-controlled equipment. An advantage in terms of competitivity against other connectors comes from the possibility of welding through galvanized profiled sheeting.

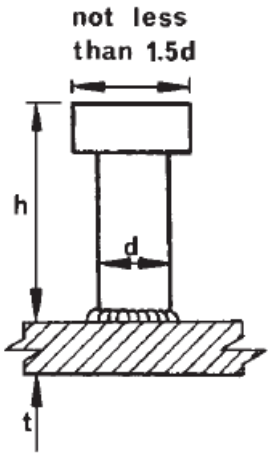

Figure 2.18 **Headed stud** [10]

A summary of literature research carried by [38] is presented in the form of load-slip curves in Figure 2.19.

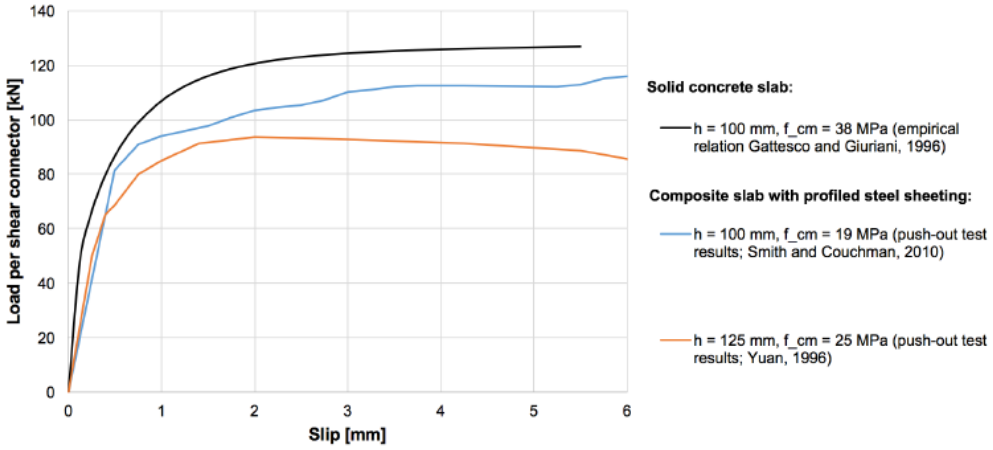

Figure 2.19 **Load-slip curve - headed studs** [38]

When analysing the formulas imposed by [18] for the shear resistance, an economic disadvantage of headed studs is revealed. The failure of the stud will always govern for concrete classes higher then C30/37. Even if the concrete industry can easily deliver high strength concrete, from a composite behaviour point of view, there won't be any benefit. Another disadvantage is the need to use special welding equipment when the studs are subjected to cyclic loading.

As the use of composite construction moved to bridges and long spans, there was a need for an increased number of shear connectors. Due to a high concentration of studs the reinforcement installation became problematic. Studies carried out by [39] concluded that headed studs with dimensions larger than usual are a good solution but they have a slightly smaller fatigue strength without taking proper measures.

2.11.2. Perfobond-rib and crestbond shear connectors

The above-mentioned problems of headed studs led to the development of other shear connectors. One of the proposed solutions is the perfobond rib shear connectors developed by Leonhardt, Andrå and Partners from Germany in the late 1980s. The vertical and horizontal forces are resisted by four components as seen in Figure 2.20 [40]:

1. Horizontal shear on the concrete ribs
2. Vertical shear on the concrete ribs
3. The transverse rebars going through the holes
4. The concrete-end bearing zone in compression.

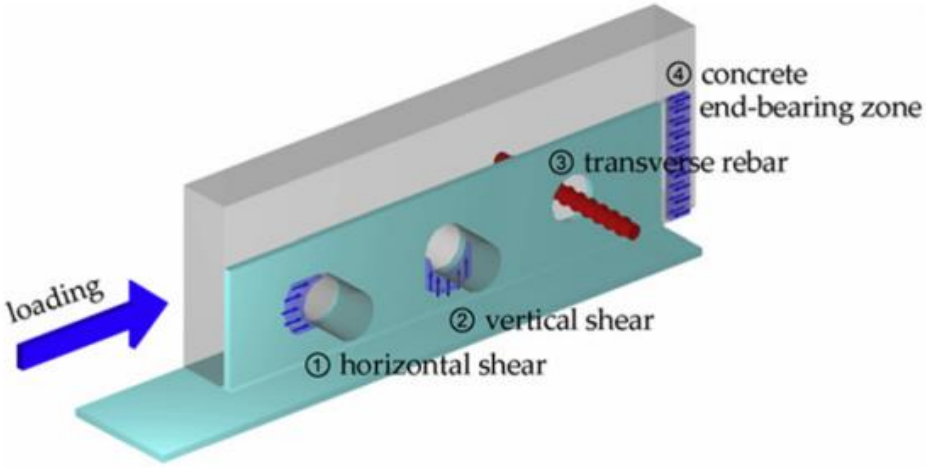

Figure 2.20 **Perfobond-rib connector** [40]

Experimental research shows that the shear capacity of a twin perfobond-rib connector is reduced to about 80% of that of a single perfobond rib. This is due to reduction in the shear capacity contributed by the concrete end-bearing zone, the concrete dowel, and the transverse rebar in the rib hole [40]. The transverse rebar has a strong influence on the ductility of the connector.

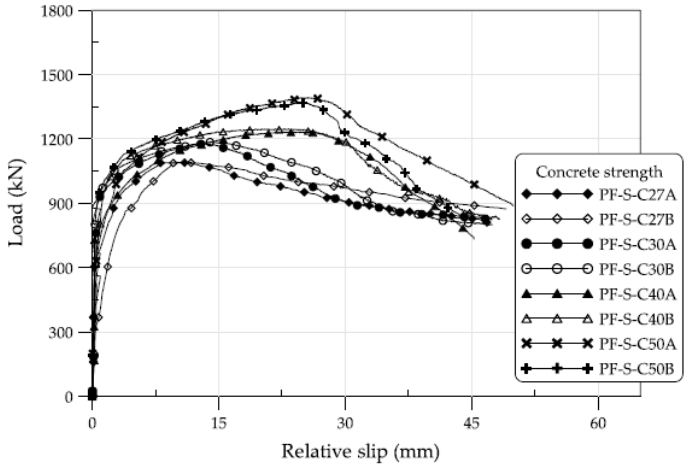

Figure 2.21 **Load-slip curve - single perfobond rib for different concrete strengths** [40]

Even though this type of connector possesses high stiffness, shear and fatigue resistance, the placement of the bottom reinforcement can be an issue. For this reason, the crestbond rib connector was developed.

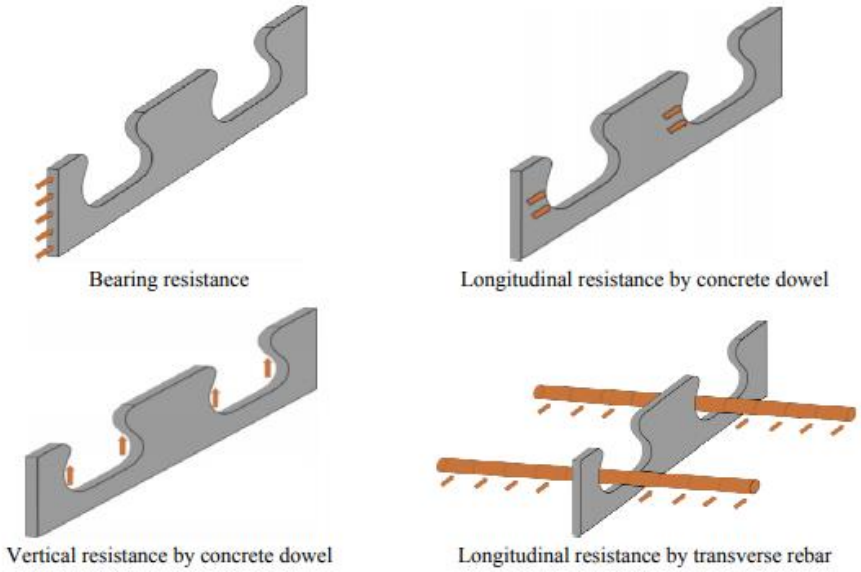

Figure 2.22 **Crestbond rib shear connector** [41]

Having similar stiffness, shear and fatigue resistance as the perfobond, the crestbond brings along the advantage of ease in installing the bottom reinforcement. It was found that the concrete strength and number of transverse rebars in the crestbond rib were significantly related to its shear resistance [41]. The dimensions of the crestbond rib have limited influence on the shear resistance.

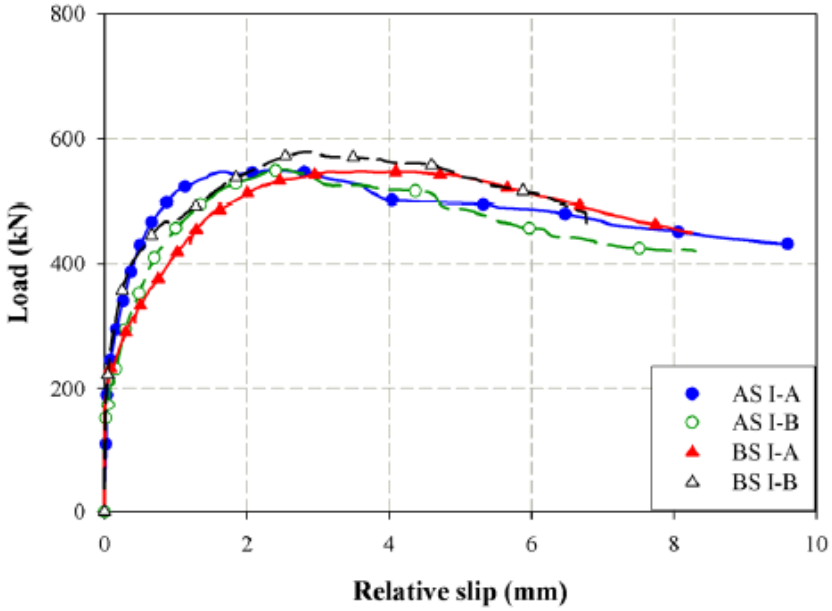

Figure 2.23 **Load-slip curve for various crestbond rib dimension** [41]

Apart from the the perfobond and crestbond other variations such as the oscillating perfobondstrip or the T-rib connector were developed.

Figure 2.24 **Oscillating perfobondstrip and T-rib shear connectors** [42]

2.11.3. Other types of welded connectors

Apart from the previously described connectors there is a wide variety of connectors such as:

- T connectors
- Channel connectors
- Bar connectors
- Pyramidal shear connectors.

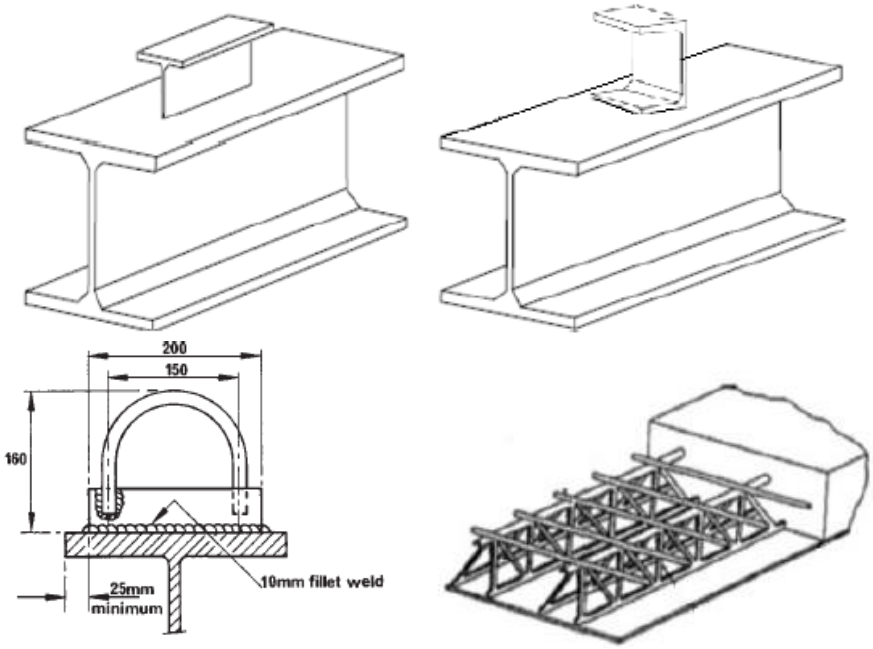

Figure 2.25 **T connectors, channel connectors** [42], **bar connectors and pyramidal shear connectors** [10](**from left to right**)

2.12 Non-welded shear connectors

2.12.1. Hilti connector

Due to welding difficulties encountered with headed studs, the need of non-welded shear connectors arises. This type of mechanical connectors does not require inspection, and the speed of construction is increased due to the ease in installation. Such a system was developed by [43] and researched by [44]. In Figure 2.26 the components of the system are represented. A cold formed L shaped anchorage leg is attached to the top flange of the beam by two powder-actuated fasteners. The X-HVB is ductile in all sizes and designed to resist longitudinal shear force, while vertical uplift is prevented by the X-HVB head and the nails [43].

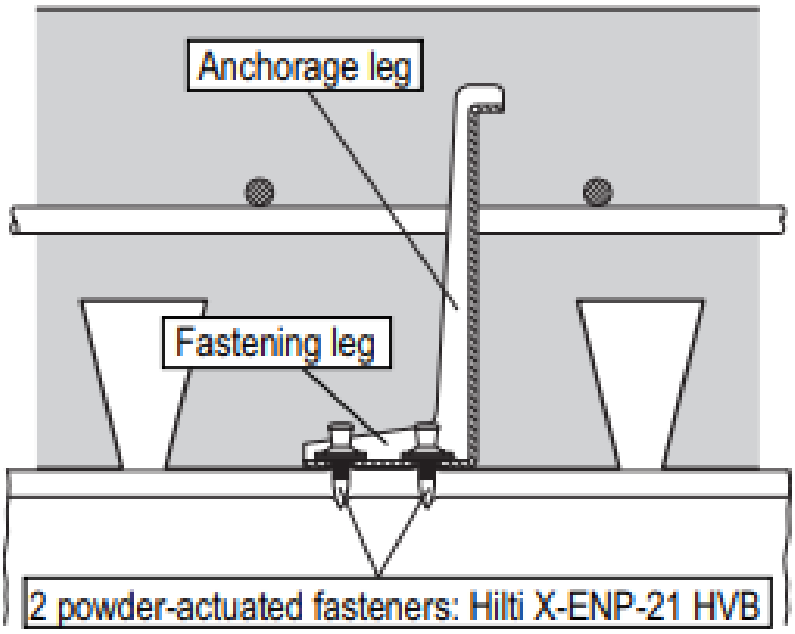

Figure 2.26 **Hilti shear connector** [43]

According to research carried by [44], three failure modes were encountered in push-out tests with trapezoidal sheeting (see figures below). If the requirements in terms of the connecter height above the rib and spacing are satisfied, the capacity and ductility are maximized.

The ductile behaviour is defined by shearing of pins, pulling out of pins and pulling out of connector (pins in place) [44].

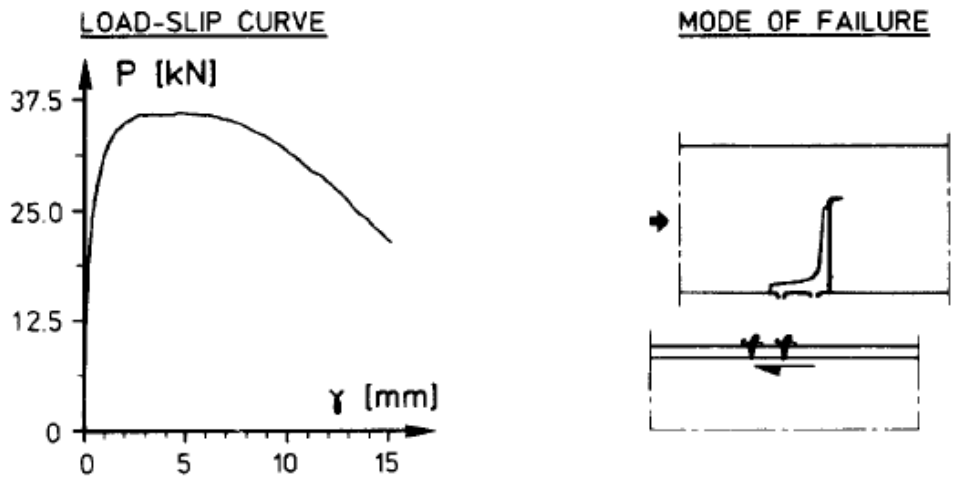

Figure 2.27 **Ductile failure** [44].

The semi-ductile failure is defined by pulling out of connector, concrete pull-out around connector, crushing of concrete at connector leg and shearing of concrete at top of ribs [44].

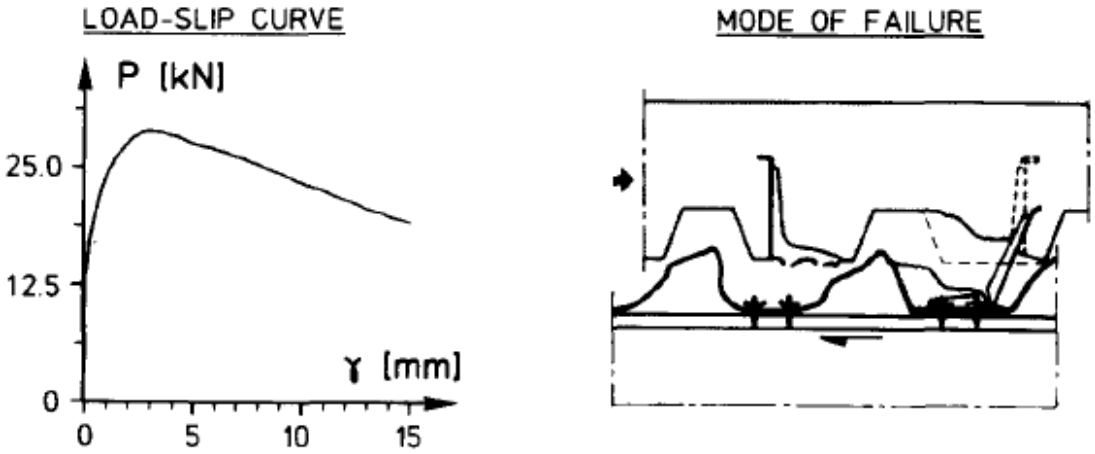

Figure 2.28 **Semi-ductile failure** [44]

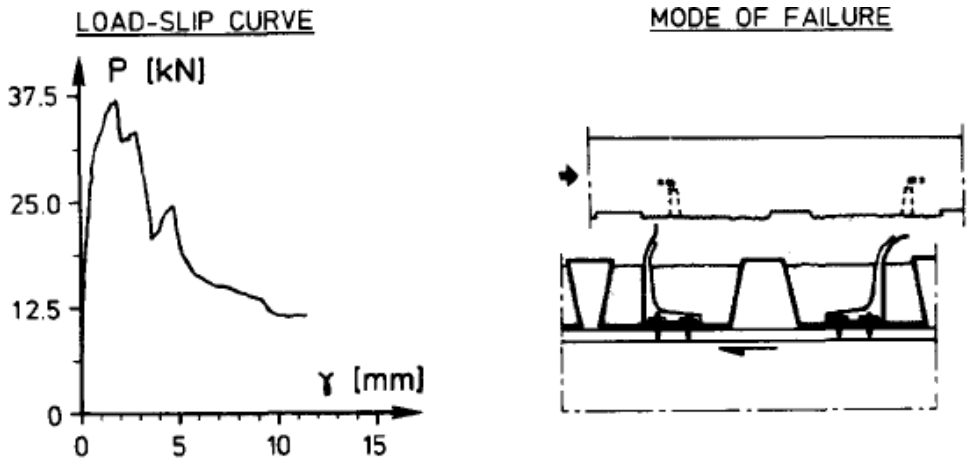

Figure 2.29 **Brittle failure** [44].

In beam test carried by [44] ductile behaviour was observed, even for low degrees of connection. The degree of connection can be lowered up to 25% for spans not exceeeding 15m.

2.12.2. Welded stud on base plate

Another solution in the form of a non-welded connector was tested by [45] consisting of a welded stud on a base plate. The failure was governed by shearing of the pins before yielding of the stud. In terms of ductility, this connector showed a lower slip capacity compared to the traditional welded headed studs. The recorded slip was in the order of 4-7mm.

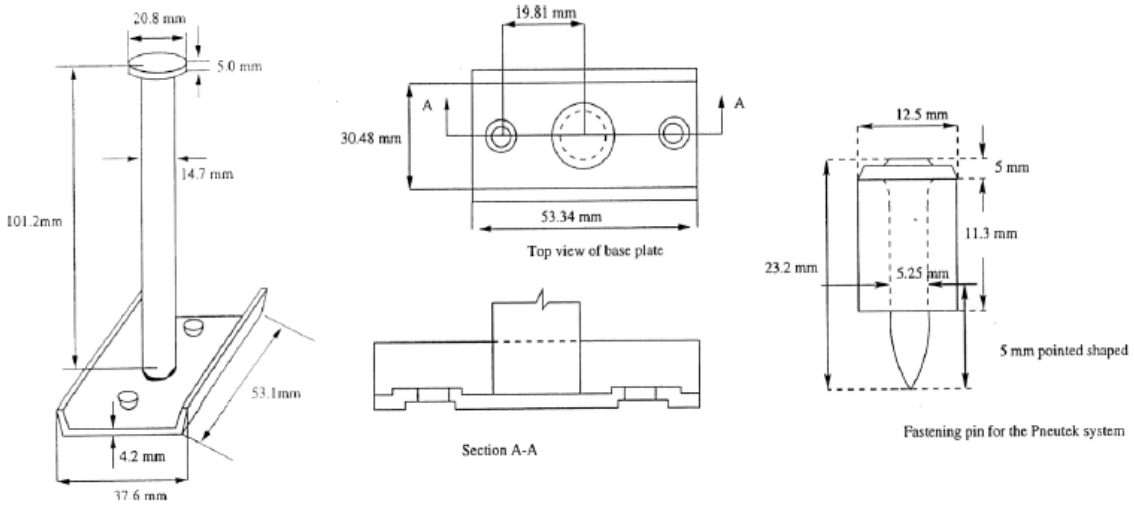

Figure 2.30 **Shear studs with base plate pin connected** [45]

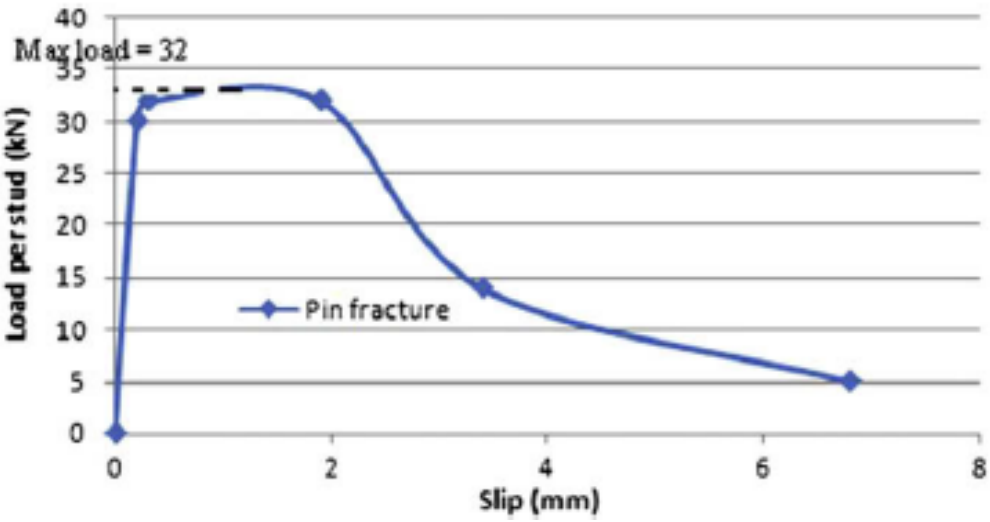

Figure 2.31 **Load-slip curve for perpedicular plate orientation and profiled sheeting CF70** [45]

The ductility and resistance can be improved by increasing the penetration depth of the pins, increased properties of the base plate and installing the base plate parallel to the beam axis.

Apart from the two solutions presented at this moment there is a wide variety of shear connectors installed using powder actuated fasteners.

2.13 Injection bolts

The combination of steel and concrete requires large oversized holes in the top flange to ensure the fit of the components and a fast execution and demounting. For this reason, after assembly the composite action is not active. The bolt will slip until it starts bearing on the hole wall. A solution to obtain slip resistant connections are resin injection which has been used since the 1970's in connections for railway bridges.

The need of large oversized holes required by demountable systems can be accommodated with ease when resin injection is used. In composite structures the resin will increase the ductility of the connectors due to its deformability without reducing the shear resistance. Regulations for injection bolts can be found in [11] and [46].

Resin injection requires a special injection bolt which has a hole in the head. Moreover, a special washer must be used in order to allow the resin to pass into the bolt-to-hole clearance. To ensure that resin will completely fill the void between the hole wall and the bolt shank there is a need of an air channel. The purpose of the channel is to provide an escape path for the air.

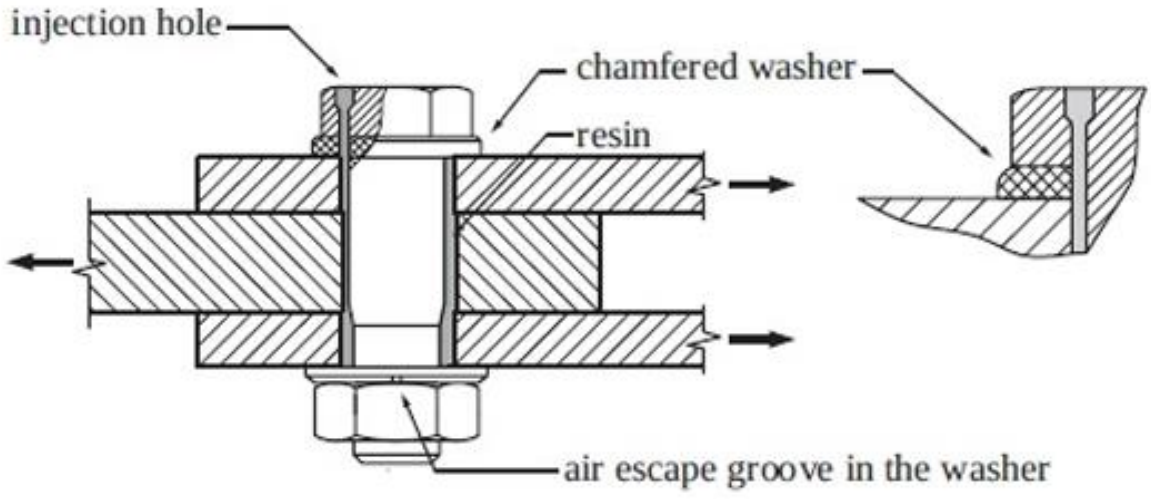

Figure 2.32 **Injection bolts in a double lap joint** [47]

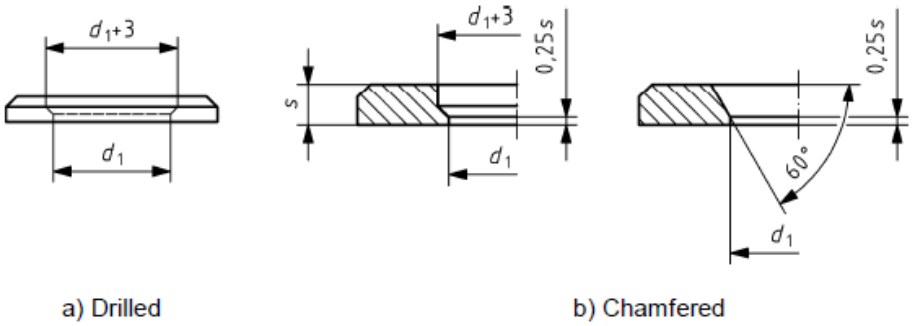

Figure 2.33 **Washer detail** [11]

2.14 Demountable shear connectors

Traditional composite structures have the disadvantage of restricting the non-destructive disassembly of the components. Therefore, the research focus of composite construction shifted towards demountable mechanical connectors. In this way, easy dismantling for the purpose of replacement, maintenance or reuse of concrete slabs is easily achieved [48].

2.14.1. Bolted shear connectors

Bolted shear connectors can represent a viable solution to the traditional headed stud. Commonly used in joints it was inherent to be adopted in composite construction. The price difference per unit is slightly higher compared to headed studs but, reducing the construction time can bring an economical advantage for bolts as means of mechanical connectors.

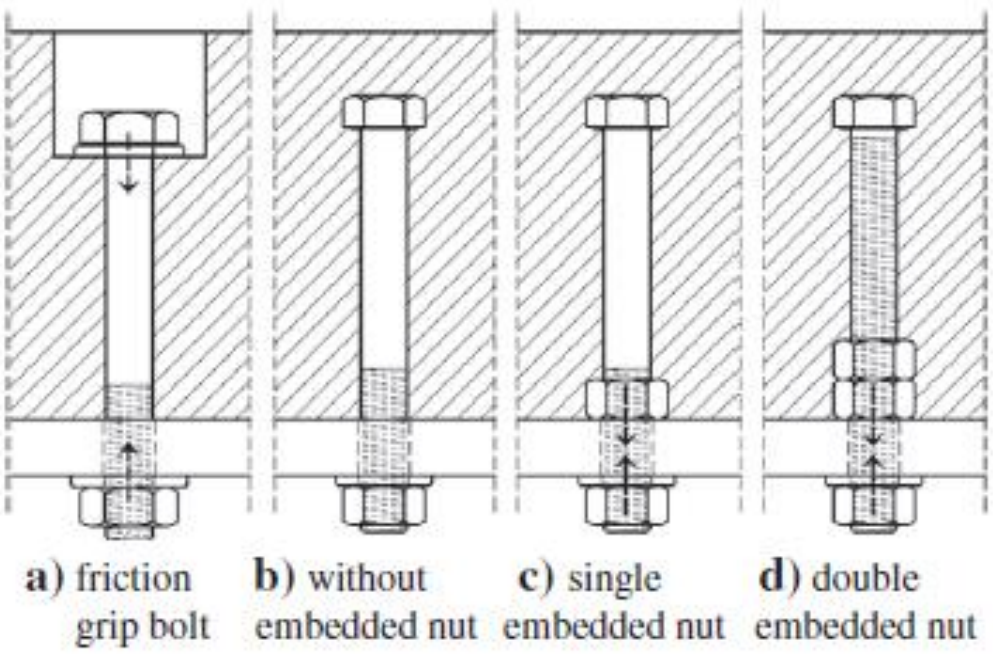

Figure 2.34 **Bolted shear connectors** [49]

2.14.1.1. Friction grip bolts solutions

Friction grip bolts (Figure 2.34 a)) resists the longitudinal shear force through friction between the steel and concrete interface. By prestressing the bolt through the thickness of the concrete slab the friction force is achieved. On the other hand, due to prestressing of the bolts, long term effects such as creep and shrinkage will influence the behaviour of the shear connection. Moreover, due to the concentrated compressive stresses around the bolt there is a need for special reinforcement and detailing. Another drawback is the increased price of high-grade bolts which are needed for preloading.

According to [50] friction grip bolts have zero slip at serviceability stage while in later stages at ultimate limit state the slip doubles compared to welded headed studs of same dimensions. Design shear resistance for friction grip bolts is defined in BS 5400-5 [51] but notably lower values than those obtained by [50].

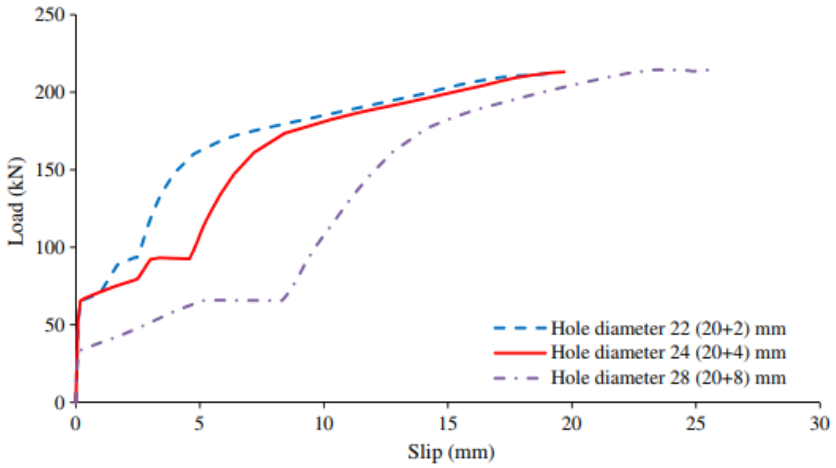

Figure 2.35 **Load-slip curve - friction grip bolt connectors** [52]

As seen from Figure 2.35 the behaviour of the connector is governed by three stages. In the beginning the shear force is transferred by the interface friction, constraining the interface slip. When the friction is overcome, the bolt slips until it starts bearing on the hole walls. In the final stage the connector is bearing on the steel and concrete walls up to failure. Because the bolts are installed from the top there is a need of separate holes in the slab and the beam. The hole tolerances in the two elements causes the large slip in the second stage.

A refined design for friction bolts is presented and tested in [57] in the form of a friction bolt with cast in cylinders. The shear connectors consist of a steel cylinder casted into the concrete slab, an L-profile around the slab edges to protect it from damage and top plate to transfer the prestressing force.

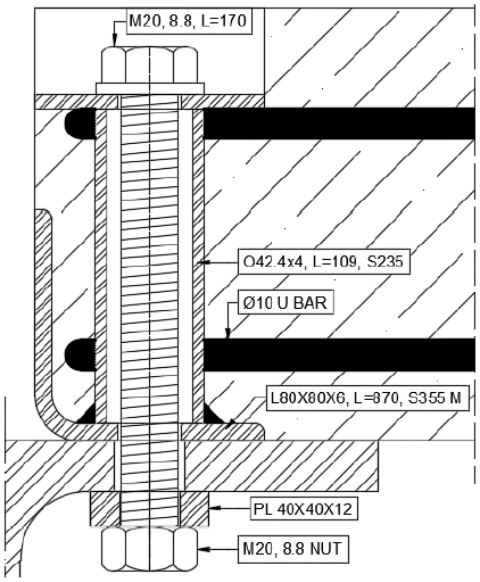

Figure 2.36 **Friction bolt with cast in cylinders** [53]

Push-out tests included solid and profiled sheeting slabs. In all tests the failure was governed by shearing of the bolt with average resistances of 150kN. A similar behaviour to the regular friction bolt was observed where the three stages were distinguished.

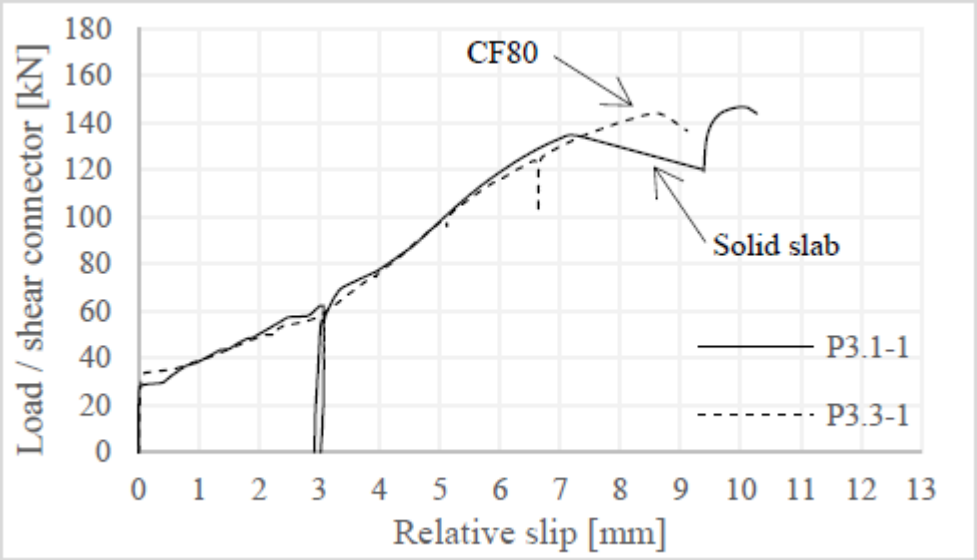

Figure 2.37 **Load-slip curves - friction bolt with cast in cylinders in solid and profiled sheeting slabs** [53]

After failure, the specimens were reassembled and tested again obtaining similar resistances and failure modes. However, lower friction resistance and larger relative slip was observed.

2.14.1.2. Bolt without embedded nut

In Figure 2.34 b) a bolted shear connection without embedded nut is represented. Literature review carried by [9, 38, 49] revealed that the shear resistance is 80% of headed studs while the stiffness is only 15%. The cause of this reduced stiffness is the slip and rotation of the bolt. Because of this reduced stiffness [54] concluded that they are not suitable as mechanical connectors.

Research was carried by [53, 55-59] on threaded headed studs in solid and profiled sheeting slabs. The studies concluded that the connectors can be demounted easily in push-out and beam tests, and simple calculations can be used to estimate the shear resistance and ultimate moment capacity.

Figure 2.38 **Threaded headed stud** [59]

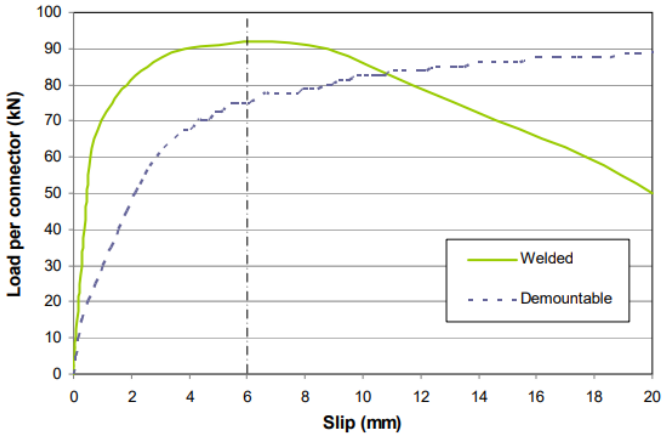

Figure 2.39 **Load-slip curve -welded and threaded studs in solid slab** [55]

Push-out tests of threaded studs in solid and profiled sheeting slab showed similar resistance as welded studs however, they have higher slip capacity but lower initial stiffness.

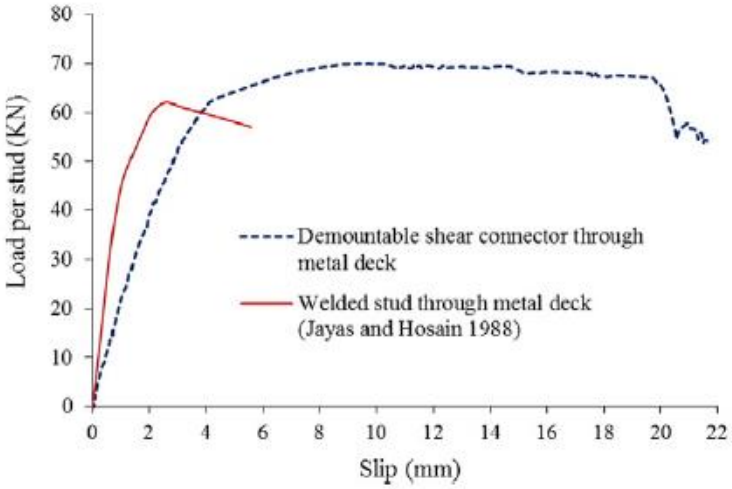

Figure 2.40 **Load-slip curves - welded and threaded stud in profiled sheeting slab** [56]

2.14.1.3. Bolts with single embedded nut

Because the rotation and slip of the bolt in the hole is the cause of the low stiffness, nuts at the base of the bolt can be embedded in concrete. (see Figure 2.34 c)). Research carried by [49] showed that bolts with single embedded nut have a resistance approximately 95% of that of headed studs. However, the stiffness is reduced by 50% due to the slip in the hole.

Two failure modes were identified by [33] for bolted connection with single embedded nut: shear failure of the bolt and pryout failure of the concrete (see Figure 2.41). At the lower bound of shear connector height to diameter ratio ($h_{sc}/d = 2.5$) slip at failure is increased above 6 mm due to concrete cone failure, leading to a ductile behaviour of a bolted shear connector [49].

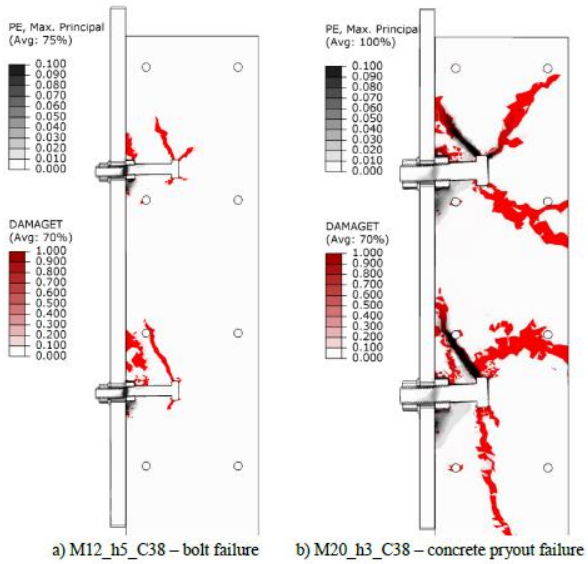

Figure 2.41 **Failure modes of bolted shear connectors influence of bolt diameter** [54]

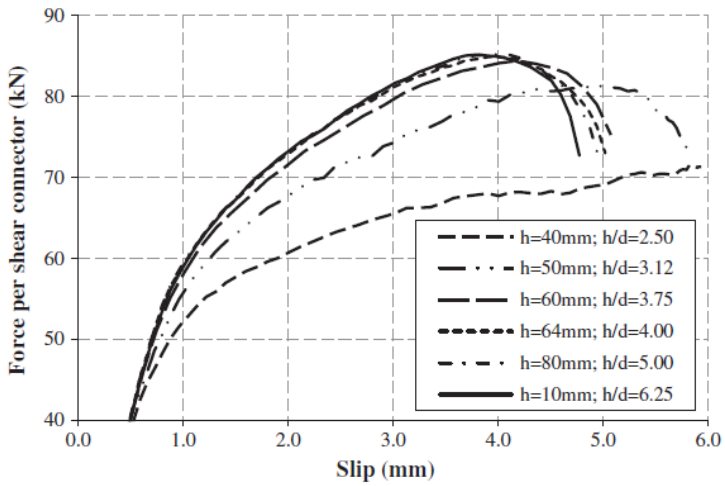

Figure 2.42 **Load-slip curve - M16 bolts with single embedded nut** [49]

Design resistance of bolted shear connectors with single embedded nut is defined by [54] following [18] framework:

$$P_{\mathrm{b,u}} = \alpha_{\mathrm{b}} f_{\mathrm{ub}} A_{\mathrm{s}} \qquad \alpha_{\mathrm{b}} = 0.6(\frac{34}{d})^{0.23}$$

$$P_{\mathrm{c,u}} = 55\alpha_{\mathrm{c}} d^{1.9}(\frac{f_{\mathrm{cm}} h_{\mathrm{sc}}}{d})^{0.4} + 22000 \qquad \alpha_{\mathrm{c}} = \frac{22.5}{d+3} \geq 1.0.$$

According to [54], adding a second embedded nut (see Figure 2.34 d)) does not have a significant influence on the stiffness and resistance. Consequently, the most viable solution for precast solid decks is the bolt with single embedded nut.

2.14.2. Resin injected bolt coupler system

The bolt coupler system comes as a solution to regular embedded bolts which are vulnerable to damage during construction and transportation. The shear connector consists of an embedded bolt and coupler which are connected from below by an injection bolt.

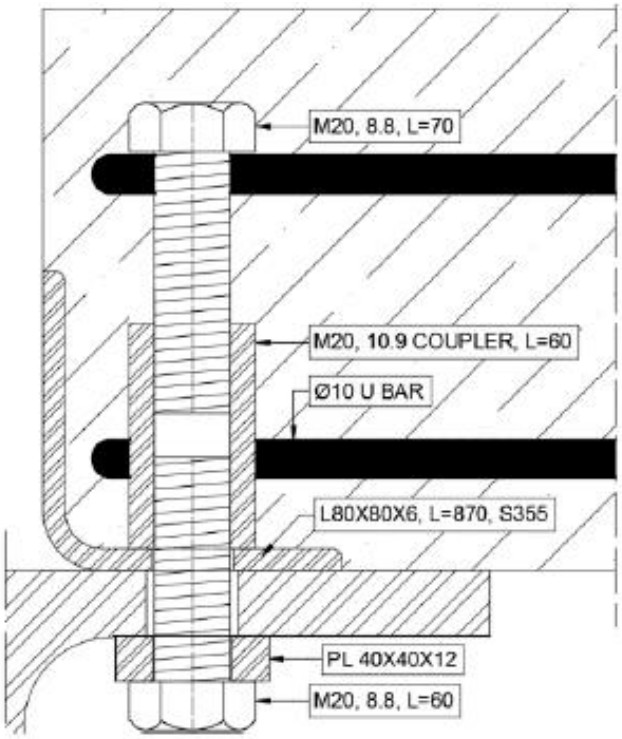

Figure 2.43 **Resin injected bolt coupler system** [53]

The coupler is designed of higher grade (10.9) compared to the external bolt in order to prevent any damage in case of overloading, ensuring the deck can be reused. The embedded bolt has the role to resist uplift forces. To protect the concrete edges during transportation and installation, L-profiles are placed all around the bottom side of the deck. The width of the decks is limited by normal transportation demands to 2.4-2.6 meters, if transported horizontally. With the application of epoxy resin, larger tolerances can be allowed without compromising the load-bearing capacity where the execution of large deck components makes it necessary [53].

Push-out tests carried by [53] for solid slabs with 150mm height failed by shearing of the bolt at an average load level of 131kN per connector. The initial stiffness decreased from 100kN/mm at load level of 50kN to 30kN/mm. Figure 2.44.

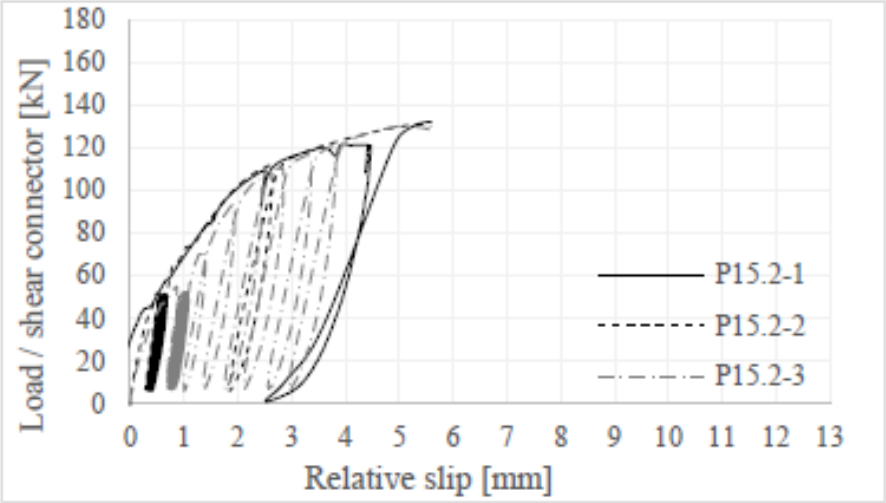

Figure 2.44 **Load-slip curves - injected bolt coupler connector in 150mm solid slab** [53]

Push-out tests have been carried by [60] on solid slabs with a thickness of 120mm. The initial stiffness was reported by [61] to 55kN/mm and a resistance of 110kN (see Figure 2.45). Beam tests have been carried out in this thesis for the bolt coupler system in 120mm thick prefabricated decks with tapered beams.

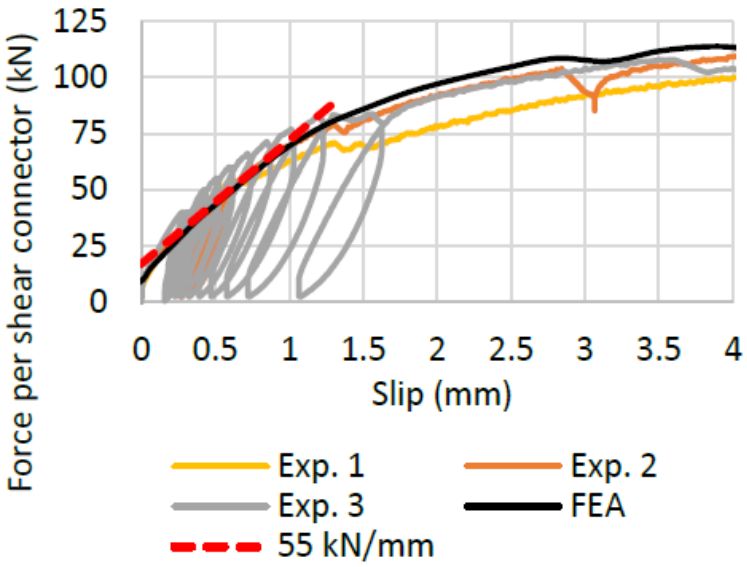

Figure 2.45 **Load-slip curve - injected bolt coupler connector in 120mm solid slab** [61]

Push-out tests have been performed by [62] on profiled sheeting slabs with a thickness of 150mm. The connector has an average resistance of 56kN with an initial stiffness of 30kN/mm. Beam tests have been carried out by [63] on demountable profiled sheeting slabs with the bolt coupler system as means of connectors.

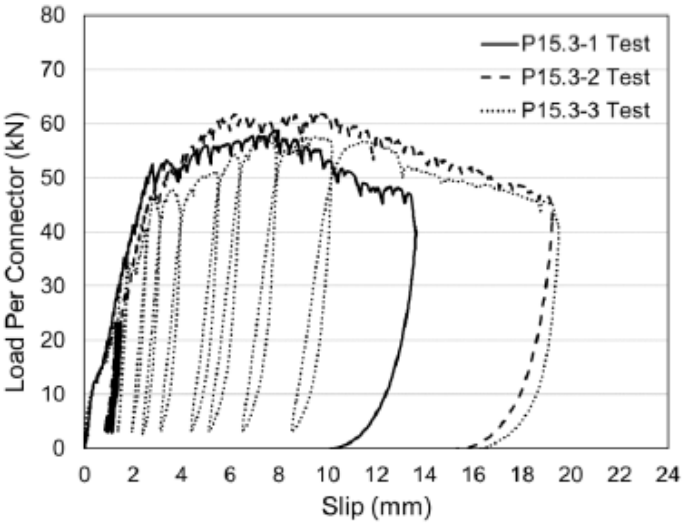

Figure 2.46 **Load-slip curves - injected bolt coupler system in 150mm profiled sheeting slab** [62]

3 Feasibility of construction

The assembly of prefabricated systems require a tight control of the tolerances in order to achieve the desired connection. Solutions involving prefabricated composite flooring systems exist but require some sort of in-situ casting. The casting increases the construction time, costs and obstructs the non-destructive demountability of the decks and beams. These issues can be overcome by using a connector which provides the possibility of demountability.

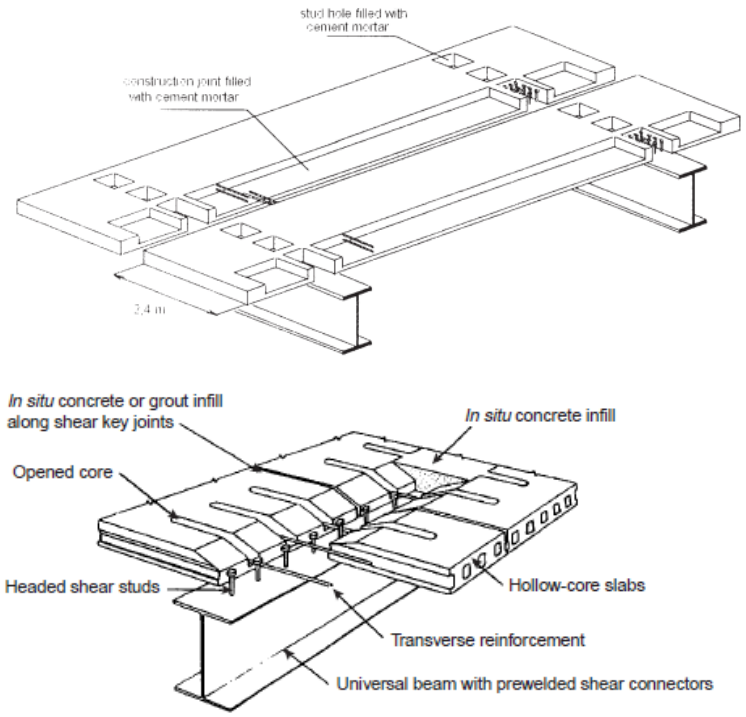

Figure 3.1 **Prefabricated solid slab with pockets [64] and composite beam with hollow core slab [31]**

The focus of this thesis is to assess the suitability of using bolt coupler connectors in large prefabricated concrete decks. The feasibility of construction will be assessed through experimental work and finite element models.

3.1 Problem definition

The outcome of this research is to understand the influencing factors and their implication on the assembly and disassembly of demountable steel-concrete composite floorings.

Manufacturing imperfections, deformation of the structure during construction and the speed of construction influences the required tolerances of the steel beam holes. The assembly and disassembly were investigated in laboratory conditions on large scale car

park specimens backed up by a wide range of imperfection measurements and finite element models.

Resin injection is used as a measure to obtain slip resistant connections. Injection of small scale push-out specimens was successful but it has not been applied to full-scale composite beams yet. Demountable flooring systems require vertical injection of a large number of bolts and the easy removal of the resin plug after disassembly. The repetitive process requires to be labour efficient and to be able to reliably fill the gap between the bolt shank and hole wall. Through injection of a large number of bolts, the quality of the injection is assessed and practical advice will be given based on experimental experience.

Research questions:

- **Which are the influencing factors for assembly and disassembly of demountable systems?**
- **Can resin injection be used reliably and labour efficiently for large demountable buildings?**

3.2 Car park specimen

Experimental research was carried out as a part of RFCS-project REDUCE (Reuse and Demountability using Steel Structures and the Circular Economy) at TU Delft's Stevin II lab. Full scale laboratory experiments were conducted to study the feasibility of construction of a novel demountable flooring system. Based on design of a car park carried out by [36], an experimental setup was manufactured.

Laboratory space constraints led to a reduction to 90% of the original car park design. The setup consists of three tapered beams and four concrete decks. The dimensions of the setup are appropriate sizes for a car park [65]. The dimensions of the tapered beam are summarized in Figure 3.2.

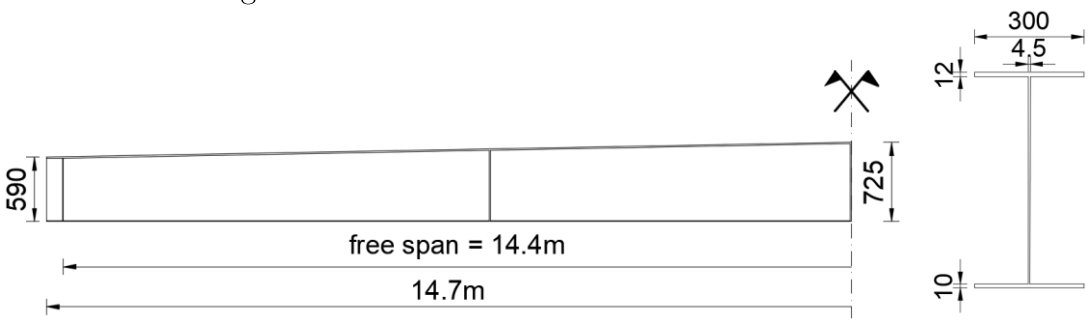

Figure 3.2 **Tapered beam dimensions**

The influence of façade columns is studied having one of external beams supported in three additional positions at a spacing of 3.6 meters. Through the testing program, the beams were braced to prevent lateral torsional buckling. As [9] pointed out, the beam is prone to instability effects during construction.

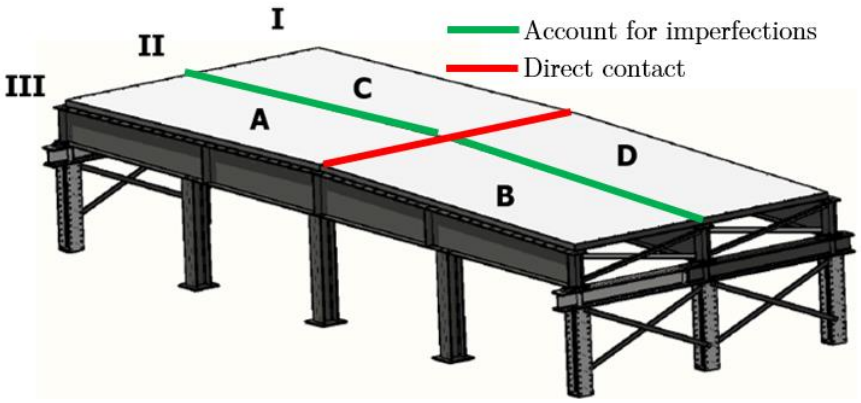

Figure 3.3 **Car park specimen** [66]

Figure 3.4 **Car park specimen in laboratory**

The dimension of the decks were 7.2 meters x 2.594 meters. The size of the prefabricated concrete decks should be as big as practically possible to reduce the amount of work at the construction site [61]. The thickness of the deck was 120mm. In longitudinal direction a gap was considered to account for any imperfections. Transversally, at mid-span, the decks were designed without an account on tolerances (see Figure 3.3). The reason behind is the necessity of the decks to transfer the normal force.

For consistency and simplicity in expressing the result, the following notation was used to define a connector position on the beam. The beams are numbered from I to III and each half-span is defined by A and B. Each connector is assigned with a number from 1 to 24 counting from support to mid-span.

During the feasibility study, the deflection was measured for beams I and II using six Sakae S13FLP50A potentiometers. The LVDTs were placed at mid-span and at 4.05 meters from the supports. Because the beams were loaded by the self-weight of the decks, the measurements are discrete. Detailed drawings of the measuring equipment are presented in 9.

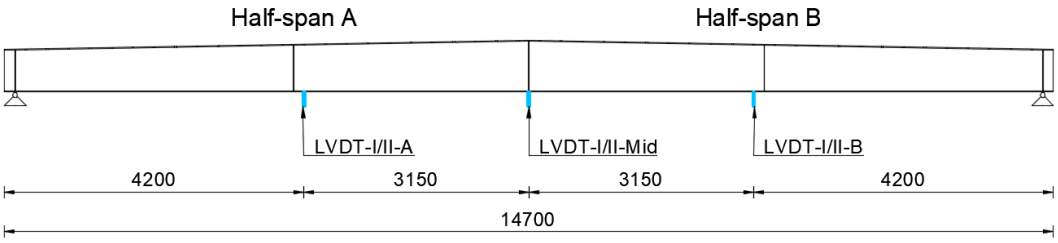

Figure 3.5 **Measuring equipment - feasibility stage**

3.3 Manufacturing process

In order to point out the source of imperfections, frequent visits were carried out to inspect and monitor the progress of the specimen fabrication.

The steel frame was produced by Lindab S.A in Luxemburg which has ensured an automatic manufacturing process, and therefore strict tolerances. The flanges and the web are welded on a single side in an automatic continuous process while the stiffeners are positioned and welded manually. 26mm holes were punched automatically.

The hole size was increased from 26mm to 32 mm in the laboratory using a magnetic drill. The reason behind the increased holes will be explained in the following sections. To avoid misalignment of the new holes, a steel template was used.

Figure 3.6 **Hole size increase from Ø26 to Ø32 mm**

The L-profiles were manufactured at the same workshop while the welding of the deck frame was done in laboratory conditions. Due to large bow imperfections, the angles were braced with tubular bars (see Figure 3.8). This aimed to ensure the rectangularity and dimensional correctness, while at the same time provide extra support during casting.

Figure 3.7 **Welded L-profile frame**

After welding the angle frame was shipped to a workshop in the Netherlands, which manufactured the prefabricated decks. Two anchors were installed to provide support for the lifting system.

The frame was placed on formwork sheets which were drilled at the connector position. The connectors were placed in the holes and tightened. The tightening ensured that no fresh concrete escape around the holes. The concrete can contaminate and influence the properties of the epoxy resin and of the release agent when the decks are injected after construction.

Figure 3.8 **Formwork and connector installation**

Debonding between the concrete slab and the L-profiles due to impact and shrinkage was observed during experiments. Extra anchoring must be added to hold the angle profiles onto the concrete slab.

On the short edge where two decks meet, a transversal joint ensures the transfer of shear forces. A section of the transversal joint is presented in Figure 3.9.

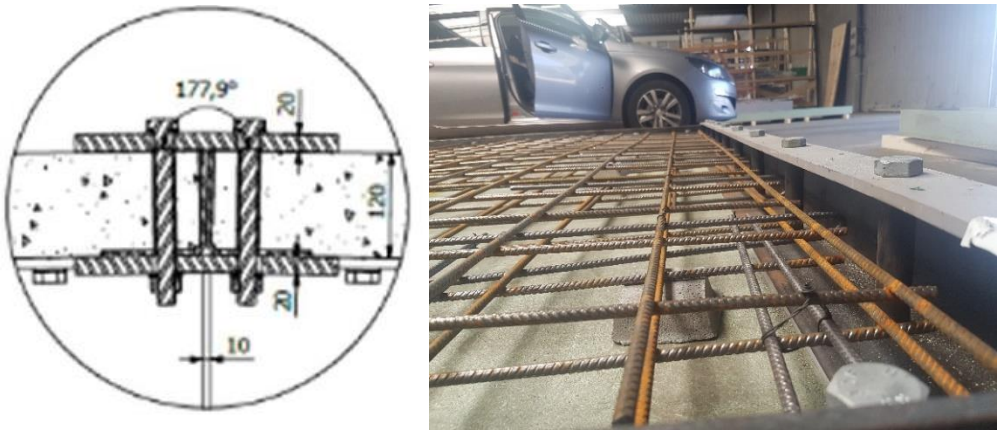

Figure 3.9 **Transversal joint section [66] and installation of the detail**

Two reinforcement meshes were installed and U-bars were placed around each connector. Standardized cubes were taken at the moment of casting from the same concrete batch.

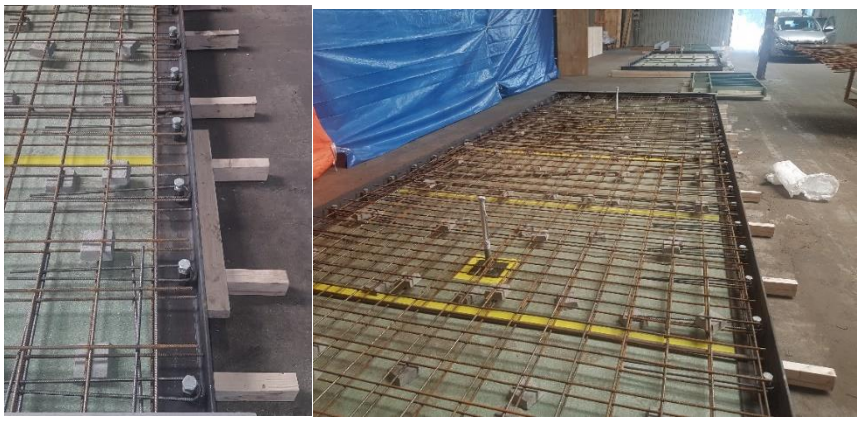

Figure 3.10 **Reinforcement installation**

Figure 3.11 **Concrete pouring and vibrating**

3.4 Feasibility of construction

The assembly and disassembly of the flooring system was tested in laboratory conditions to study the influence of imperfections and deformability of the system. To investigate the influence of façade columns, two construction sequences were tested. Following the notations from Figure 3.3, the sequences are ABCD and DCBA.

3.5 Construction method and sequence

The novelty of the system requires a new approach on how to handle the installation of the large prefabricated decks. The method must ensure complete safety for the workers and machinery, fast erection and prevent any damage to the components of the flooring during installation.

Due to the large self-weight of each deck and small tolerances, the sensitivity of the crane and the experience of its operator are of paramount importance. However, there is still a need of additional workers to fit the decks in the required position. Therefore, at any moment in time, the deck should be either fixed to the crane or to the steel beam for safety reasons.

Figure 3.12 **Installation of deck**

A first approach to assemble and disassemble the decks safely was presented by [9] (see Figure 3.13). Threaded rods are placed into the couplers at the corners and at the mid-span of the deck to aid the installation of the decks. The threaded rods will also act as lateral support for the top flange which is prone to lateral torsional buckling during construction. After all the decks are lowered into position the injection bolts are installed. In a similar fashion, prefabricated decks with embedded bolts are assembled.

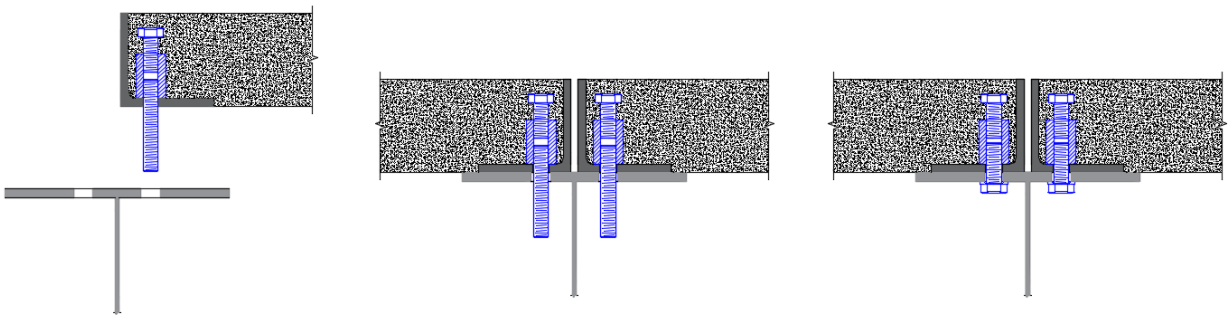

Figure 3.13 **Construction method - Threaded rods**

However, this method comes with the risk of damaging the decks. During experiments the method was tested and due to large imperfections, the rods did not fit into the top flange holes. The rods acted as support points for the deck self-weight (see figures below). The concentrated force applied by the rods lead to punching of the connector through the concrete.

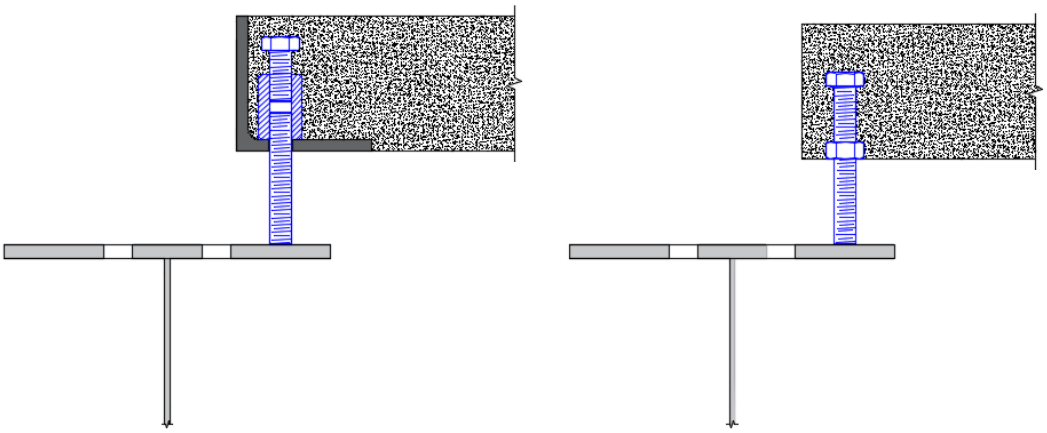

Figure 3.14 **Bolts acting as support points**

Figure 3.15 **Damage due to supported deck on threaded rods**

Prefabricated decks with embedded bolts pose a greater risk of damage during assembly due to the large number of connectors which can misalign. The possibility of damaging the deck requires a different approach on the assembly method.

A solution which does not sacrifice safety and speed is to progressively align the deck from mid-span towards the support with the help of long bolts. Workers have the task to install the long bolts, from below, into the couplers on both sides of the deck.

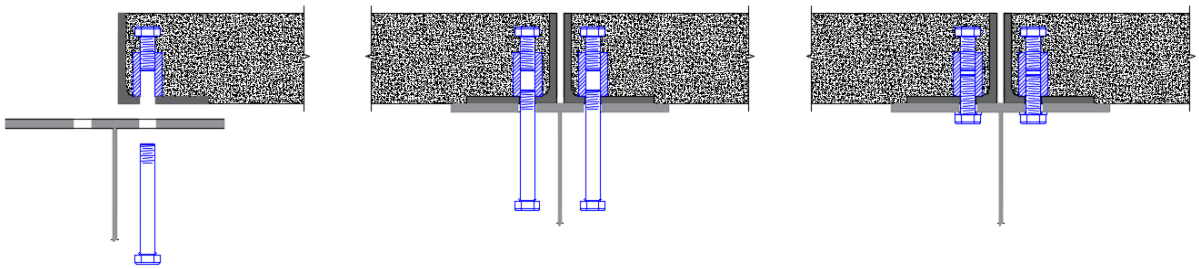

Figure 3.16 **Construction method - Long bolts**

Figure 3.17 **Long bolt**

The long bolts will correct the position of the deck while it is lowered. Moreover, the bolts will act as lateral support for the top flange and will prevent the deck from slipping off the flange which can endanger the workers. The taper of the steel beams requires the assembly to be carried progressively from mid-span towards the supports. As the deck is lowered, additional long bolts are installed at the corners and middle of the deck.

For the 6 mm hole clearance, M20 bolts were sufficient to aid the alignment of the couplers with the holes. However, for larger oversized holes such as 32mm there is the need of an increased diameter of the long bolts to centre the bolts as much as possible in the middle of the holes. In this way any rotation around the vertical axis of the deck during installation will be limited. A solution is to add sleeves which increases the diameter only to the unthreaded part.

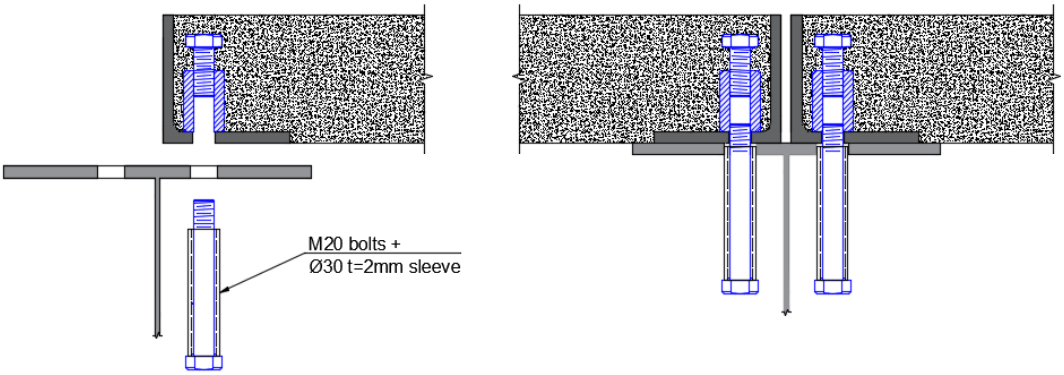

Figure 3.18 **Construction method - Long bolts for large oversized holes**

Figure 3.19 **Long bolt with sleeve**

The construction method was successfully tested during assembly ensuring a fast and safe erection and without damaging any parts of the system.

Figure 3.20 **Installation of the resin injection bolts in oversized holes (12mm clearance)**

The presence of façade columns was investigated by trying two construction sequences, namely ABCD and DCBA. During experiments, no additional hindrance was encountered between the two sequences. Even though the issue of differential deflection between beams exists, it had no significant influence on the assembly of the flooring.

3.6 Finite element model

For a better understanding of the construction process, a finite element model was developed based on previous work by [9, 13, 38]. The finite element software of choice was Abaqus. The model is extended in the following chapter to account for the in-use phase of the building.

The prefabricated concrete deck was modelled as a solid part using eight node brick elements with reduced integration (C3D8R). The edge L-profiles are not included as their influence on the global behaviour of the structure is limited. For the tapered steel beam four-node elements with reduced integration (S4R) are used. To prevent lateral torsional buckling during the construction phase, the structure was braced. The bracing system is modelled with 2-node linear beams (B31) and tied to the tapered beam.

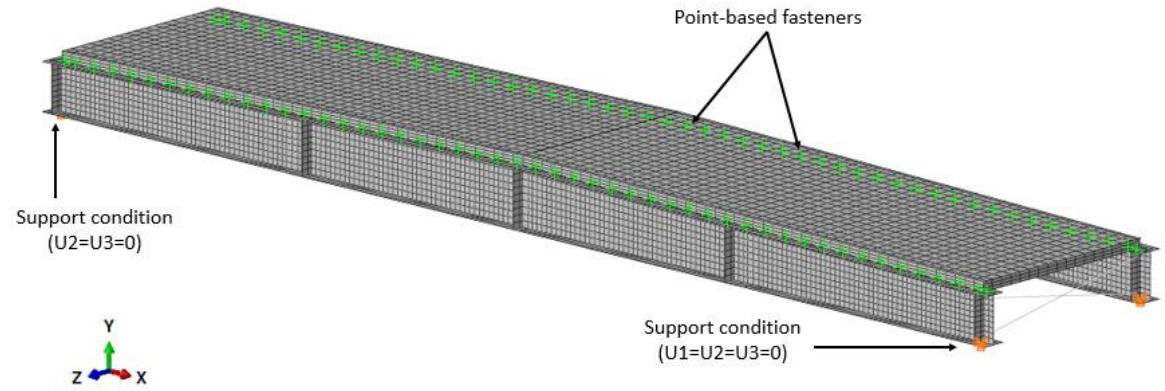

Figure 3.21 **Boundary conditions unsupported span**

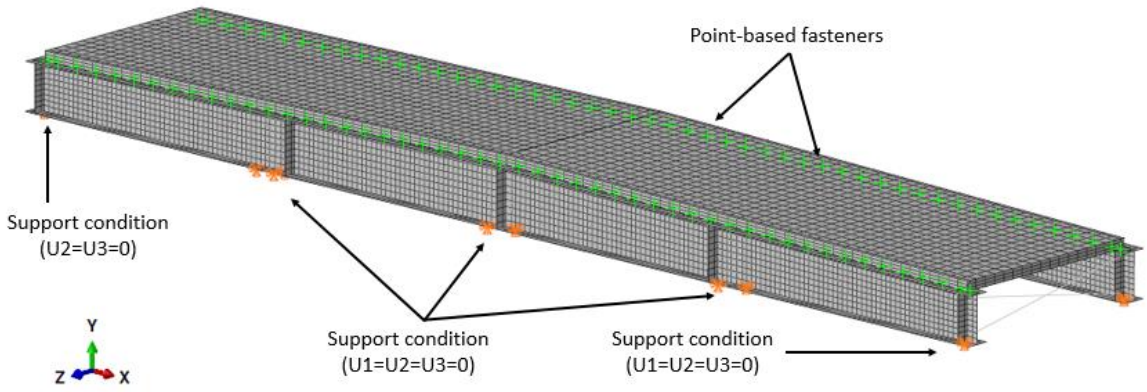

Figure 3.22 **Boundary conditions supported span**

In order to simulate the sequential installation of each deck, a step-by-step analysis is used. Using superposition, the final load-deflection and load-end slip relations are obtained using a reduced size model. The boundary conditions of the model are shown in the figures above. The self-weight of the decks is applied as pressure on the top surface of the slab.

The model starts with both decks active as seen in the figures above. However, one of the decks should not contribute to the structural system thus its material properties have to be modified. Before loading the previously inactive deck, the material properties are changed and the strains have to be removed.

The longitudinal shear connection is modelled using two sets of Point-based fasteners:

- Longitudinal component of each connector
- Vertical component of each connector.

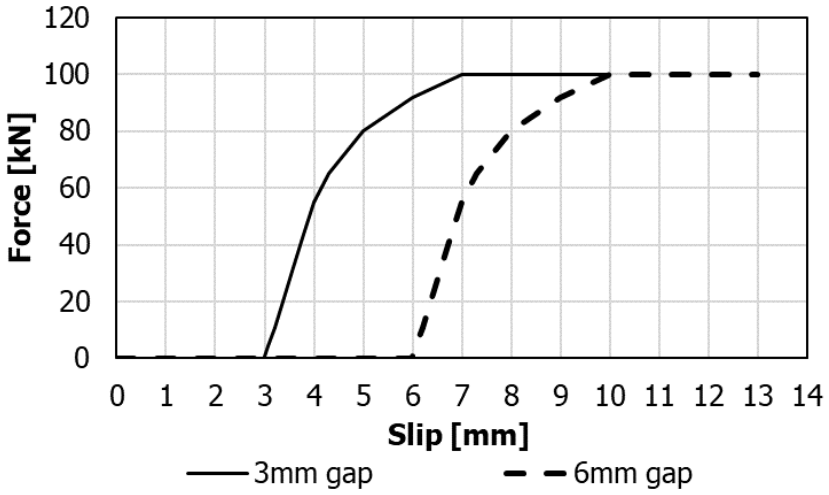

Figure 3.23 **Load-slip curves - bolt coupler system in oversized holes**

The longitudinal component is described by a non-linear curve as seen in Figure 3.23 for 6 and 12 mm clearance.

The material behaviour is modelled linear elastic. As provided by the manufacturer, the steel grade is S355 corresponding to an elastic modulus of 210 GPa. The concrete properties were determined by tests at the TU Delft laboratory on five standardized concrete cubes. The concrete falls in nominal concrete strength class C30/37.

The interaction is handled by General contact characterized by “Hard” Contact in normal direction and a friction coefficient of 0.6. The large friction coefficient can be explained by the uneven interface between the top flange of the steel beam and the L-profile. In order to handle the complex contact interface at mid-span, between the decks, a tie constrain is used. The simplification is reasonable because the bending stiffness of the deck is very small compared to the steel beams.

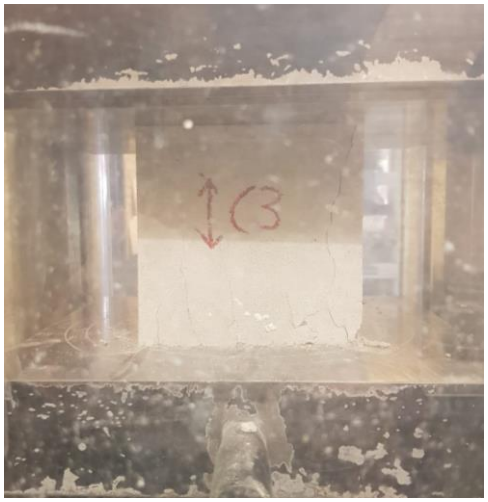

Figure 3.24 **Concrete compression test**

The end slip could not be recorded during experiments because the decks collided at mid-span during installation. Due to the impact, the deck shifts towards the support, making the recording inconsistent. Although experimental measurements could not be taken, insight can be obtained through finite element models.

In the figures below, the load-displacement curves are compared to results obtained from experiments. The model comes in good agreement with the experiments with a maximum deviation of 4.5%. A possible reason for the deviation can be explained by the flexibility of the supporting structure. For beam I this phenomenon is visible throughout both measurements.

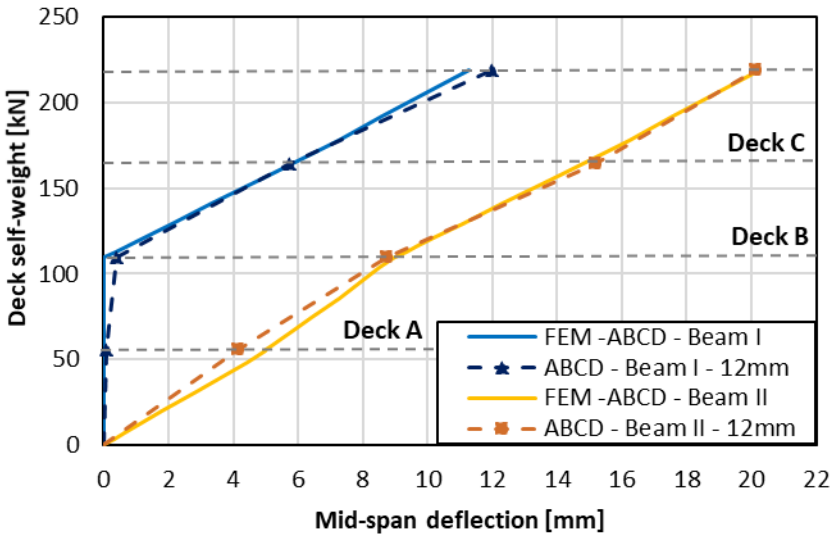

Figure 3.25 **Load-deflection curves - FEM vs experiments, ABCD sequence**

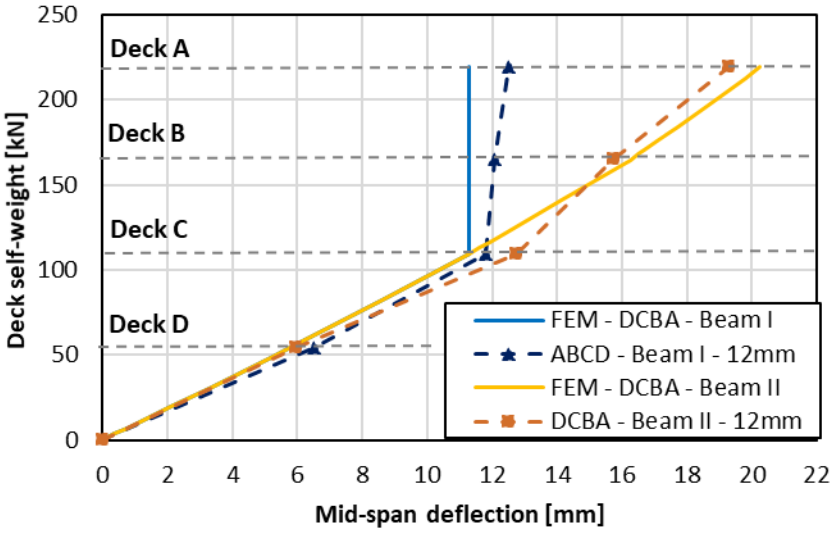

Figure 3.26 **Load-deflection curves - FEM vs experiments, DCBA sequence**

In the figures below the measured deformed shape of beam II is plotted after each deck installation.

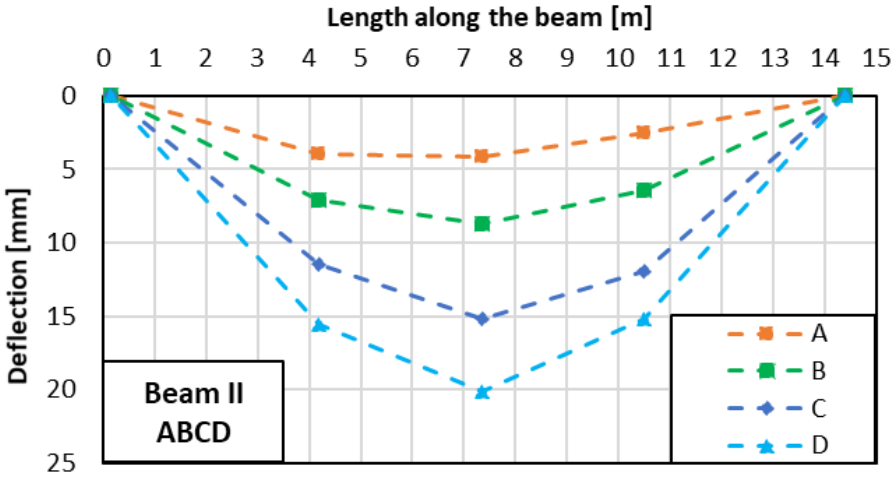

Figure 3.27 **Measured deformed shape of the beam II- sequence ABCD**

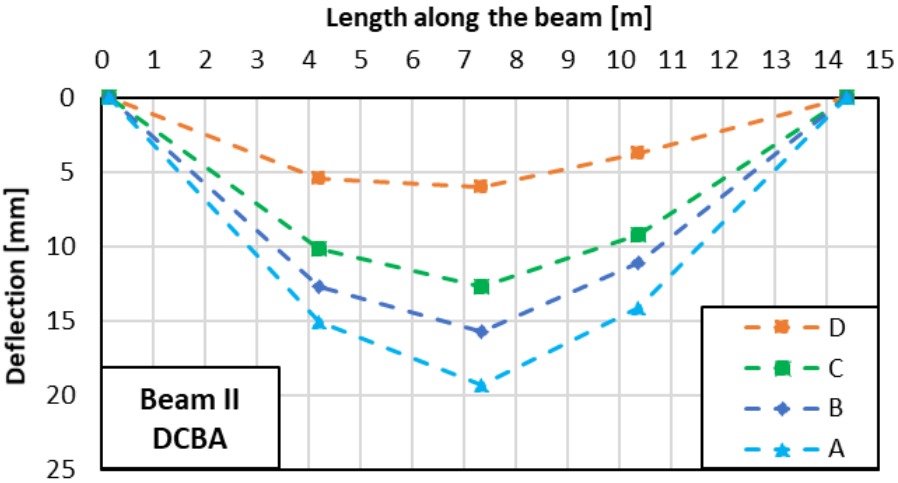

Figure 3.28 **Measured deformed shape of the beam II- sequence DCBA**

The deformed shape obtained by finite element models comes in good agreement with the measurements.

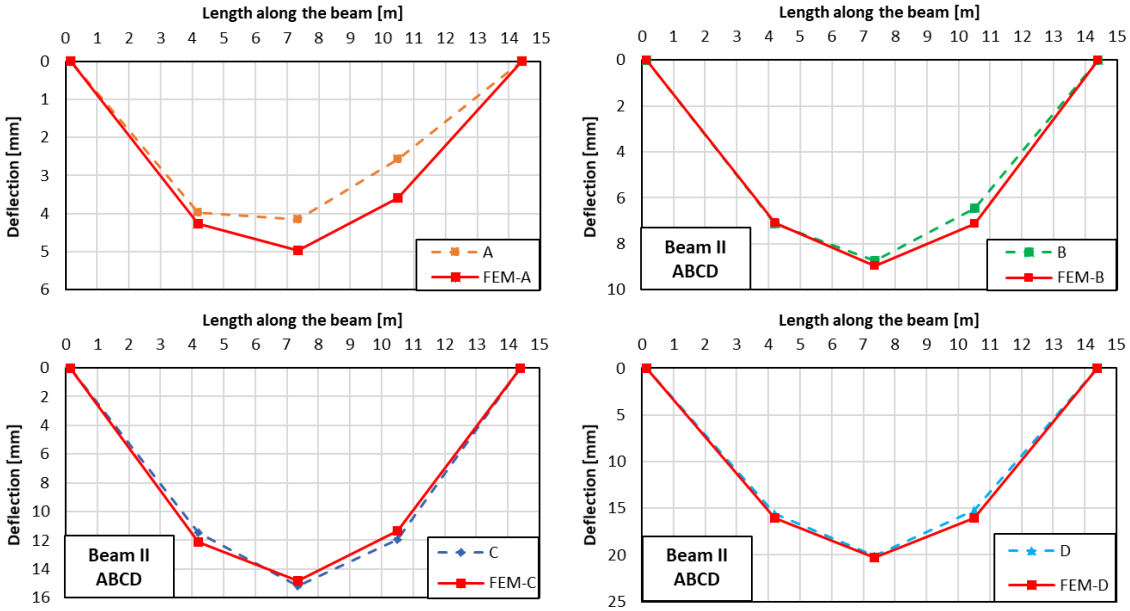

Figure 3.29 **Deformed shape of the beam - FEM vs experiments, ABCD sequence**

3.7 Oversized holes

To ensure the assembly, disassembly and reassembly of bolted connection there is a need for increased tolerances. As defined by [11] the nominal clearance is as follows:

$$Nominal\ hole\ clearnce = Hole\ diameter - bolt\ diameter$$

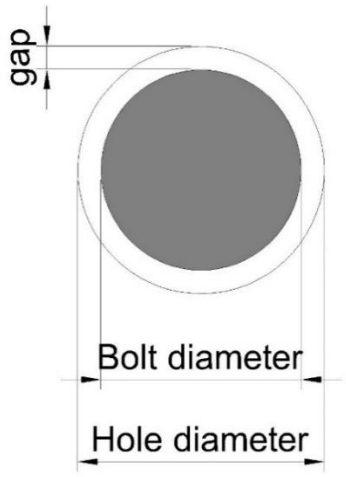

Figure 3.30 **Oversized hole**

Preliminary results from Abaqus simulation indicate that a 6 mm hole clearance (3 mm bolt-to-hole gap) would be sufficient for a typical span of 16 m consisting of large pre-fabricated concrete decks of 8.00 x 2.60 metres [67]. The finite element model results

used for determining the clearance can be found in [9]. The 6mm clearance was adopted when manufacturing the experimental specimen.

Given that the specimen spans only 14.4 meters and one of the beams is supported, the 3mm gap is a conservative estimation for the end slip. Using finite element models the estimation of the end slip reduces to 1.45 mm. Therefore, the 3mm gap already accounts for 1.55 mm in terms of imperfections and tolerances required for a rapid installation.

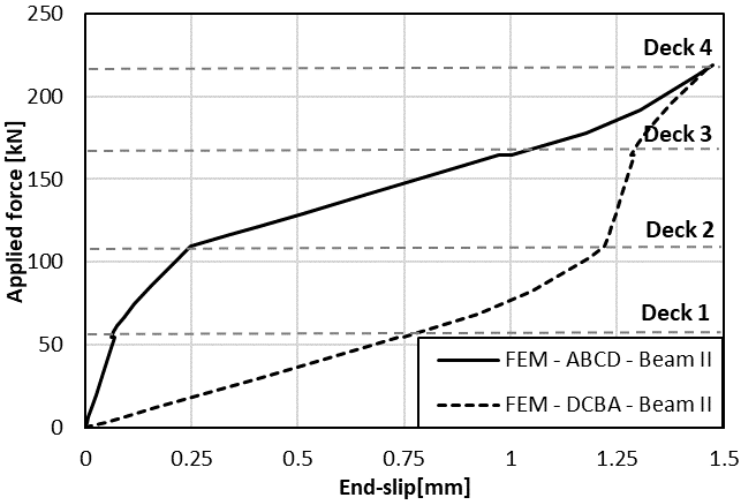

Figure 3.31 **End-slip depending on construction sequence**

Assembly for 6 mm clearance was not possible and based on measurements which are described in the following sections, the hole clearance was doubled. Evidence of the insufficient clearance can be seen in Figure 3.32 where the mid-span deflection for the 6mm and 12 mm clearance is presented. For 6mm clearance the deflection is reduced to some extent by composite action achieved by the long bolts during construction.

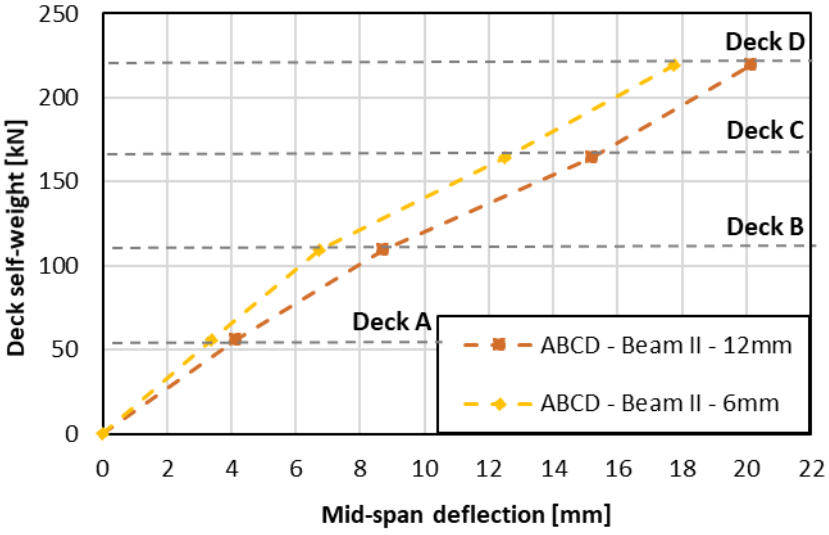

Figure 3.32 **Load-deflection curves -12mm and 6mm clearance**

The increased hole clearance was sufficient to assemble and disassemble the decks. Moreover, increasing the hole clearance will speed up the installation of each deck. The ease of the construction should always be considered when designing the hole clearance.

3.8 Influence of deviations and slip on construction

Following the guideline [11], manufacturing and execution tolerances were quantified and their influence on the assembly and disassembly is investigated. The imperfections were measured using simple measuring tools and database of roughly 1300 measurements was built up to quantify the most influential imperfections. The assessment of imperfections and execution deviations is done considering the misalignment of the holes in longitudinal and transversal directions. Due to the nature of the setup, the influence of the columns can be ignored. In longitudinal direction, the spacing between the holes and the length of the deck influences the hole clearance. In transversal direction, the hole size will have to account for the straightness of the beams and L-profiles and spacing of the beams.

In addition to the measured deviations, the deformation of the system under the self-weight of the decks will influence the assembly and disassembly. The finite element described in the previous section is used to estimate the deformation of the structure during construction.

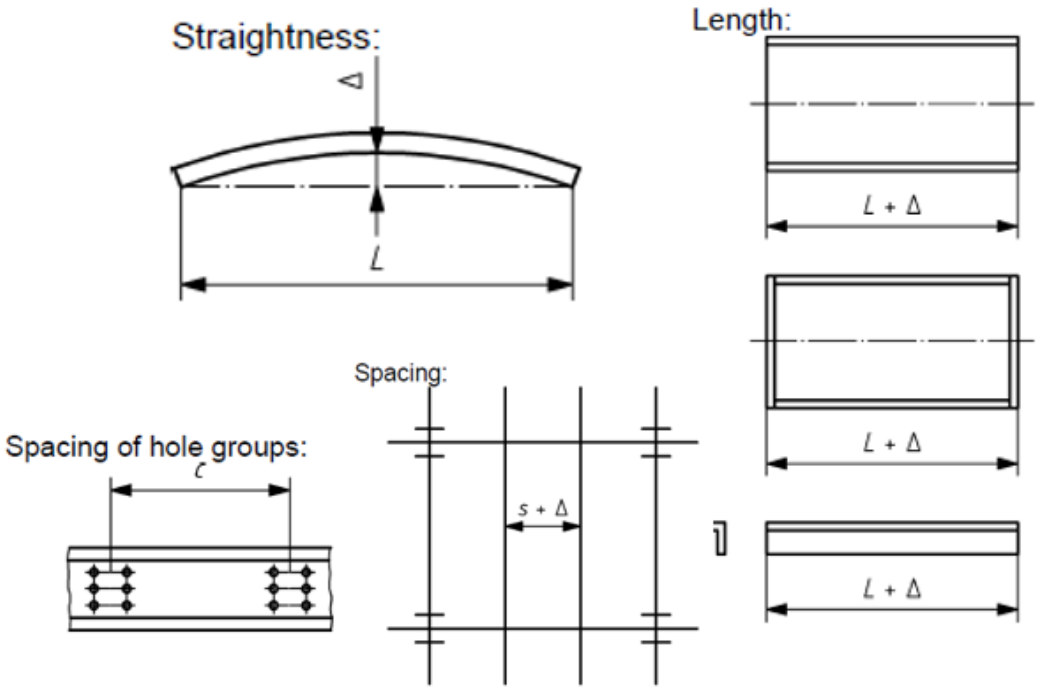

Figure 3.33 **Imperfection categories defined by** [11]

3.8.1. Transversal direction

After placing the tapered beams onto the supporting frame, the cross-braces were installed. Out of straightness and spacing of the beams led to deviations up to 10mm. For this reason, eight equally spaced construction braces were installed in each bay to reduce the deviation. Afterwards the transversal deviations were measured using a wooden template.

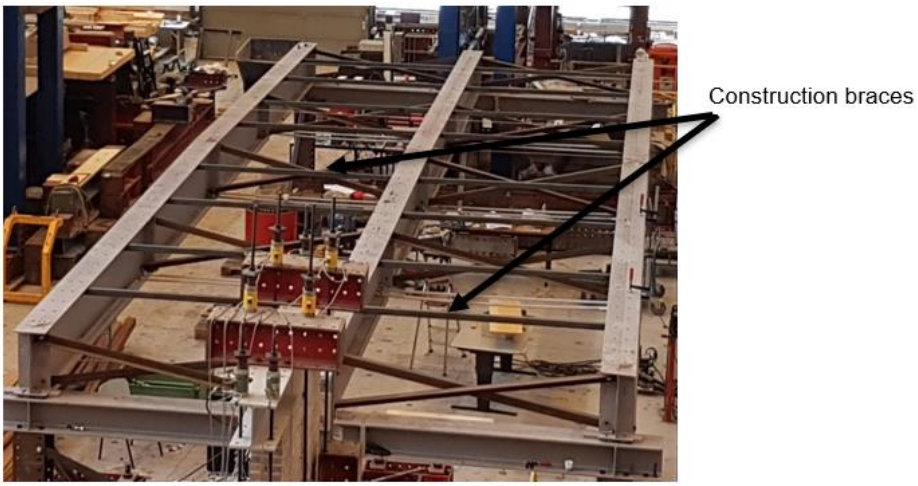

Figure 3.34 **Construction braces position**

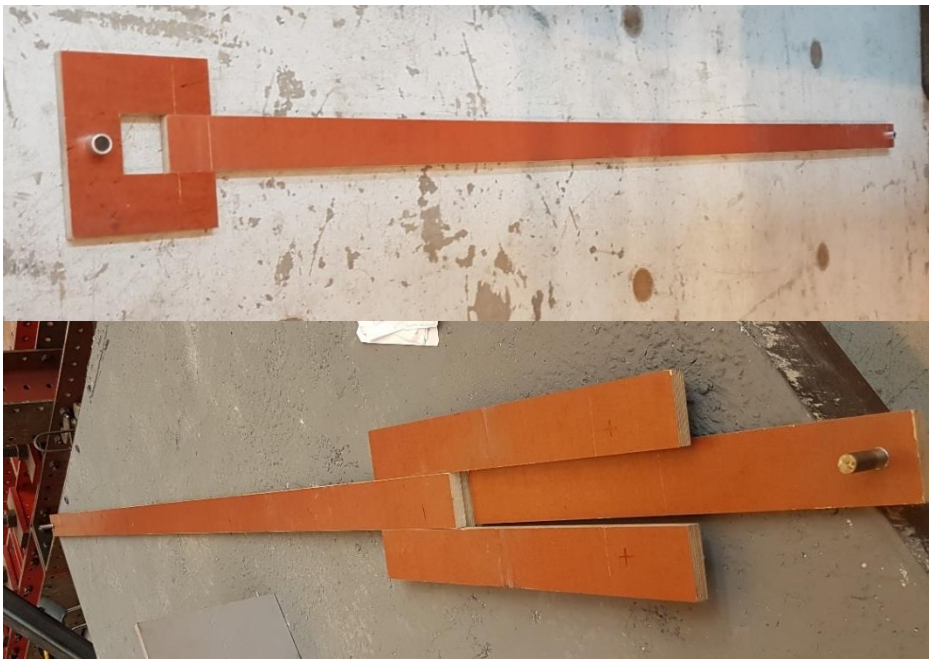

Figure 3.35 **Measuring templates - beam and deck**

The measurement was repeated at all the connector positions for all decks and beams. The obtained values represent the transversal distance (spacing) between the centres of the connectors, not the real deformed shape of the beams or decks.

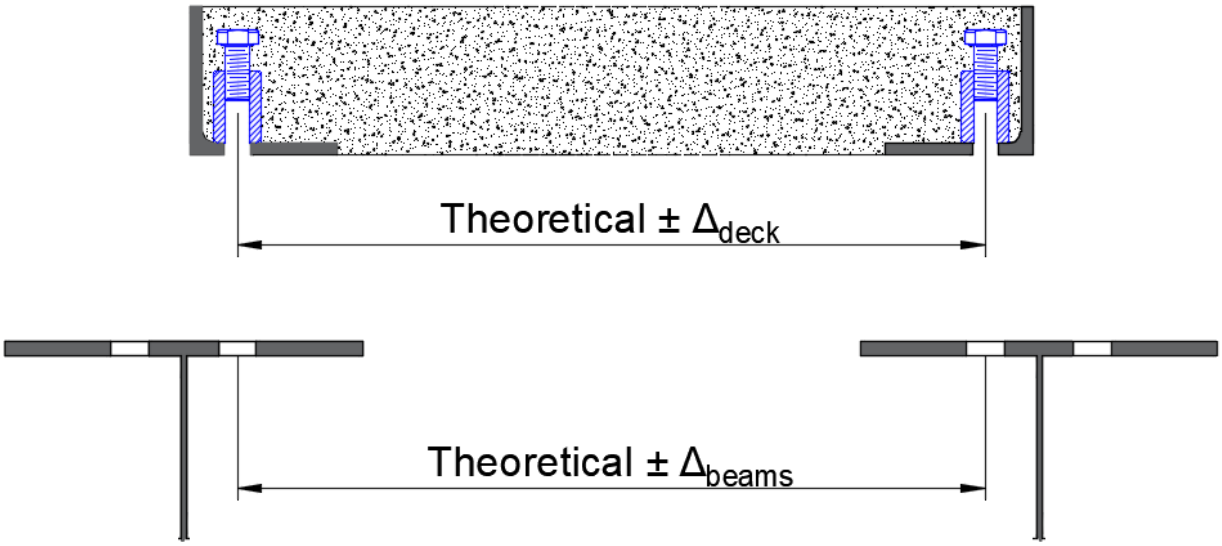

Figure 3.36 **Graphical representation of transversal direction**

In the graph below beam II is assumed perfectly straight while the other two beams incorporate the deviations which were scaled by a factor of 200. As mentioned before, this is not the real deformation but it helps to understand where the deviations are localized.

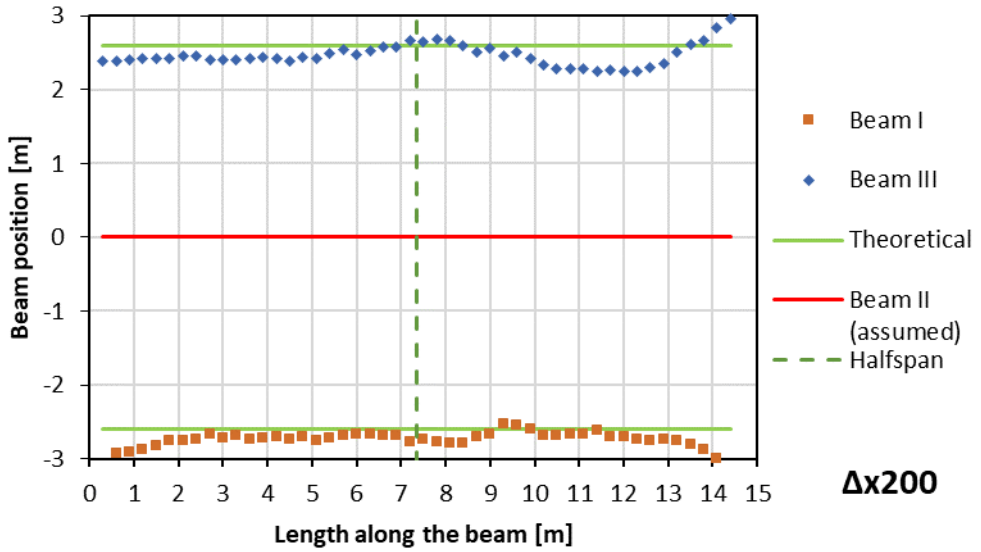

Figure 3.37 **Schematic illustration of beam transversal deviations**

The transversal deviations of the beams are localized close to the supports and reduce along the beam where the construction braces are installed. This confirms the effectiveness of the braces.

In the same manner, one edge of the deck was considered perfectly straight while the other edge accounts for the average deviations of all four decks. The position of the connectors in the deck is set by the L-profile thus, any out-of-straightness will offset the

connector from its intended position. The transversal distance is highest at the middle of the deck and reduces towards the welding points. Given the fact that the L-profiles were braced and welded in laboratory conditions points out the necessity of a change in the manufacturing process in order to avoid these deviations.

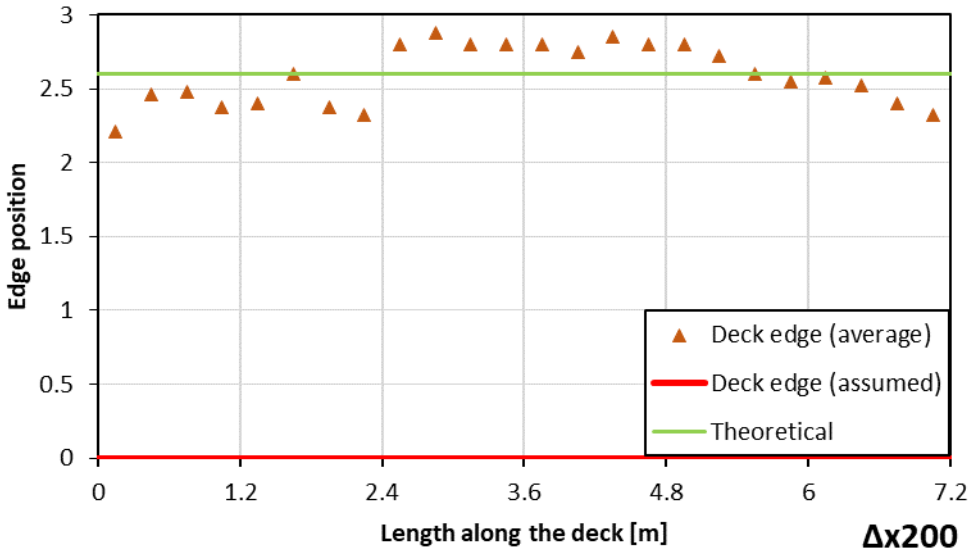

Figure 3.38 **Schematic illustration of deck transversal deviations**

To assess the required hole clearance, the measurements have to be judged in terms of deviations. The scatter of the points is rather limited for the beams with an average of -0.69mm and an absolute maximum of 2.72mm.

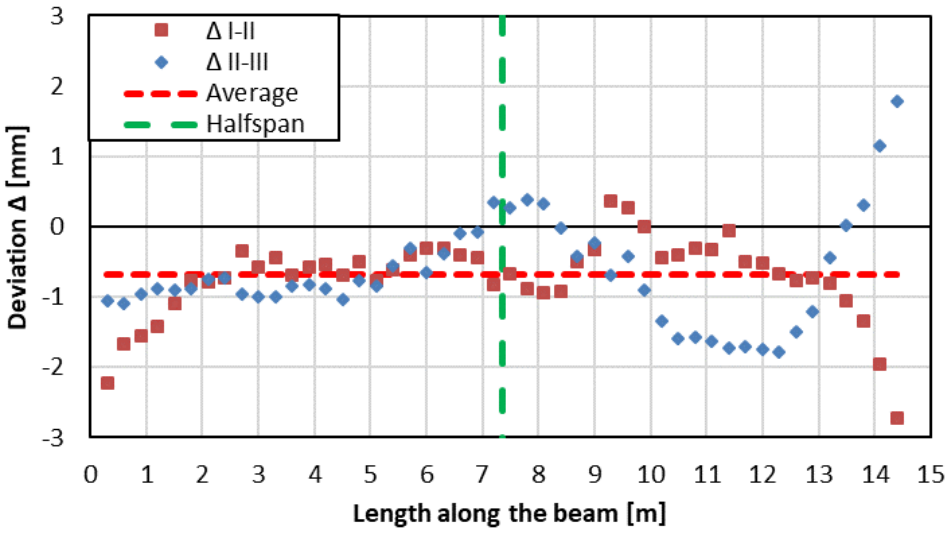

Figure 3.39 **Distribution of beam transversal deviations**

On the other hand, the measurements of the deck are scattered around the -0.05mm average with an absolute maximum of 3.5mm.

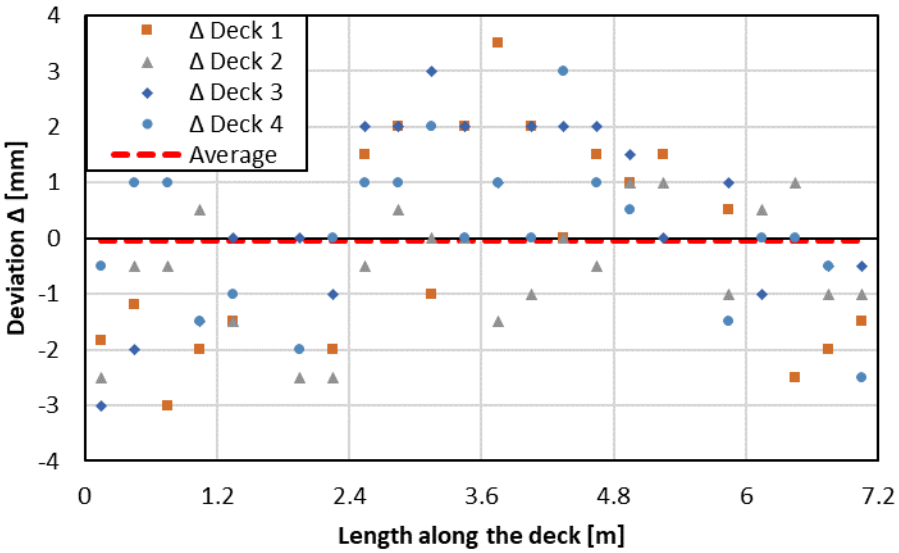

Figure 3.40 **Distribution of deck transversal deviations**

The two measurements must be put together in order to judge what hole clearance is necessary. During construction the steel beams represents the fixed part while the decks are the movable one. Therefore, the decks whether they are wider or narrower, need sufficient beam hole clearance for assembly. In Figure 3.41 the two cases are presented for a hole clearance of 6mm. The 3mm hole gap on each side of the deck will contribute to accommodate its transversal deviations.

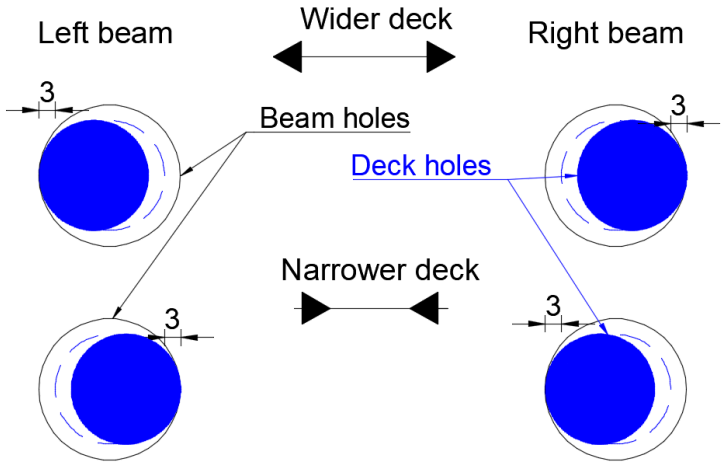

Figure 3.41 **Schematic illustration of transversal clearance**

Combining Figure 3.36 and Figure 3.41 the clearance requirement is determined:

$$\text{Theoretical} + \Delta_{\text{deck}} = \text{Theoretical} + \Delta_{\text{beam}} \pm \text{gap}_{\text{left}} \pm \text{gap}_{\text{right}}$$

The requirement allowing for assembly is rewritten as follows:

$$\Delta_{\text{deck}} \leq \Delta_{\text{beam}} \pm \text{clearance}$$

For simplicity, the average deviation of the beam spacing is offset with the hole clearance. In Figure 3.42, the average was offset for 6 and 12mm clearance. Since all deck deviations lie in between the green lines the equation above is satisfied. Consequently, no constrain on the hole clearance is imposed by the transversal misalignment of the holes.

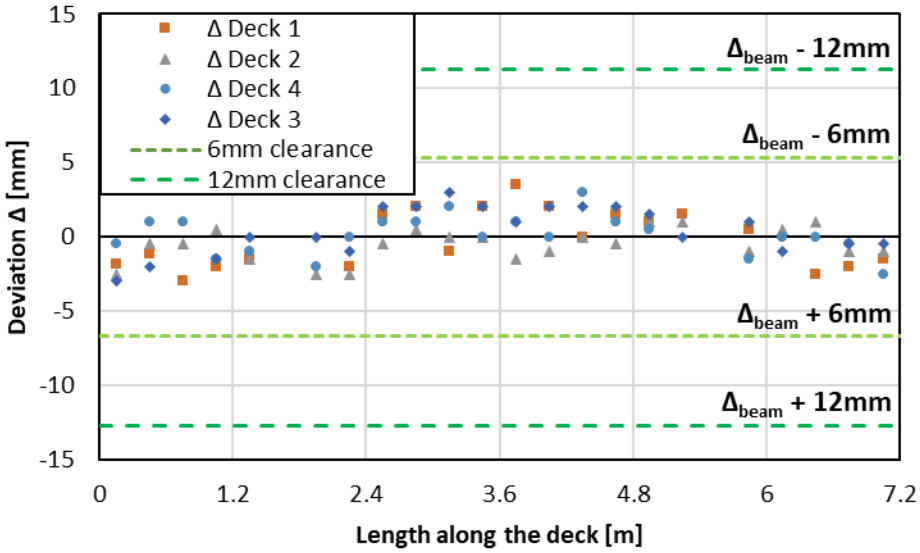

Figure 3.42 **Transversal deviations check**

In the graph below, the maximum 10mm deviation measured before the spacing was corrected by the installation of the construction braces is considered. Because no exact measurements were carried before the installation of the braces the deviation distribution is unknown. For this reason, the positive and negative values of the deviation are accounted for. From the graph it can be seen that the deviations of the deck cannot be accommodated by the hole clearance of 12mm. This confirms the need of the construction braces.

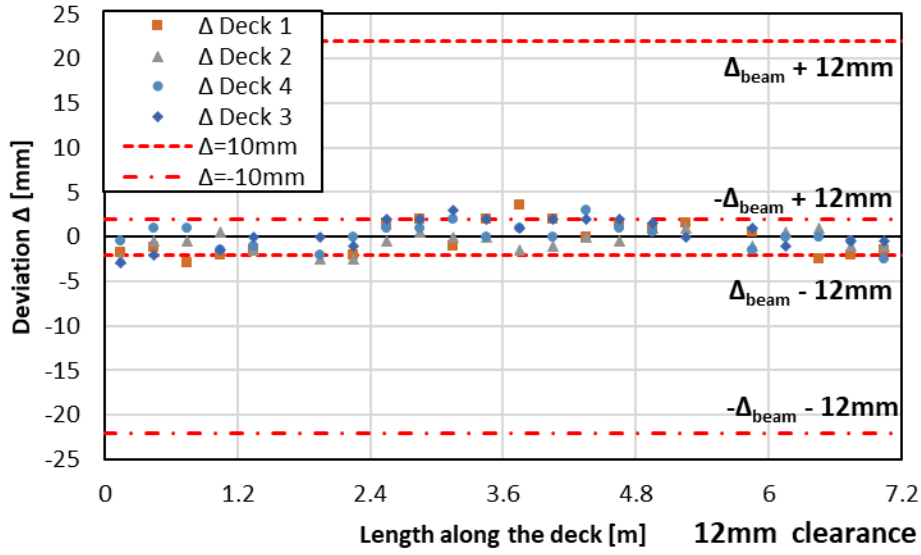

Figure 3.43 **Transversal deviations check - before installation of the construction braces**

The width of the decks was designed considering possible imperfections (see Figure 3.3). Figure 3.44 shows the decks being in contact as a consequence of large out of straightness of the L profiles. However, the combination of the reduced deck width with the 12mm clearance holes was sufficient for assembly.

Figure 3.44 **Picture from mid-span to supports and from supports to mid-span**

3.8.2. Longitudinal direction

Apart from the transversal direction, the alignment in longitudinal direction of the connectors with the beam holes is critical. The manufacturing deviations will add up to the interface slip generated by the installation of the decks. As mentioned previously, at mid-span, the decks must transfer the normal force in order to achieve composite action. To ensure this transfer, the decks were designed to be in contact without any additional measures (see Figure 3.3), thus no account was made for possible manufacturing deviations of the decks.

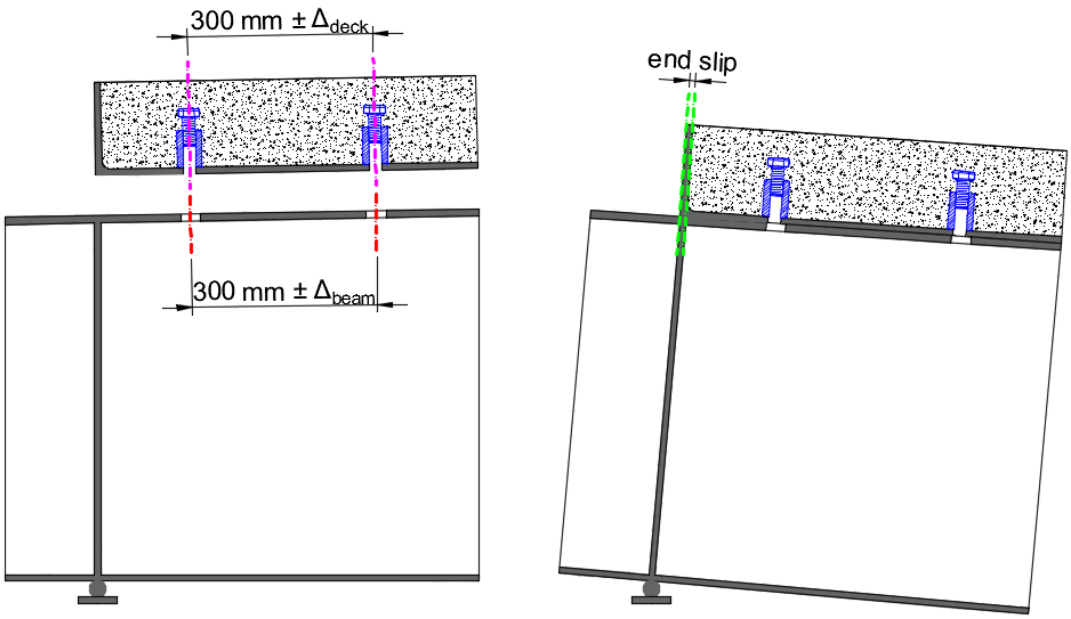

Figure 3.45 **Contributions to hole clearance - imperfections and end slip**

In longitudinal direction, the hole spacing is 300mm for both the deck and the steel beam. Any deviations of these two spacings will require an increased hole clearance. In the graphs below, the distribution of the deviations is presented.

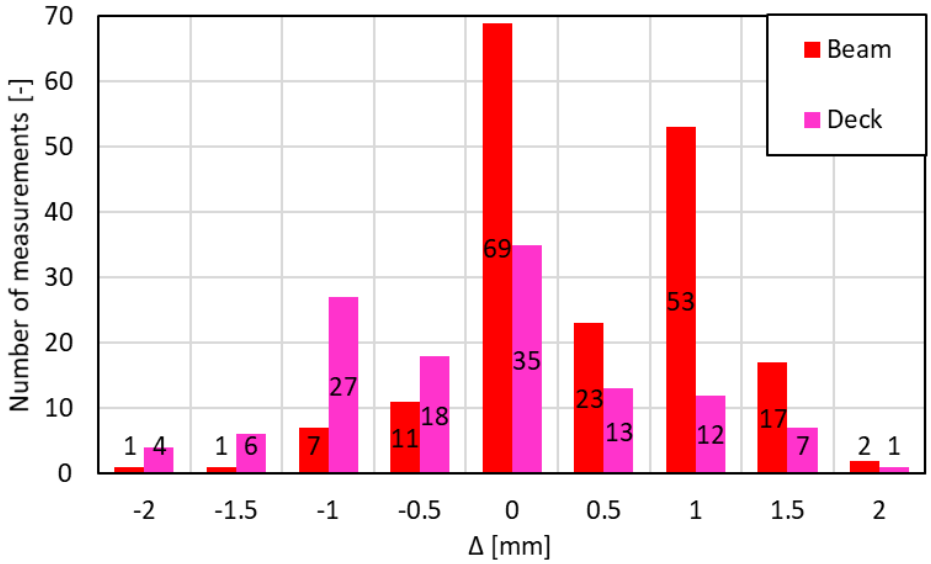

Figure 3.46 **Distribution of spacing deviations**

The measured deviations are limited to the value of 2mm found in [11] for functional manufacturing tolerances class 2. When designing the hole clearance, the most unfavourable situations have to be accounted for. This is the case when the deviations of the deck and beam are distributed in opposite direction from one another as seen in Figure 3.47. To account for situation the absolute value of these two deviations has to be summed up to the interface slip.

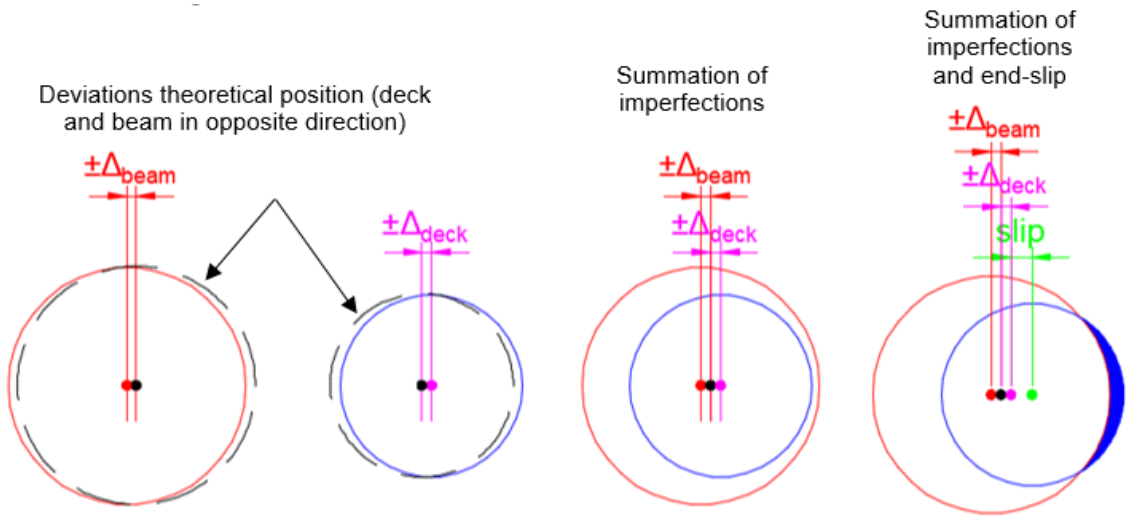

Figure 3.47 **Imperfections and end-slip contributions**

The hole clearance should be design as follows:

$$\text{clearance} \geq 2 \times (\Delta_{\text{deck}} + \Delta_{\text{beam}} + \text{end slip})$$

Summing up the measured deviations of 2mm and the end slip of 1.5mm obtained from finite element (see Figure 3.31), leads to a gap requirement of 5.5mm. This justifies the decision of increasing the hole size to 32mm.

Because no tolerance was considered at mid-span between the two decks (see Figure 3.3) any manufacturing deviations of the decks in terms of their length will influence the installation of the flooring system. Measurements pointed out that the decks were longer on average by 4.75 mm with a recorded maximum of 8mm.

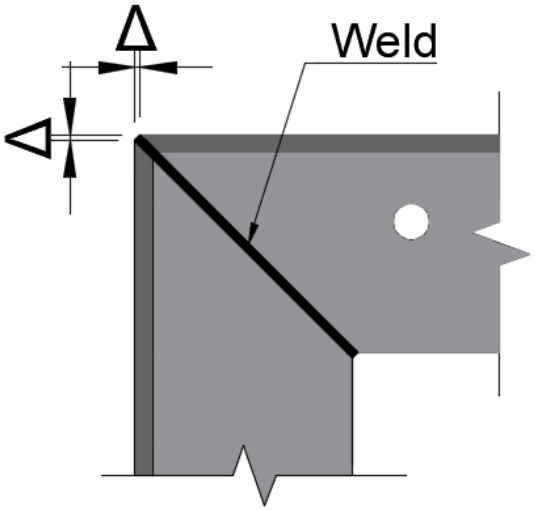

Figure 3.48 **Length imperfection due to welding**

The deviation lies behind the welding quality of the corners. The L-profiles were cut at with an angle of 45^0 at the ends. During welding, any misalignment and length deviations

of the L-profiles led to an increased length of the deck. This manufacturing problem contributes also to an increase in the transversal spacing at the ends of the deck (see Figure 3.38 and Figure 3.44). During experiments, measures to reduce the excess material were taken.

At mid-span a gap of at least 16mm should be included in the design to accommodate the large deviations found lengthwise. The contact between the decks can be achieved afterwards by forcing steel plates or grouting the gap. This will reduce the necessary hole size and the required control on the manufacturing of the decks.

3.9 Feasibility of resin injection

Injection was never used for full-scale composite beams and its reliability of filling the clearance was certified only for small scale push-out specimens. During the experimental programme, a large number of bolts were vertically injected to verify the quality of the injection and to provide practical advice based on experimental experience.

One of the most commonly used two component epoxy resins in injected bolted connections is Araldite/RenGel SW 404 in combination with hardening agent Ren HY 2404. [68]. The hardened resin has the ability to transfer the forces in order to achieve composite action. Araldite is a thermosetting polymer; its properties are achieved after hardening but cannot come back to its initial state by adding heat. The properties of the resin will change due to ageing and aggressive environments. Another drawback of the epoxy resin is that creep influences the behaviour of the connection. Extensive research has been carried by [69] and [70] to investigate the behaviour of epoxy resins based on the one used as part of this thesis. The solution of reinforced resin was proposed by [68] and further investigated by [69] and [71].

During the experimental work, apart from the previously mentioned hardener, another type with an increased pot time was used and compared in terms of workability and feasibility for common working conditions. The mix ratios and properties of the two hardeners in combination with the resin are according to the manufacturer [72] as follows:

Mix ratio	Parts by weight	
RenGel© SW 404	100	100
Ren© HY 2404	10	-
Ren© HY 5159	-	8

Table 3.1 **Mix ratio** [72]

Resin/Hardener mix:	Volume	Unit	SW 404 HY 2404	SW 404 HY 5159
Appearance			Blue	Blue
Pot life at 25ºC	250 ml	min	15	50
Demoulding time		h	12	12

After cure: with HY 2404: 14 hours at 60°C
with HY 5159: 14 hours gradually to 80°C

Density	ISO 1183	g/cm^3	1.8	1.8
Hardness	ISO 868	Shore D	85-90	85-90
Deflection temperature	ISO 75	°C	80	100
Abrasion	Taber	mm^3/100U	4-6	4-6

Table 3.2 **Resin properties** [72]

Because hardening is an exothermic reaction, the exterior temperature at the moment of injection influences the pot time of the resin. Experience acquired during injection at an exterior temperature higher than 30^{0}C showed that HY2404 will lead to a rapid increase in viscosity. The high viscosity increases the injection time which will require very small mix batches to be used efficiently.

The advantage of the hardener with an increased pot time is that it gives the worker the flexibility to finish a larger batch of resin therefore, reducing the time required for preparing multiple small batches and replacing the caulk tube. Another benefit of using the hardening agent HY5159 is the initial reduced viscosity of the resin mix, which makes the injection faster without leaking back from the hole through the injection channel. Using HY5159 the resin mix can be injected in batches of 500g RenGel SW 404 which corresponds to roughly 20 holes. The time required to inject one hole reduced by a factor of 5 to 30 seconds.

Figure 3.49 **Epoxy resin mix (SW404** [73] **+ HY2404** [74] **or HY5159** [75]**) and release agent ACMOS82-2405** [76]

To increase the efficiency of the injection process two persons working in parallel are required. One of the worker prepares batches of 500g of RenGel SW 404 which are injected by the second worker in roughly 10 minutes. The worker injecting the resin will require to carry out the operation while standing on a lifted platform or ladder.

During the experimental programme, an electrical and a manual caulking gun were compared. Using the manual gun proved to be more advantageous in terms of cleanliness, time and costs. Because the injection is done vertically and a high pressure is applied by the electrical gun to the tube containing the mix generates large quantities of leaked mix. The unhardened resin stains the steel beams and enters into the components of the device. Eventually without periodical and time-consuming cleaning of the caulking gun, the motor will get stuck by the hardened resin. Consequently, using cheap manual caulking guns is far more advantageous than the expensive electrical tool.

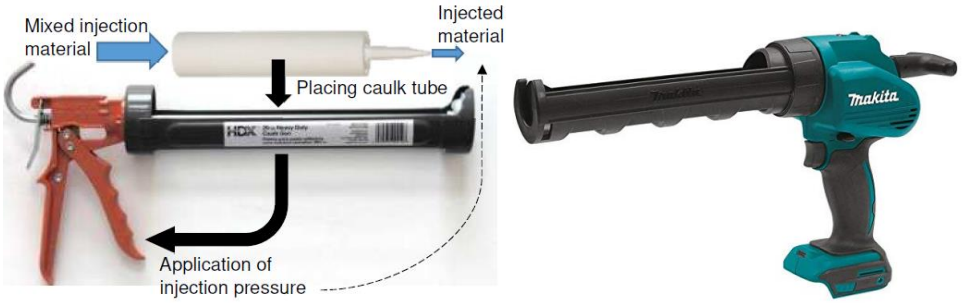

Figure 3.50 **Manual caulking gun [68] and electrical caulking gun [77]**

To ensure the resin will completely fill the void between the hole wall and the bolt shank there is a need of an air channel. The purpose of the channel is to provide an escape path for the air (see Figure 3.52). As soon as the resin is seen leaking from the air channel, the pressure on the caulking gun can be removed and the hole can be considered injected.

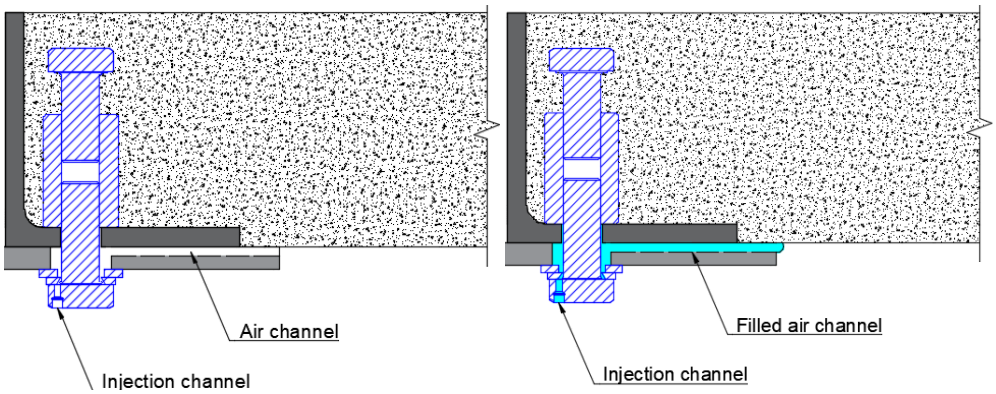

Figure 3.51 **Cross-section of the connector before and after injection**

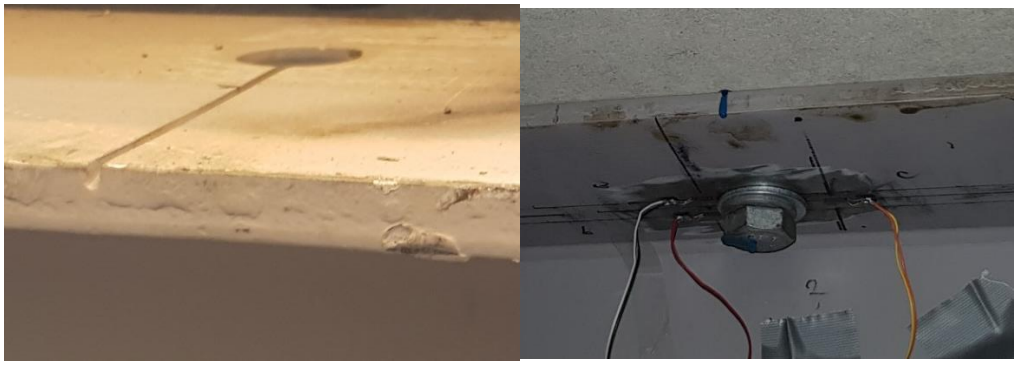

Figure 3.52 **Air channel and leaking resin from the air channel**

During the experimental programme roughly 150 bolts were injected and inspected (see Figure 3.53). The injection completely filled the clearance for all holes with minor defects such as air inclusions.

Figure 3.53 **Injected holes**

To include the proposed flooring system in the circular economy philosophy, all the parts should be fit for reuse in a second life cycle. However, due to adhesion, without precautions the bolts and the resin plug cannot be removed after hardening. The formation of such an adhesive bond can be prevented by the use of a release agent, amongst which are wax-, silicon-, PFTE- and PVA-based products [68]. ACMOS 82-2405 was used to spray all the surfaces which interfere with the resin. The process is fast, and one spray

tube can be used for approximately 50 bolts or holes. After four-point bending tests, the bolts were easily removed. The plug from the bolt holes and injection channel was removed (see Figure 3.54).

Figure 3.54 **Removing resin plug and cleaned injection bolt**

3.9.1. Influence of imperfections on resin injection

The imperfections of the top flange influence the required amount of epoxy resin. Based on [11] two types of measurements were carried before placing the decks.

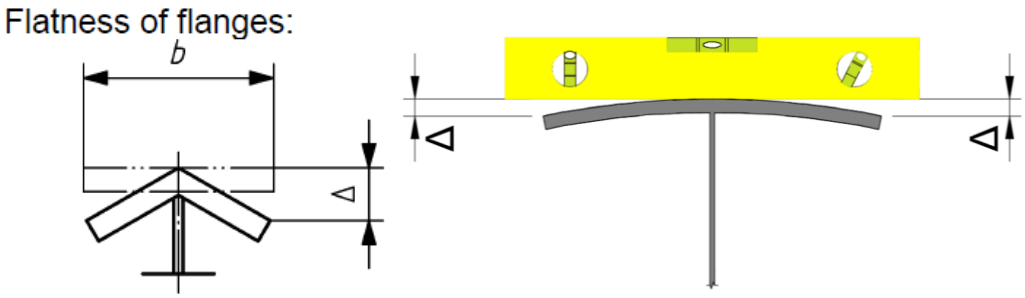

Figure 3.55 **Flatness of flanges according to [11] and measuring procedure**

The flatness of the flanges was measured as seen in Figure 3.55. The summary of the measurement can be found in Table 3.3. A higher deviation was recorded on the welded side as consequence of welding the flange to the web only on one side.

Value	Δ on welded side	Δ on unwelded side
Maximum	5mm	2mm
Average	3mm	1.3mm

Table 3.3 **Results measurements - Flatness of flanges**

The second tolerance as defined by [11] is the flange distortion of the I section. The imperfection was investigated using a tensioned wire placed on the top flange above the holes as seen in Figure 3.56. No flange distortion was observed in this case. Still, this type of imperfection should not be excluded in case of discontinuous welding.

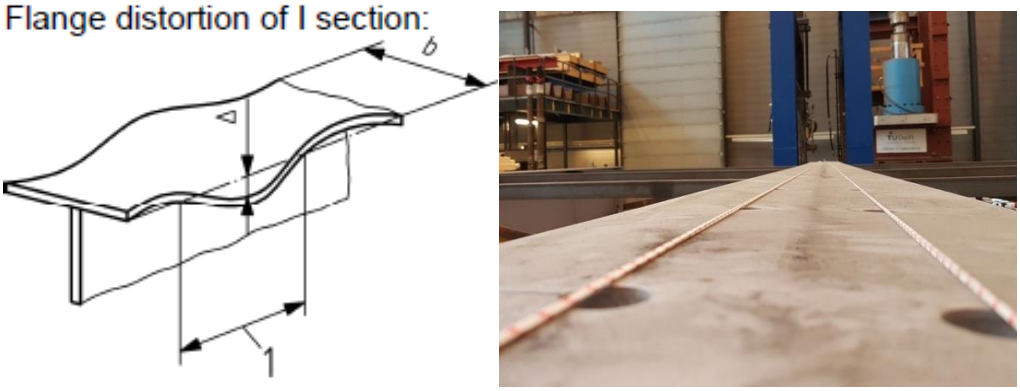

Figure 3.56 **Flange distortion of I section according to [11] and measuring procedure**

After placing the decks on top of the steel beams, gaps up to 8mm were observed. However, by hand tightening the bolts, the gap was closed except close to the stiffeners which act as supports for the top flange. Closing the gap was possible due to the slenderness of the top flange and web which can locally deform. Therefore, account should be taken in case of stocky steel sections.

Figure 3.57 **Gap between deck and top flange before and after tightening the bolt**

After the testing program ended, the decks were removed in order to investigate the influence of the above-mentioned imperfections. Even though the gap between the deck

and flange was closed, large volumes of epoxy resin leaked around the hole. As expected the leakage was more pronounced at the holes close to the stiffeners. The excess resin had a thickness of up to 3 mm.

Apart from the imperfections of the top flange the manufacturing of the decks contributed to this leakage. Due to the flexibility of the formwork, the concrete creates an overgrowth at the edge of the L-profile (see Figure 3.58). The overgrowth acts as a support on the top flange opening a leakage point.

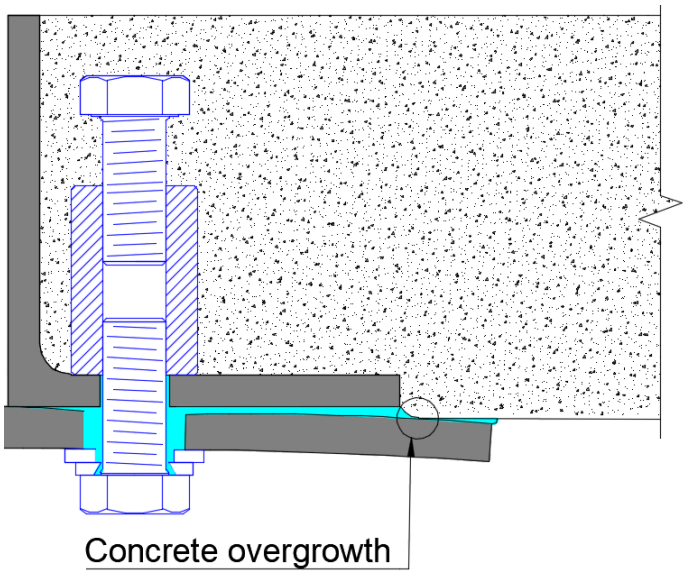

Figure 3.58 **Leakage around the bolt due to manufacturing imperfections of the deck**

Figure 3.59 **Leaked resin on top flange and deck**

3.10 Conclusions

1. Experimental research confirms that the construction of demountable composite flooring systems consisting of large prefabricated decks is feasible if construction tolerances are designed appropriately.
2. The construction tolerances are achieved by using oversized holes. The hole clearance design is influenced by:
    a. Deformability of the system during construction in the form of end slip,
    b. Imperfections of the beam and deck in longitudinal and transversal direction,
    c. Speed of execution and demounting.
3. The most influential imperfection is the spacing of the couplers in the deck and the beam holes in longitudinal direction. According to [11] and confirmed by measurements, the spacing deviations can be up to 2mm, so the hole clearance should be increased by at least 8mm to account for these imperfections.
4. Deviations in transversal direction do not constrain the hole clearance if the beams are braced to correct the beam spacing before the installation of the decks.
5. L-profile are installed around the deck in order to protect the concrete from damage during assembly and disassembly. However, long angles profiles are prone to large imperfections such as out-of-straightness which must be considered when designing the hole clearance.
6. The frame around the decks is consists of four profiles welded at the corners. The welding quality of the corners will affect the length of the deck. For this reason, at mid-span a gap should be designed to account for lengthwise deviations. After construction, the gap can be closed using steel plates or grout in order to transfer the compression force.
7. Embedded bolt connectors are prone to damage during transportation and construction. Experimental experience shows that any misalignment during deck installation will lead to punching of the connector. Using the bolt coupler connector and an appropriate construction method, the decks can be installed easily, safely and without any damage to any of the flooring components.
8. The construction sequence does not influence the feasibility of construction if sufficient clearance is adopted.
9. Vertical resin injection of oversized holes investigated on roughly 150 bolts confirms that it be can be reliably and labour efficiently used in case of demountable buildings.
10. An increased hole clearance will greatly ease and speed up the construction without influencing the injection of the bolt to wall gap.
11. It was observed that a hardening agent with a longer pot time (HY5159) reduce the injection time by a factor of five compared to a faster hardening agent (HY2404) even in case of high ambient temperatures. The injection process takes approximately 30 seconds per bolt.

12. The required amount of resin is influenced by the imperfection of the top flange and deck and by the position of the hole relative to the vertical stiffeners.
13. Reusability of all components of the flooring will not be obstructed by the adhesion of the resin if preventive measures are taken.
14. Manual caulking guns proved to be more advantageous compared to electrical one in terms of cleanliness and economy.

4 Mechanical behaviour of demountable composite floorings

Headed studs have been used extensively as means of shear connectors in composite beams. However, they obstruct the non-destructive demountability of the components. The bolt coupler connector (see Figure 4.1) will ensure the transfer of longitudinal shear, while at the same time enables the possibility of demounting and reusing the concrete slabs and the steel beams.

So far, experimental research on demountable composite beams was performed by [57, 58] [78, 79] with different types of connectors. The experimental programme which took place at TU Delft as part of RFCS-research project REDUCE (Reuse and Demountability using Steel Structures and the Circular Economy) aimed to investigate the behaviour of composite beams using a bolt coupler system as means of shear connector.

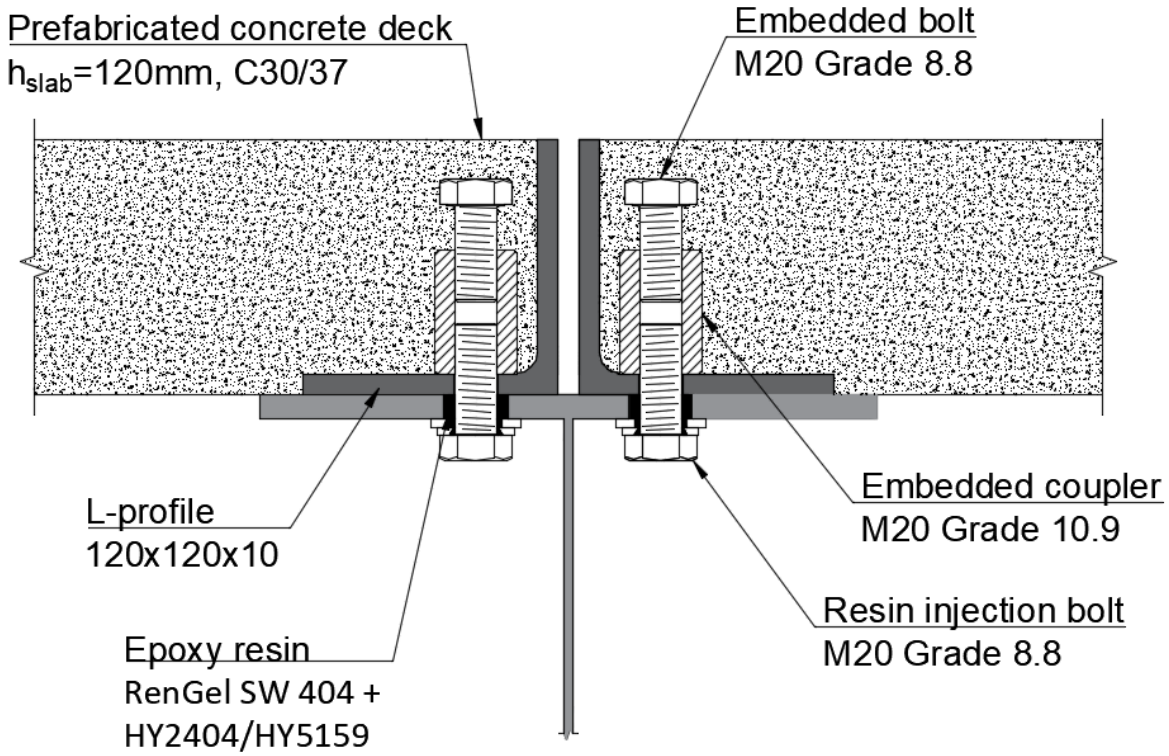

Figure 4.1 **Cross-section of the demountable shear connector**

4.1 Problem definition

Demountable floorings require increased tolerances to ensure the assembly and disassembly of the system. This translates into an increased hole size which will affect the composite behaviour of the beam. After installation, due the oversized holes, the bolt shank will not be in direct contact with the hole wall. In order to achieve the composite behaviour, the connectors need to slip until they reach contact. Resin injection represents

a solution to fill the gap and achieve composite action without any initial slip of the bolt in the hole.

To include a structure in the circular economy philosophy, its components must be recovered and reused. Consequently, the structure should not suffer any damage during their first life cycle. For this reason, the main focus of this master thesis is to investigate the elastic behaviour of a demountable composite beam under four-point bending. The applicability of push-out tests results is studied using finite element models which aim to provide insight in the load-deflection behaviour of the composite beam.

Due to transportation requirements the length of the prefabricated concrete decks is limited. This creates a discontinuity of the slab influencing the shear and axial force transfer. Experimental research coupled with finite element analysis aims to investigate how is the composite beam behaviour affected by this discontinuity.

The high price per unit of installed connector requires an efficient design to satisfy serviceability requirements with limited costs. Following the slip distribution along the length of the beam, the connector arrangement can be optimized through a non-uniform distribution. Concentrating the shear connectors towards the support, where they are most effective, will transfer the longitudinal shear force more efficiently, but raises the problem of vertical separation. An investigation carried by [21] using a validated analytical model shows that in the elastic range the vertical uplift for uniformly distributed loading is limited. Through a finite element model, the vertical separation phenomenon will be investigated under different loading conditions in the elastic range. The study aims to determine the most efficient connector arrangement in terms of longitudinal shear transfer and vertical separation.

Research questions:

- **What is the load-deflection behaviour of resin injected demountable composite beams?**
- **Which is the optimal connector arrangement to achieve an economical design?**

Finally, the setup was tested to failure using a non-uniform connector arrangement. The results of the experimental programme and of the finite element model can also be found in [61].

4.2 Four-point bending specimen

The mechanical behaviour of composite beam was studied using a reduced size specimen compared to Figure 3.4. The new setup consists of two tapered beams and their corresponding decks. The dimensions of beams and decks can be found in Figure 3.2, Figure 4.1 and Figure 4.3.

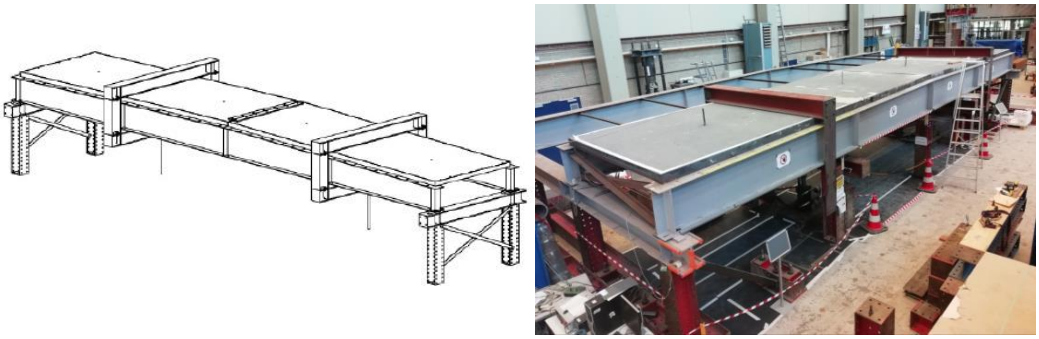

Figure 4.2 **Beam setup** [61, 66]

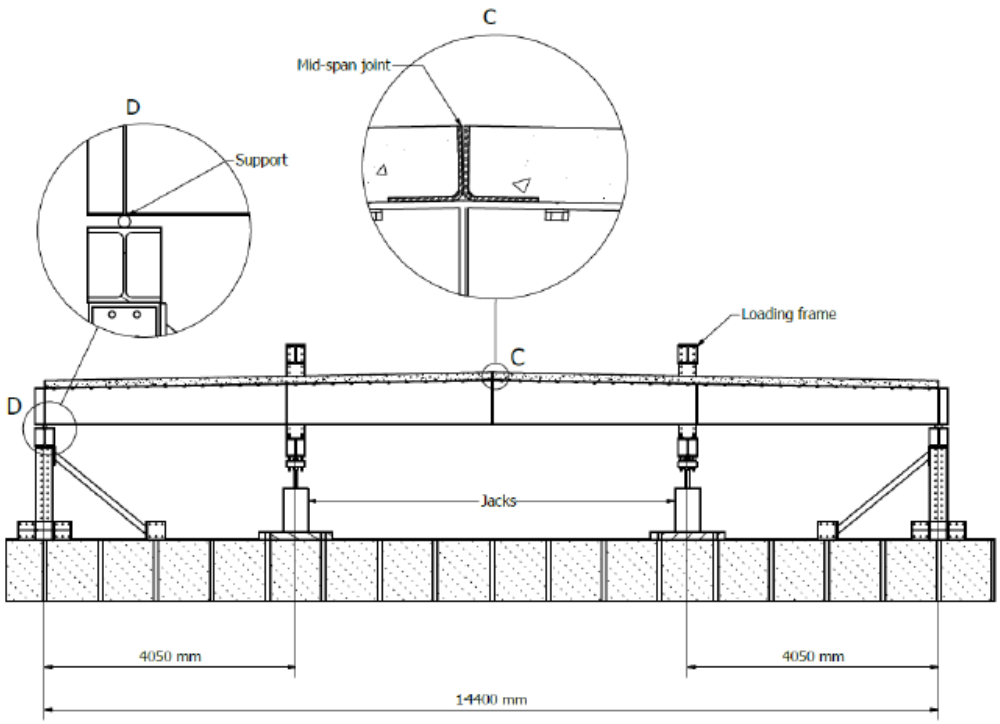

Figure 4.3 **Detail setup drawing** [61]

The point loads were applied at 4.05 meters from the supports. To ensure an even distribution of the load between the two beams the uneven surface of the deck was flattened. To reduce any influence of catenary forces roller supports were installed. At mid-span, the gap between the decks was closed by forcing steel plates in between and finally grouted to ensure a continuous transfer of the compression force. The setup was braced to avoid lateral torsional buckling and horizontal bracing was used to increase the

torsional inertia of the setup which ensures that the beams deform only under uniaxial bending.

The structure was extensively monitored during loading to avoid any plastic deformation. A number of six Sakae S13FLP50A potentiometers were installed to record the deflection of the beam. At the four corners of the decks, ETI SYSTEMS LCP8 potentiometers were installed to measure the end-slip. The stresses were recorded using 98 TML FLA-6-11 strain gauges. On each beam the stresses were measured using three strain gauges along the depth of the steel section. Along the length of the beam in each half-span the strain gauges were placed at mid-span and at the position of maximum predicted longitudinal stress. On top of these strain gauges the stress situation around the hole was measured to ensure no local yielding takes place. Schematic drawings of the installed measuring equipment can be seen in the figures below and 9.

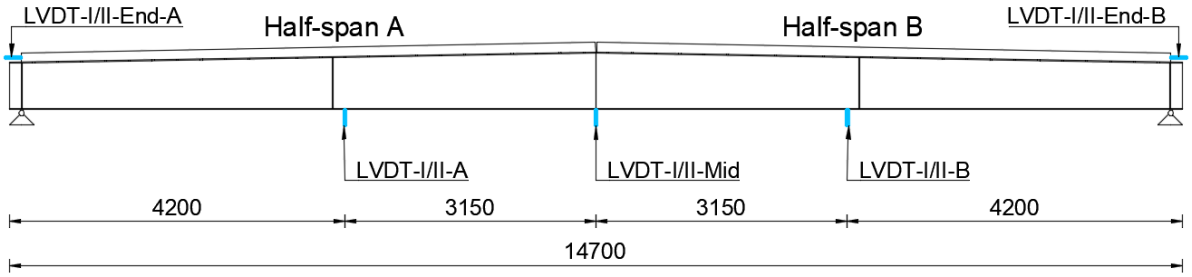

Figure 4.4 **Potentiometers locations**

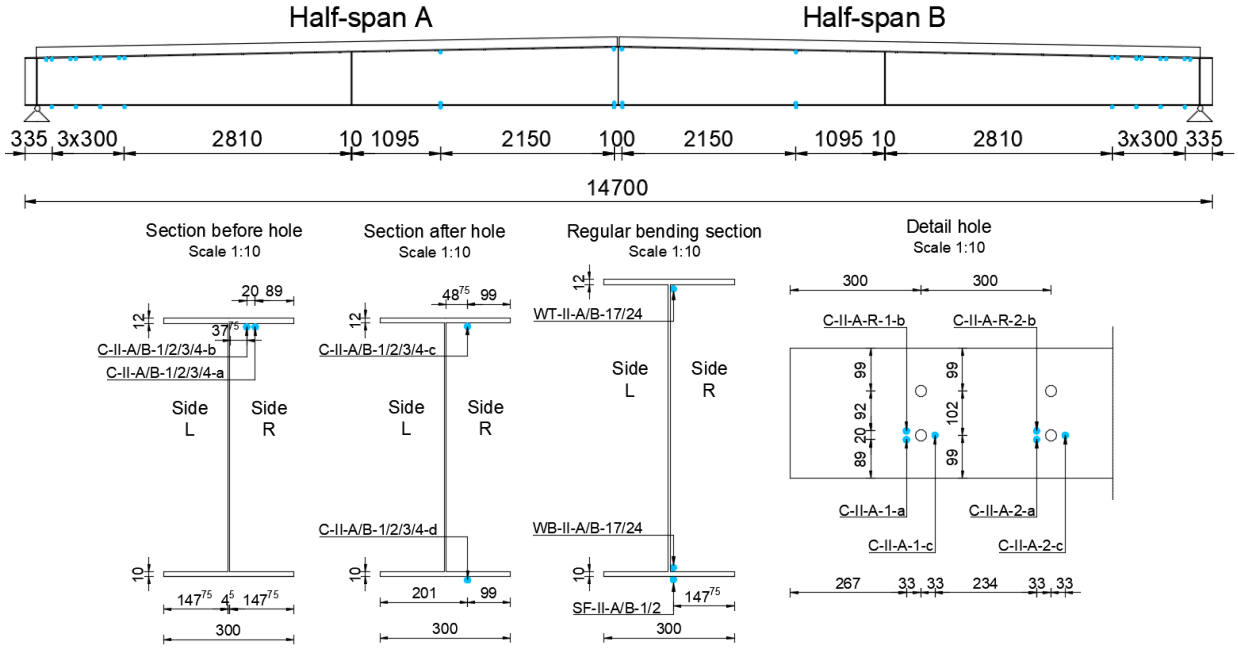

Figure 4.5 **Strain gauges locations**

The load was applied using two hydraulic jacks with a maximum capacity of 550kN. The jacks were displacement controlled throughout all four-point bending tests. To check

the consistency of the results five loading and unloading cycles were applied for each test. In Figure 4.6, the loading regime is presented. The applied displacement differed on the connector arrangement tested.

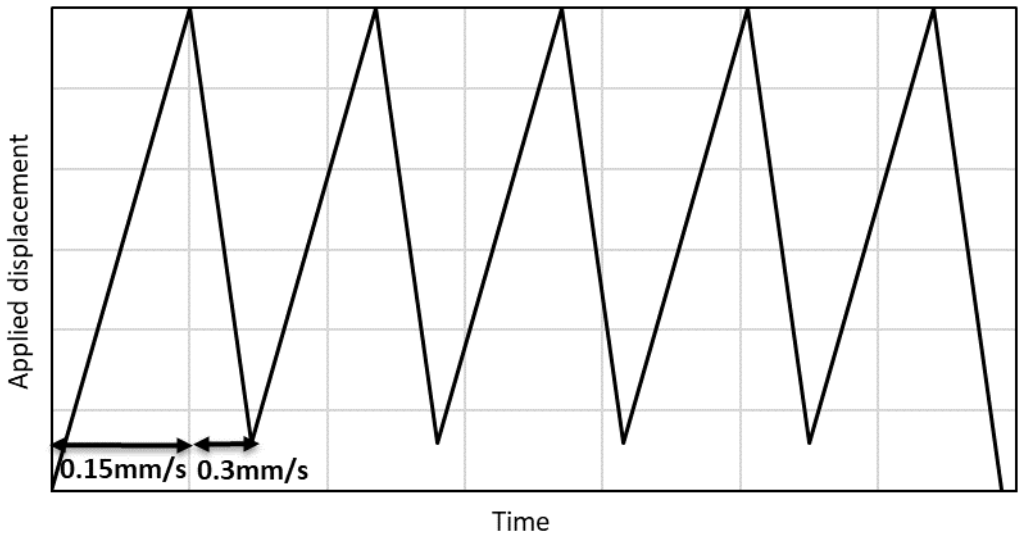

Figure 4.6 **Jack loading regime**

4.3 Connector arrangements

In current practice the mechanical connectors are uniformly distributed along the length of the beam to achieve composite action. However, by following the slip distribution (see Figure 4.7) the arrangement can be improved by concentrating connectors close to the supports.

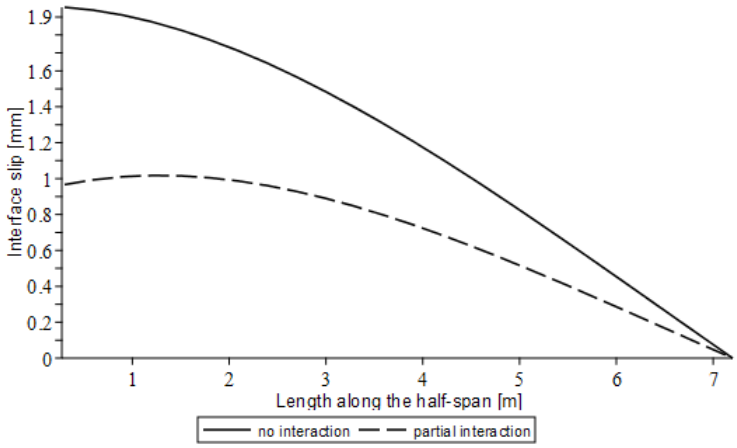

Figure 4.7 **Slip distribution**

The 300mm spacing allows for various connector arrangements to be tested in order to assess their performance.

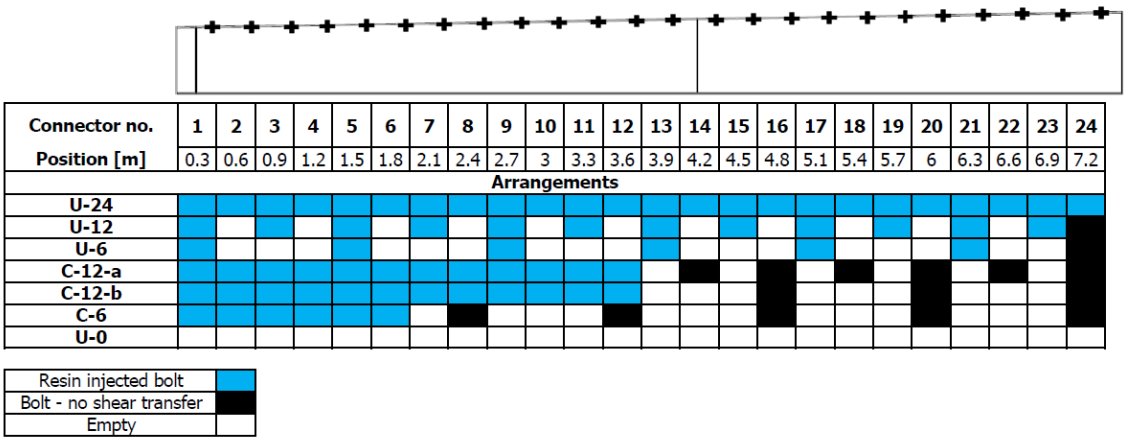

Figure 4.8 **Tested connector arrangements**

Seven elastic tests were performed to study the load-deflection behaviour of the composite beam. In Figure 4.8 the arrangements tested are presented in two categories. The capital letter U stands for uniformly distributed arrangements while C denotes the concentration of connectors towards the supports.

Starting with U-24 the number of connectors is reduced to U-12 and U-6. The uniform distribution is afterwards compared with the non-uniform arrangement C-12 and C-6. Two options were tested for C-12-a and C-12-b to study the influence of increasing the spacing between non-active shear connectors which have the role to prevent the vertical separation. No significant differences were observed between the two arrangements in terms of deflection, end-slip and stresses.

Finally, all the connectors were removed and the setup was tested to study the influence of the interface. The last test was to bring the composite beam to failure. For this test the connector arrangement C-6 was chosen with a spacing of the non-active connectors of 600mm.

4.4 Finite element description

The finite element model described in the previous chapter was modified to account for the in-use phase, namely the composite action of the beam. Therefore, the a step-by-step analysis accounts for both the construction sequence and the four-point bending phase.

The size of the model was reduced to one quarter and a spreader beam was added. The four-point bending is modelled using a displacement-controlled boundary condition at

the end of the spreader beam. The displacement control solves the convergence problems encountered by load control (see Figure 4.9). The level of detail of the model was increased by adding the L-profiles as an integrating part of the solid concrete slab.

Including the geometry of the loading system in the model will generate a realistic load transfer from the spreader beam to the composite beam. Roughly 86% of the load is transferred above the steel section (see Figure 4.10). Simply applying a load along the width of the deck was not sufficient to match the experimental results.

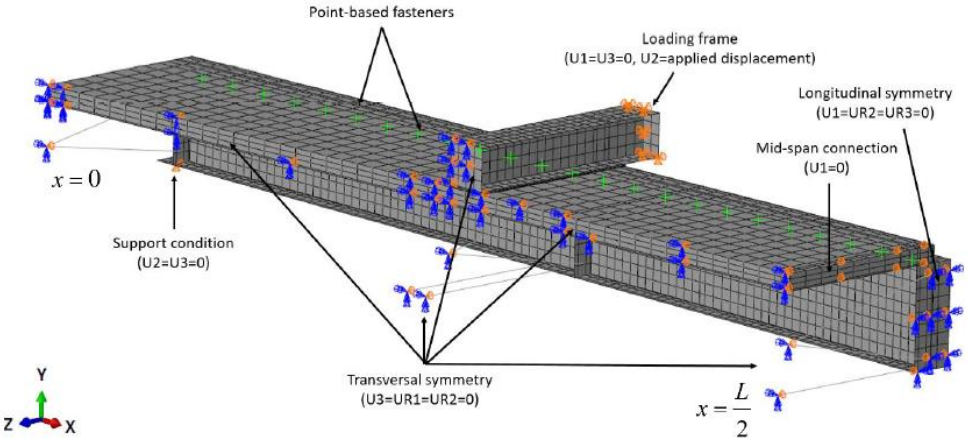

Figure 4.9 **Finite element model** [61]

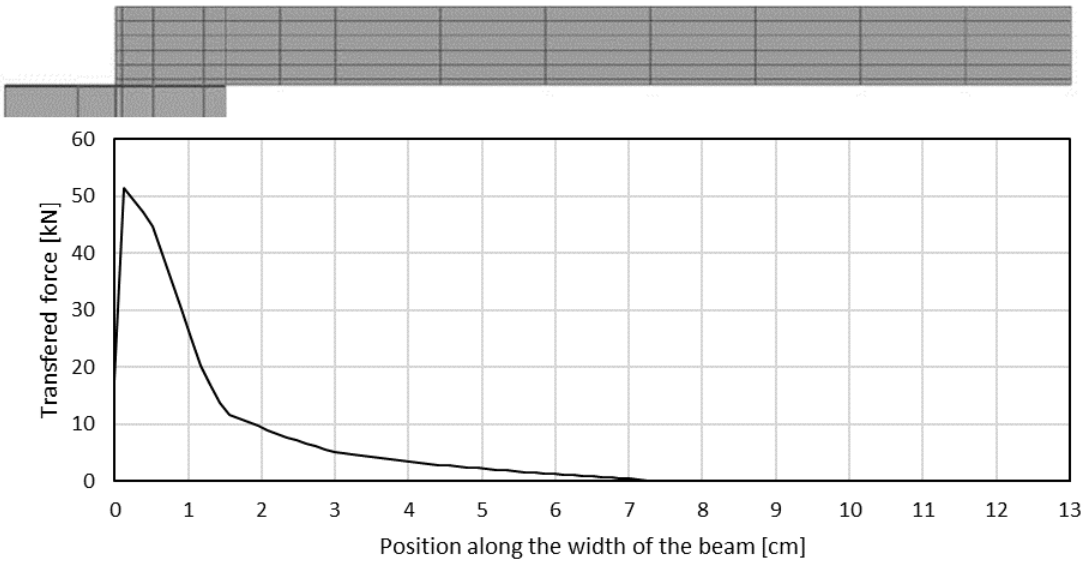

Figure 4.10 **Load transfer from spreader beam to deck**

The shear connection is modelled using three sets of Point-based fasteners:

- Non-resin injected connector
- Resin injected connector
- Vertical component of each connector.

Using Model change interaction, the fastener sets are activated or deactivated at different steps throughout the analysis. This is required because the injected connectors will be active at the same time only after the gap is filled with resin. The Model change command requires a change in the input file when applied to Point-based Fasteners. From the graphical interface, the command is assigned to the set defining the position of the springs. However, the command can only be applied to element sets so the input file must be changed before running the model.

```
*Model Change, add
~~300mm-spacing,~~
_Resin_pf_,
```

Figure 4.11 ***Model change - Abaqus input file**

The spring section is defined coupled on the motion, having an initial stiffness of 55kN/mm (see Figure 2.45 and Figure 3.23). The springs corresponding to a bolt in 12mm hole clearances will accumulate slip during the construction stage and can be activated during the loading phase for high applied loads. The vertical spring prevent the uplift of the concrete slab.

The interaction is handled by General contact characterized by “Hard” Contact in normal direction and a friction coefficient of 0.3.

To capture the failure of the composite beam, the concrete was modelled using concrete damaged plasticity. The material behaviour of the beam is described considering hardening effects.

Engineering Stress (MPa)	Engineering strain	True Stress (MPa)	True Strain
0	0	0	0
355	0.001690476	355.600119	0.001689049
360	0.0125	364.5	0.01242252
470	0.05	493.5	0.048790164
520	0.1	572	0.09531018
520	0.175	611	0.161268148
504	0.23	619.92	0.207014169
360	0.26	453.6	0.231111721

Table 4.1 **Steel stress-strain values** [80]

To predict the elastic behaviour of the composite beam, the non-linearities of the materials and the construction stage can be ignored. However, to capture the failure the stress situation during construction and the material non-linearities are necessary.

4.5 Elastic tests

The goal of these experiments was to investigate the elastic load-deflection behaviour of the demountable composite beams while also reusing the setup multiple times. For this reason, finite element models were employed to limit the applied jack displacement. The longitudinal stresses and the end-slip were constrained to the elastic range. Push-out tests on the resin injected bolt coupler system have been performed by [53, 60]. The maximum allowable connector slip during the experiments was set to 1 mm to ensure linear-elastic behaviour of the shear connection [61] (see Figure 2.45). After injection, all the bolts were removed, and the specimen was loaded to break the adhesion between the top flange and deck. Any possible adhesion could contribute to the composite behaviour of the beam making the validation of the finite element difficult.

In Figure 4.14 and Figure 4.15 the load-deflection and load-end-slip curves are presented. The self-weight is excluded from all the plots. Depending on the number of connectors and arrangement the applied displacement was reduced to ensure the elastic behaviour of the setup. The end-slip of 1 mm was never overcome and the load-deflection curves are linear throughout the 5 loading cycles. The longitudinal stresses at mid-span and at the position of maximum predicted stress do not exceed the elastic limit.

For validation, the effective bending and slip stiffness and the longitudinal stresses are compared to results obtained from the finite element model. The stiffnesses were computed as the average result over the number of load repetitions, taken over the interval 15-25mm deflection at mid-span. For arrangements U-0 and U-6, the results were taken over the last 10mm of deflection [61]. The specified intervals will avoid considering the influence of flexibility of the supporting system which is more pronounced in the first parts of loading. The results of the finite element analysis closely match the experimental results both in terms of deflection (average deviation 2%), curvature (average deviation 0.7%) and stresses (average deviation 4.9%) [61] (see Figure 4.16 Figure 4.17).

$$k_{\mathrm{b,eff}} = \frac{\Delta F}{\Delta W\left(x = \frac{L}{2}\right)}$$

$$k_{\mathrm{s,eff}} = \frac{\Delta F}{\Delta u(x = 0)}$$

Arrangement	$k_{b,eff}$ [kN/mm]			$k_{s,eff}$ [kN/mm]		
	Experiment	FEM	Diff.	Experiment	FEM	Diff
U-24	6.89	7.13	3.4%	514	301	-41.4%
U-12	6.35	6.35	2.8%	330	294	-10.9%
U-6	5.82	5.82	0.9%	199	188	-5.5%
C-12	6.69	6.69	3.9%	487	190	-61.0%
C-6	6.18	6.18	1.6%	389	128	-67.1%
U-0	4.1	4.1	-0.7%	98	51	-48.0%
	Average		**2.0%**	**Average**		**-39%**

Table 4.2 **Comparison of experimental and finite element results**

However, the effective slip stiffness is underpredicted on an average by 39%, literature study carried by [61] indicate multiple publications such as [81, 82] which confirm these differences in end-slip. The influence of the interface on the end-slip was studied experimentally by removing one of the decks and greasing the surfaces. The interface conditions of the other deck were not changed, and five cycles of loading were applied to C-6 connector arrangement. No significant difference in end-slip was observed in either half-spans, indicating that adhesion and friction at the interface may only have had a small effect in the original test series [61]. The stiffness of the beam without connection matches the stiffness obtained by finite element indicating that no significant shear interaction (e.g. due to adhesion and friction) was present [61]. Future research on composite beams should focus on understanding the interface slip in order to identify the source of deviation.

The connector strain gauges give valuable information in terms of the magnitude of the stress around the holes. The concentrated force transferred by the connector to the top flange should not lead to local yielding. For comparison the live load for car parks specified by [83] is 3kN/m^2 and generates a maximum moment equal to 202kNm, which corresponds to an applied jack force of 50kN. The applied jack force during the test ranged between 100kN and 250kN, much higher than the loads specified by [83]. The stresses did not exceed 80MPa for the applied loads which certifies that with a good design, the stresses around the holes will not exceed the yielding point in the serviceability stage.

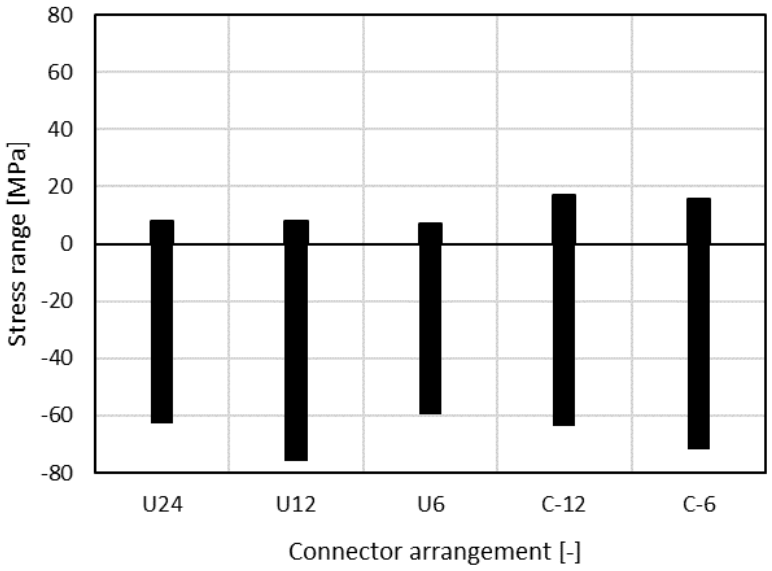

Figure 4.12 **Stress range - connector strain gauges**

In Figure 4.13, the effective bending stiffness is plotted against the number of resin injected shear connectors. The effectiveness of concentrating shear connectors towards the ends of the beam is clear when comparing the two curves. Reducing the number of resin injected connectors to half and concentrating the remaining at the ends results in a decrease of effective bending stiffness of only 2%. When the number of connectors is quartered the reduction in effective bending stiffness is 11%.

After the all the connector arrangements were tested the bolts were easily removed using a pneumatic gun without any visible damage to the resin. As expected there was no sign of damage to the couplers, bolts, steel beams and decks. As presented in the previous chapter, the resin can be cleaned and the beam and decks are fit for future use.

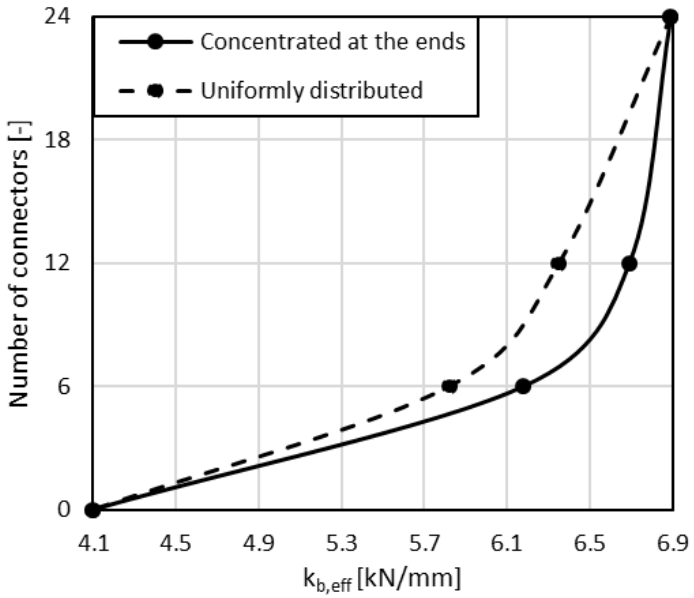

Figure 4.13 **Number of connectors against effective bending stiffness - beam tests**

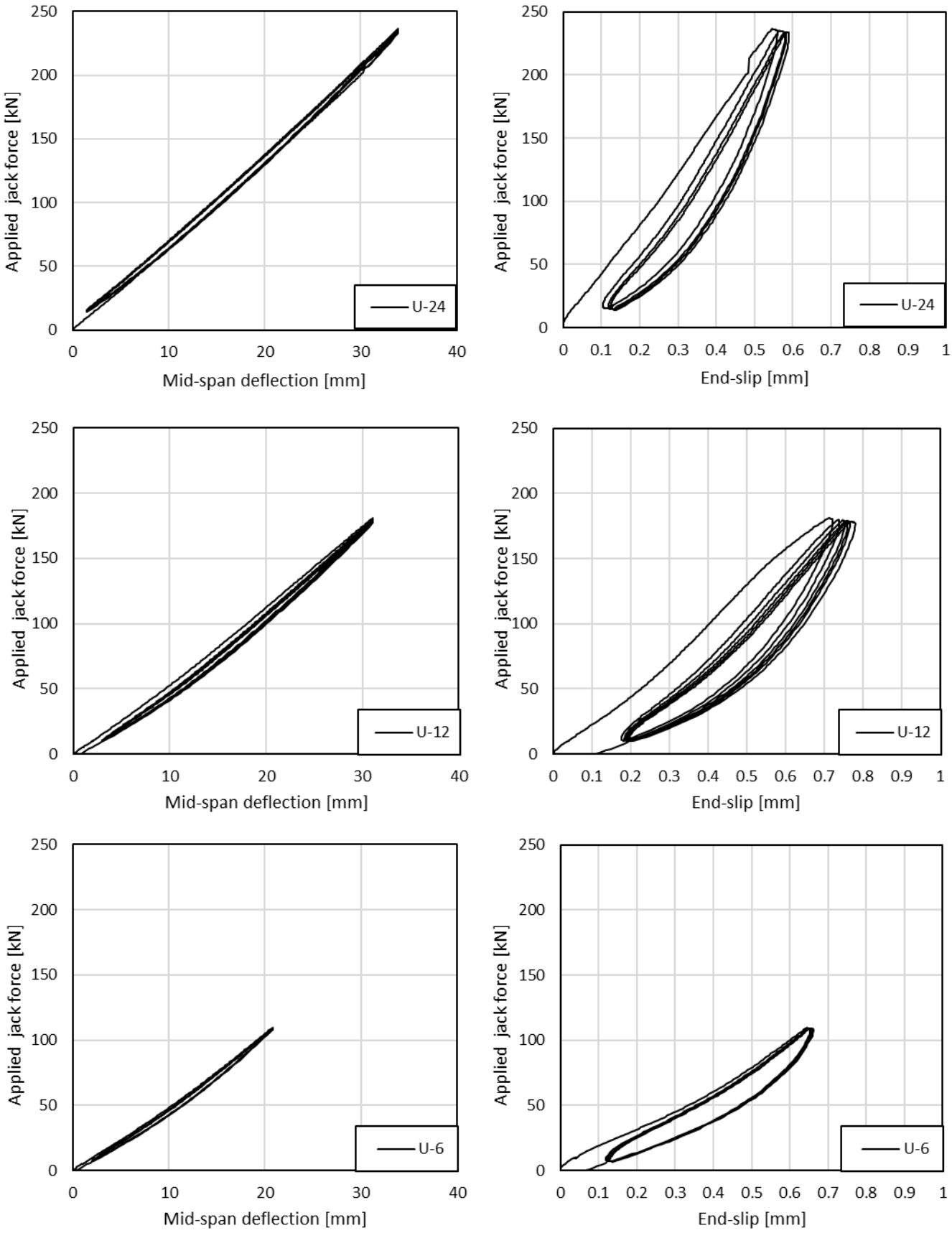

Figure 4.14 **Load-deflection and load-end-slip curves - U-24, U-12, U-6**

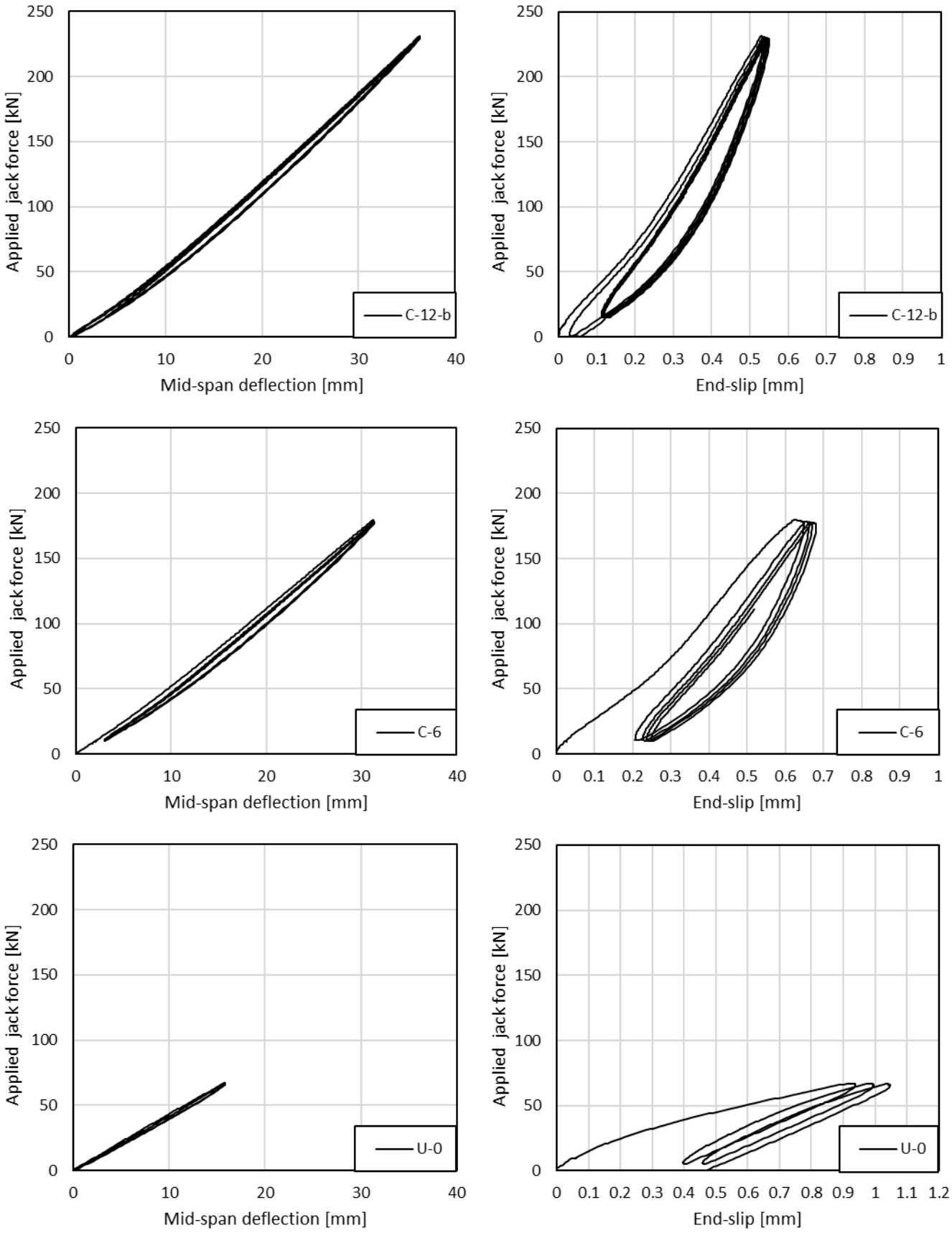

Figure 4.15 **Load-deflection and load-end-slip curves - C-12-b, C-6, U-**

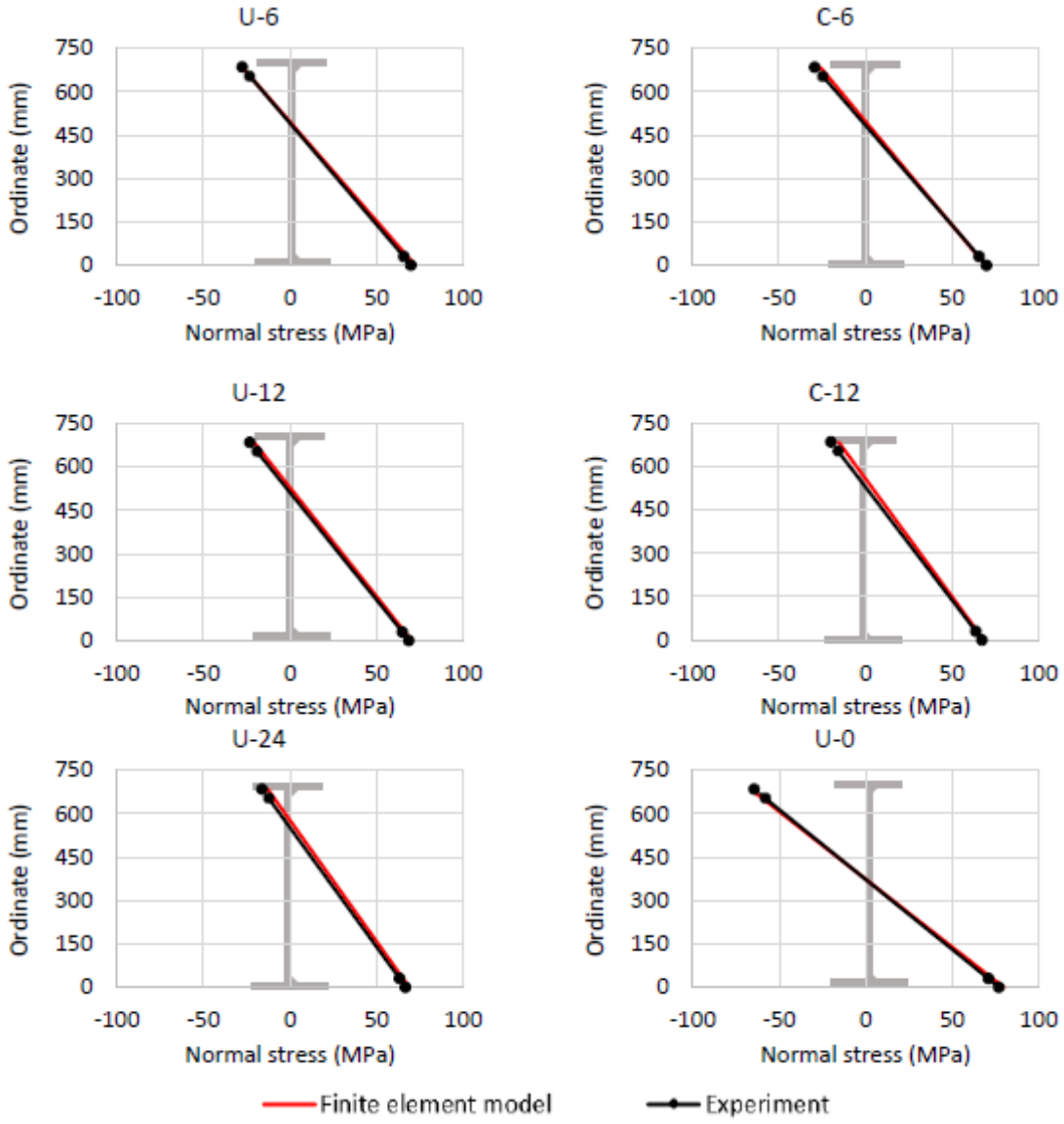

Figure 4.16 **Comparison of beam stresses during four-point bending** [61]

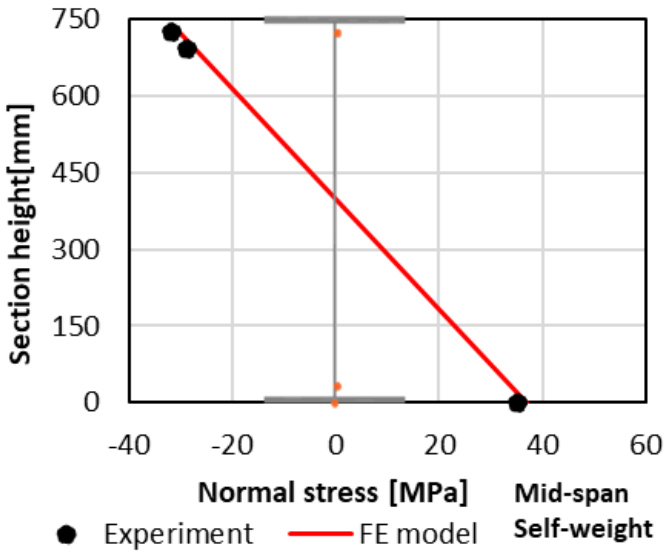

Figure 4.17 **Comparison of beam stress due to self-weight**

4.6 Failure test

After all the connector arrangements were tested in the elastic range the setup was loaded to failure using connector arrangement C-6-a. Because the holes were injected multiple times and the groove was never cleaned lead to two clearances not being fully injected. For this reason, the connector arrangement will be regarded as C-5-a. In Figure 4.19 and Figure 4.20 the total applied load, including the self-weight, is plotted against the mid-span deflection and end-slip for both the experiments and finite element results.

Figure 4.18 **Plasticlly deformed setup**

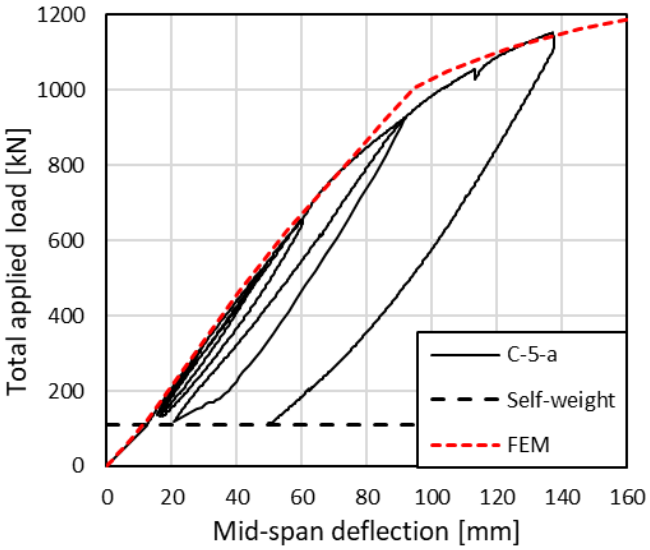

Figure 4.19 **Comparison of load-deflection between finite element and experimental results**

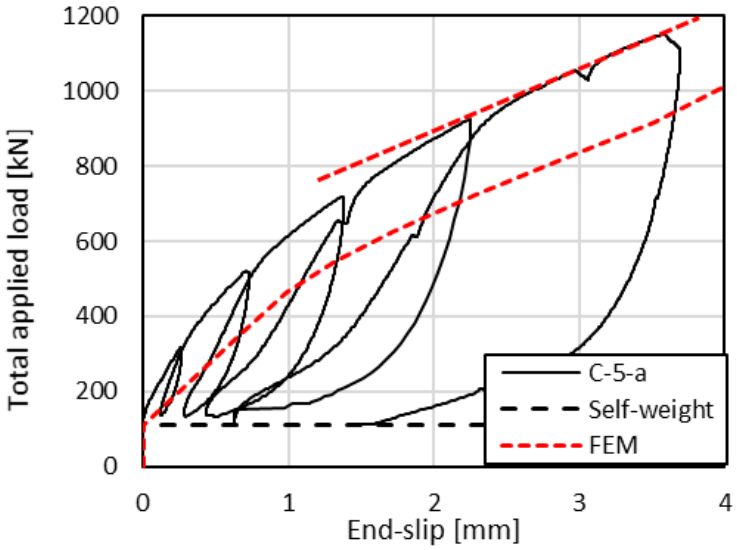

Figure 4.20 **Comparison of load-end-slip between finite element and experimental results**

The jack force was limited to 550kN for safety reasons, and because of this the beam was loaded only up to 135mm of mid-span displacement. However, the serviciability limit state requirement of L/250 was overcome by a factor of roughly 2.3. From Figure 4.19 one can notice the elastic range is exceeded at a load level of 800kN and is followed by a non-linear part up to 1150kN. After unloading a permament deformation of 50mm was observed. A good match is observed for the initial stiffness of the beam while the non-linear part started at a lower level during experiments. This is explained by the fact that the steel beams yield at different load levels due to possible flexibilities of the support or an uneven transfer of the applied force between the steel beams. In terms of slip, the same trend is observed in the elastic range. However, the effective slip stiffness shows a good match in the non-linear range.

The superposition of the self-weight and of the jack loads leads to a maximum bending moment of 2306kNm. The first yielding of the bottom flange of one of the beams takes place at a load level of 870kN (see Figure 4.21) which corresponds to a bending moment of 1737kNm. Because no instability effects were observed during experiments the elastic bending moment capacity of the two beam is equal to 1670kNm. The difference of 4% between the first measured yielding and the predicted elastic moment can be due to the unquantified composite action.

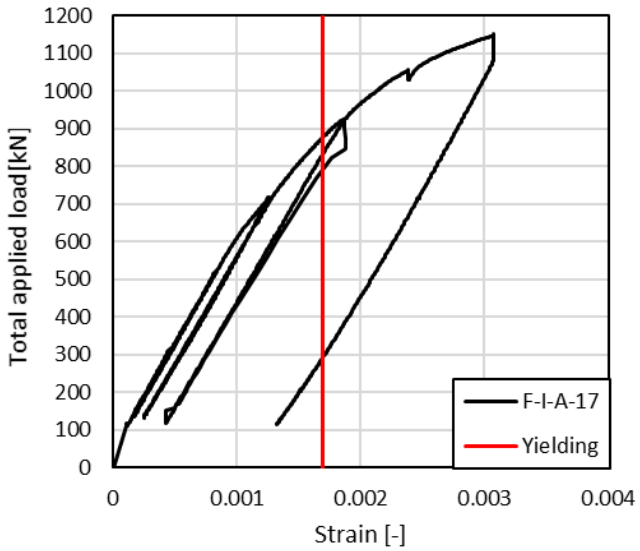

Figure 4.21 **Strain agains applied load** - beam failure

Averaging the recorded stresses at the position of maximum predicted stress shows a good match between the finite element and the experiments. Partial plastification of the tensile part is obtained at the highest applied load which confirms the failure of the beam.

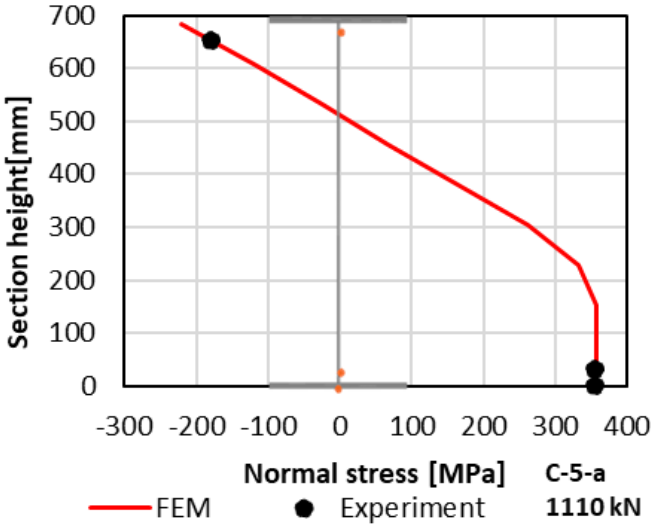

Figure 4.22 **Stress distribution - finite element model and experiment (beam failure)**

The stresses around the holes give additional proof that yielding will not take place during the servicibility limit state. Yielding around the holes was recorded only after the beam was plasticly deformed.

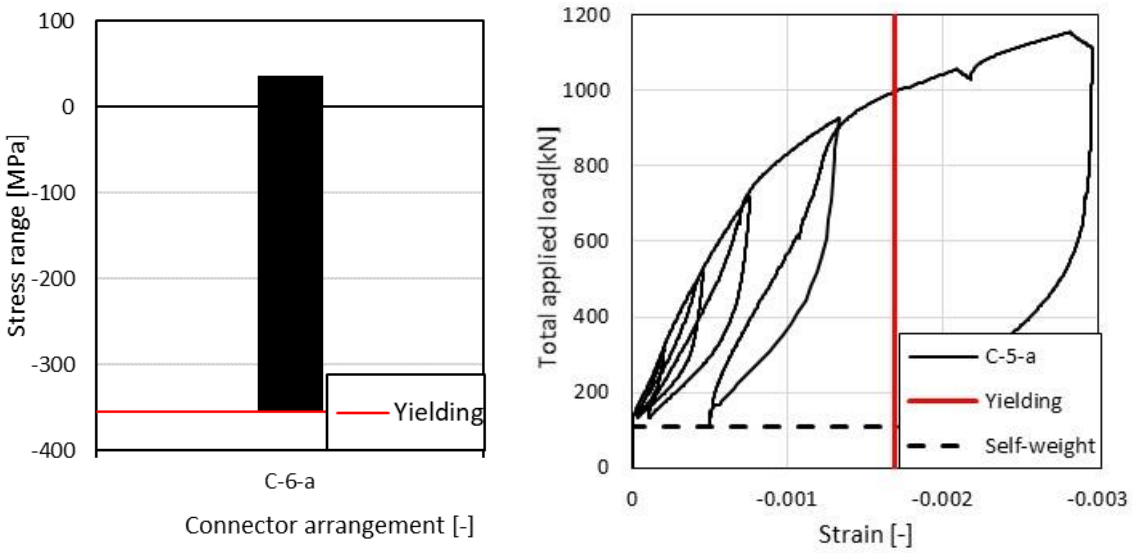

Figure 4.23 **Stress range around and strain vs applied load the holes - beam failure**

Even though, large slips were recorded at the interface, the bolts were easily removed and the structure was demounted. Consequently, a demountable flooring can give an edge even after exposed to extreme loading since the structure can be easily deconstructed instead of a long and dangerous demolition process.

Consequently, the results from push-out tests are a good approach to describe the connector behaviour in composite beams. The beam elastic behaviour can be captured in terms of deflection, curvature and stresses using finite element. However, the elastic effective slip stiffness is underpredicted but a close match is found in the plastic range.

4.7 Optimization of shear connector arrangement

The high unit price of the bolt coupler connector and intensive manufacturing process requires an optimization of the shear connector arrangement in order make the demountable flooring solution economically viable.

4.7.1. Longitudinal shear

As previously mentioned, the slip distribution is not constant along the length of the beam (see Figure 4.7), which leads to the necessity of a non-uniform connector arrangement. It was confirmed by experimental beam tests that concentrating the shear connectors towards the supports will reduce their number with only minor decrease in beam stiffness (see Figure 4.13). This was also theoretically confirmed by [84, 85].

The analytical model developed by [37] presented in 2.8.1 and the developed finite element model were used to understand the behaviour of the longitudinal shear connection. The analysis was carried out on the geometry of the experimental setup subjected a

uniformly distributed load of 3kN/m^2 as defined by [83]. Four decks were considered in the analysis (see Figure 4.30).

In Figure 4.24 the cumulative shear force along the length of the beam for U-24 is plotted. In the plot below, the red line marks the quarter span position. The 12 connectors found in first quarter span resist roughly 77% of the total longitudinal shear force. At L/8, marked by the blue line, the shear force resisted by the 6 connectors present up to this point is approximately 45%. This confirms that outer connectors are most effective in transferring the longitudinal shear force.

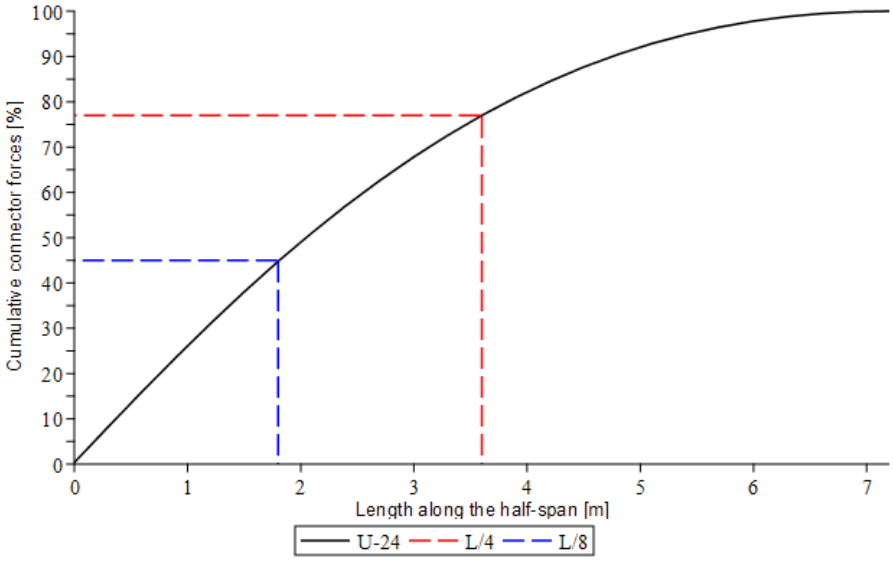

Figure 4.24 **Cumulative connector force along the length of the half-span**

The plot from Figure 4.13 was generated again, this time considering uniformly distributed loads. The advantage of non-uniform connector arrangement is clear from the reduction in the beam stiffness by only 3% when the number of connectors is halved.

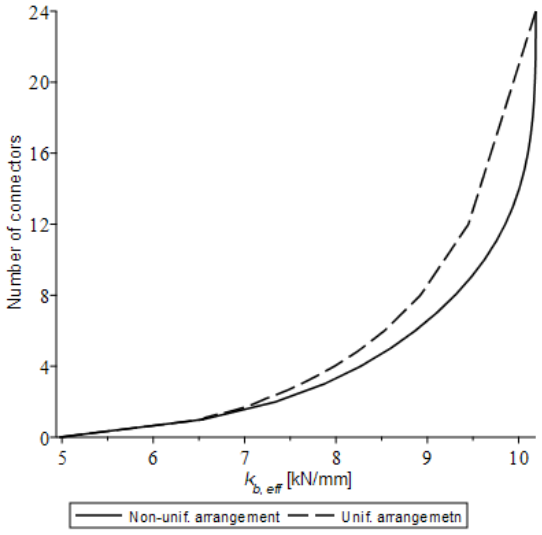

Figure 4.25 **Number of connectors against effective bending stiffness**

The relationship between the beam stiffness and the number of shear connectors can be approximated by an exponential function. In Figure 4.26 the ratio between the maximum bending stiffness allowed by the number of holes and the effective bending stiffness is shown. Common design starts by incrementing the number of connectors until the stiffness requirements are satisfied. Analysing Figure 4.26, one can notice that after a certain number of connectors the beam stiffness will no longer increase. Consequently, in order to design the optimum number of connectors, the steep part of the exponential function should be avoided because it brings no benefit in terms of beam stiffness.

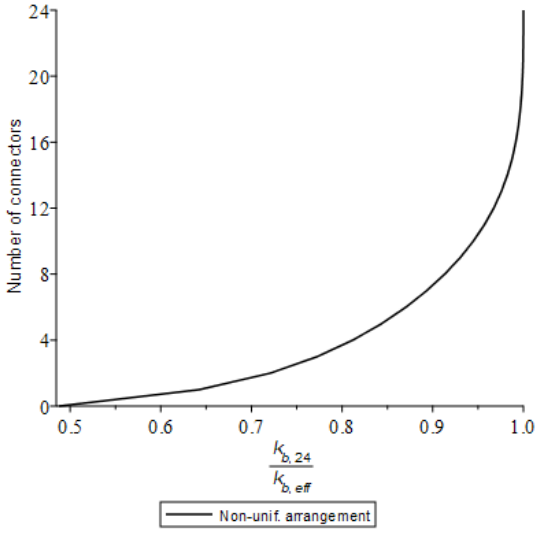

Figure 4.26 **Number of connectors against ratio of maximum and partial interaction**

Looking at the connector force distribution for arrangements U-24 and C-12 one can observe that the longitudinal shear force is distributed more evenly when the shear connectors are concentrated at the ends of the beam. In this way the connectors are used more efficiently. The abrupt change in curve slope for C-12 can be explained by the sudden change in connection stiffness. The slip will follow the connector force distribution.

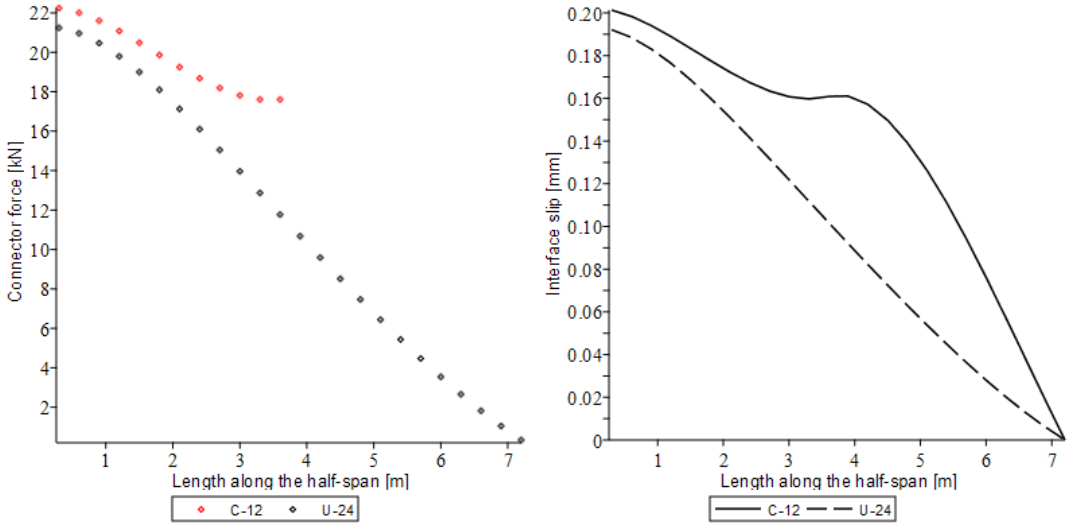

Figure 4.27 **Connector force and slip distribution - C-12 and U-24**

4.7.2. Vertical separation

EN 1994-1-1 [18] requires that the connector spacing should not be less than 800mm in order to prevent vertical separation. The economic benefits of a non-uniform connector arrangement will be reduced by this requirement. It was already shown by [21] that the vertical separation is limited while the beam is kept in the elastic range. Because the vertical separation was not measured during experiments, its influence is studied by finite element analysis.

The validated finite element model is used to study different load combinations in order optimize the number of connector necessary to prevent uplift. The longitudinal shear connection studied is C-6. Vertical shear connectors are modelled as elastic springs acting only in tension. The stiffness of the vertical springs is assumed equal to 160kN/mm based on experimental pull-out tests carried by [86, 87]. The two authors performed pull-out tests on headed studs with same dimensions and material properties but different slab thicknesses, reinforcement and concrete compression strength. In Figure 4.29 the results of the pull-out curves are presented. From the plot it can be observed that the initial stiffness of the studs is similar and is independent on the concrete class, slab thickness and reinforcement.

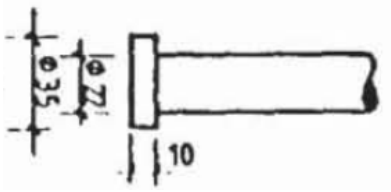

Figure 4.28 **Headed stud dimensions** [86] **- 130mm height**

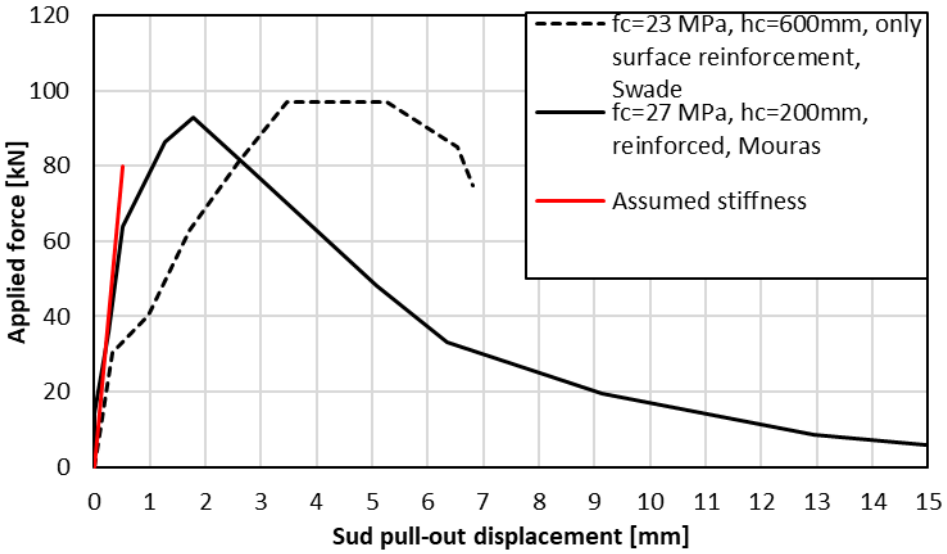

Figure 4.29 **Pull-out experiments**

As mentioned in the previous chapter, there is a need for long bolts, while installing the decks, at least at the corners and middle of the deck. Keeping in mind this requirement, the verifications study whether additional connectors are required.

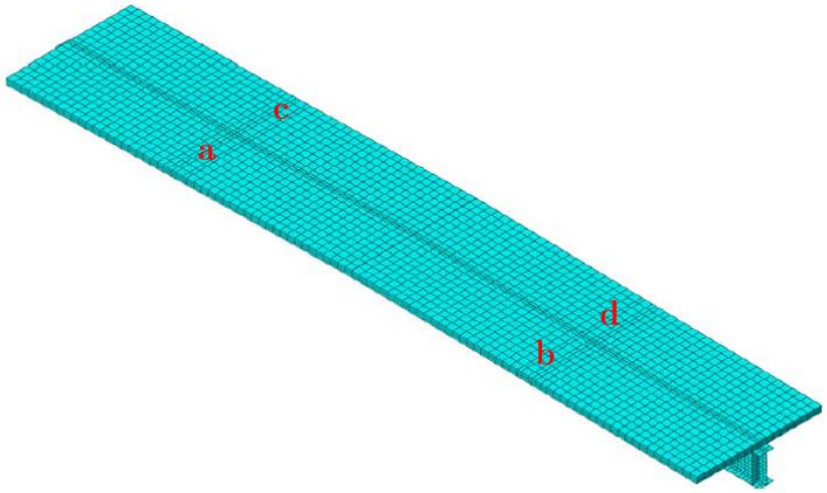

Figure 4.30 **Finite element model - uniformly distributed loads**

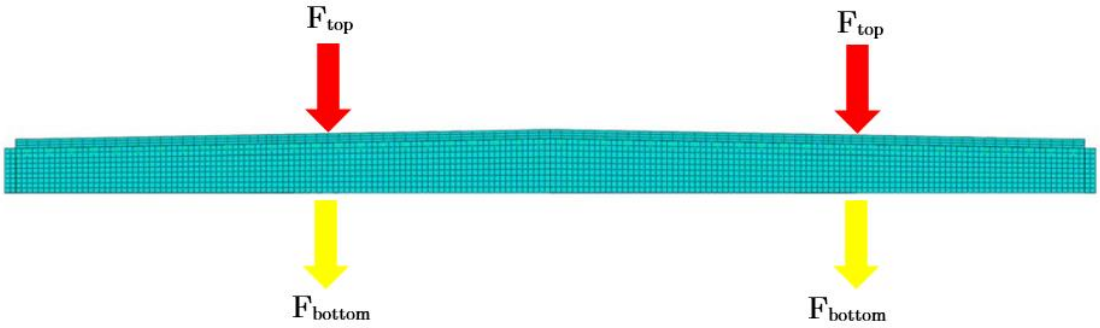

Figure 4.31 **Finite element model - concentrated loads**

A number of 10 load cases were studied to obtain the maximum vertical separation and connector uplift force. Uniformly distributed loads were applied on the top surface with the magnitude of 6kN/m^2 (twice the SLS load) and concentrated forces with the magnitude of 112kN which corresponds to the uniformly distributed load applied in one half-span. The self-weight was not factored as it contributes to the reduction of the vertical uplift. The magnitude of the loads was chosen higher compared to usual cases in order to prove that the uplift phenomenon will not govern the design of the connector arrangement.

Number	Load case	Maximum uplift force [kN]	Maximum vertical separation [mm]
1	a+b+c+d	1.45	0.0095
2	c+d	2.42	0.016
3	c+b	0.96	0.017
4	c	1.3	0.012
5	F_{top} (left and right)	1.21	0.013
6	F_{top} (left)	2.02	0.014
7	F_{bottom} (left and right)	1.61	0.016
8	F_{bottom} (left)	1.98	0.018
9	F_{bottom} (left)+F_{top} (right)	3.87	0.040
10	**F_{bottom} (left)+F_{top} (left)**	**8.3**	**0.073**

Table 4.3 **Results of finite element analysis for vertical separation**

The results of the finite element analysis are presented in Table 4.3. The obtained vertical separation is very low with a maximum of 0.073mm and a maximum connector force of 8.3kN.

The pull-out resistance of the connector can be obtained using the formulation proposed by [88]. The expression accounts for the edge distance of the connector, height of the shank, diameter of the shank and head and concrete class. The diameter of the shank and head are considered equal keeping in mind the coupler extends for most of the connector height. The pull-out resistance of the connector is equal to 20.4kN. Accounting for safety factors from [46], the resistance reduces to 14.7kN and the utilization ratio is equal to 0.56. However, one should have in mind that the L-profile will contribute through bending to the pull out resistance of the connector. The expression to determine the pull-out strength proposed by [88] is the following:

$$P_{\mathrm{u}} = 0.85\pi(d_{\mathrm{h}} + h_{\mathrm{s}})\ h_{\mathrm{s}}(0.267 f\hat{}_{c}^{\frac{2}{3}})\sqrt{\frac{1}{2}\frac{e - \frac{d_{\mathrm{s}}}{2}}{h_{\mathrm{s}}}}$$

Where:
d_{s} - diameter of the shank
d_{h} - diameter of the head
h_{s}- height of the shank
$f\hat{}_{c}$ - compressive strength of the concrete

The vertical separation is lower than 0.01 mm which can be considered sufficiently small for engineering purposes. The reliability of the numerical results should be confirmed by experimental data.

To verify whether the reduced number of connectors will have an influence on the beam stiffness, the optimized arrangement was compared to the situation where all other vertical connectors are installed. Finite element results show a reduction in beam stiffness of 1%.

The analysis performed investigated only the case of tapered beams therefore, prismatic beams should be the focus for future research. However, experimental research carried by [63] on demountable composite floorings with profiled sheeting slab in combination with prismatic beams recorded similar values in terms of vertical separation.

Consequently, having all these in mind the arrangement can be optimized by concentrating the connectors at the ends of the beam while using only 2 additional one to reduce the uplift of the deck.

4.8 Assessment of mid-span joint

4.8.1. Shear force transfer

As part of the experimental program, the mid-span joint was investigated in terms of its suitability to transfer the shear forces between the decks. Because the flooring is made up of two decks, the differential deflection can create a discontinuity at mid-span. The differential displacement of the decks can create discomfort to the passengers or in the case of a rigid surface finishes it can damage them.

Figure 4.32 **Loading frame - mid-span joint experiment**

Two experiments were performed by applying a concentrated load on top of one of the decks while the differential displacement was measured underneath the deck at the position of the load and at the symmetric position of the unloaded deck. In order to study the suitability of using a mid-span joint two situations were tested. In the first, the shear transfer was ensured by bearing of the L-profiles while in a second experiment the transfer was aided by a mid-span joint as seen in Figure 4.33.

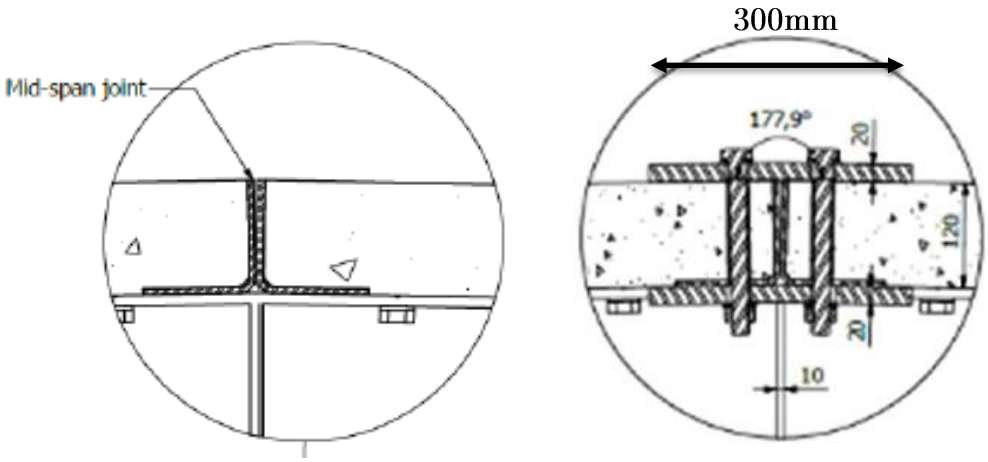

Figure 4.33 **Mid-span conditions** [61] [66]

The concentrated load was applied using a square surface with a width of 200mm as defined by [83] for category G. In order to capture an unfavourable situation the load was applied on the concrete at a distance of 300mm from mid-span.

Experimental measurements show that using a transversal joint reduces the differential displacement between the two decks by 90%. The maximum axle load defined by [83] for category G is 90kN. At a concentrated load level of 45kN, the differential displacement between the two decks was 0.75mm when the transversal joint was used.

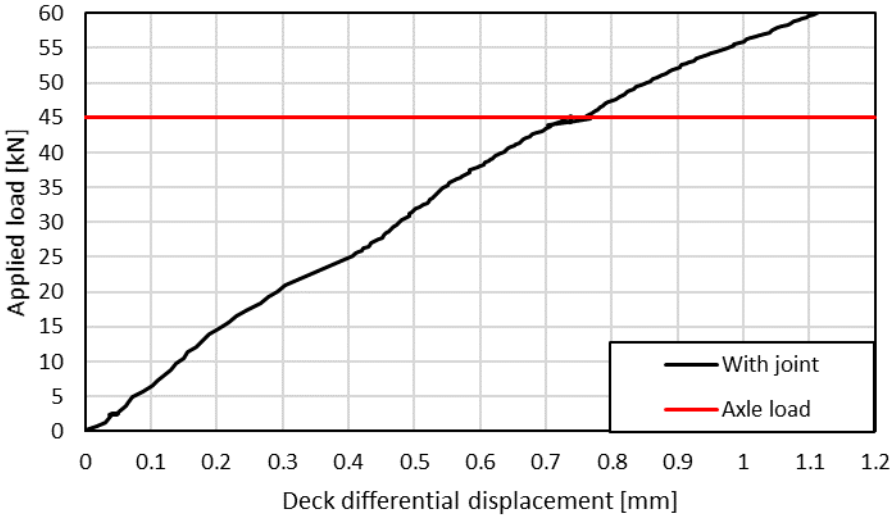

Figure 4.34 **Load-deck differential displacement**

The joint reduces the differential displacement, however the current solution using two cover plates is difficult and unsafe to install. Therefore, a more suitable solution should be proposed. Even though, the differential displacement is limited and would not affect the passenger comfort it should not be disregarded if a rigid finishing is applied.

4.8.2. Compression force transfer

At mid-span during the four point bending, the decks were in direct contact and the experimental results closely matched the finite element model where the slab was considered continuous. However, as emphasized in the previous chapter, the lengthwise deviations of the L-profiles require a gap at mid-span (see Figure 3.3) to accommodate these imperfections.

For this reason, the situation when the gap is not filled was assessed through finite element model in order to quantify the loss in bending stiffness due to the discontinuity in the compression force transfer. For connector arrangement C-6, the composite beam was loaded by a uniformly distributed load equal to 3kN/m^2. The bending stiffness reduced by 60% in this case because composite action was not achieved. The stiffness of the composite beam reduces to the stiffness of the steel section. Moreover, the discontinuity in the compression force transfer results in an increase of the longitudinal stresses. The magnitude of the stresses in the top and bottom flange changed significantly as shown in Table 4.4.

Mid-span condition	Top flange stress [MPa]	Bottom flange stress [MPa]	Mid-span deflection [mm]
In contact	21	66.8	21
Without contact	67.6	77.38	13.1
Difference [%]	31%	86%	160%

Table 4.4 **Study of mid-span gap**

The assessment of the mid-span joint presented in this master thesis represents only a preliminary step out of an extensive research topic which should be further investigated.

4.9 Conclusions

1. The possibility of disassembly and reusability of the demountable composite flooring system consisting of large prefabricated concrete decks and tapered beams connected by means of resin injected bolt coupler connectors was confirmed in case of an elastic design. Moreover, it was possible to disassemble the structure even after the steel beam has been plastically deformed. This can give an edge by avoiding labour intensive and potentially dangerous demolition.
2. Resin injection of the large oversized holes allows for higher manufacturing imperfections and reduced construction time while at the same time enables composite action of all the connectors under live loads.
3. The elastic and plastic beam behaviour can be captured by finite element models which confirms the suitability of the push-out tests to describe the demountable shear connectors. The results of the finite element analysis closely match the experimental results both in terms of deflection (average deviation 2%), curvature (average deviation 0.7%) and stresses (average deviation 4.9%) [61].
4. The measured end-slip is smaller by up to 52% compared to results from finite element models. This overprediction was also observed in experiments performed by other authors. The influence of interface friction and adhesion was investigated and can be excluded as a possible cause of these deviations.
5. Extensive monitoring of the stress situation around the holes confirms that the concentrated load generated by the shear connectors can be transferred to the top flange without local yielding.
6. To make demountable solutions as economically viable as possible, non-uniform connector arrangements can be used to optimize the longitudinal shear connection. The relation between beam stiffness and number of connectors follow the shape of an exponential function (see Figure 4.26). In order to design the optimum number of connectors, the steep part of the exponential function should be avoided because it brings no benefits in terms of beam stiffness.
7. Concentrating the connectors towards the supports will lead to a more uniform connector force distribution compared to traditionally uniformly distributed arrangements.
8. Numerical analysis show that the effect of vertical separation is sufficiently small to be ignored for engineering purposes. The number of connectors which prevent uplift can be reduced significantly with only a minor decrease (1%) in beam stiffness.

9. Experimental research shows that using a mid-span joint to aid the shear force transfer between decks will reduce differential displacement by 90%. The deck differential deflection at a load level of 45kN will drop to less than 0.8mm. The measured discontinuity will not affect passenger comfort, however it should be regarded in case of a rigid surface finishing.
10. Using finite element models, the requirements for ensuring a continuous transfer of compression force was studied. It was shown that a discontinuous concrete slab will not achieve composite action and the load will be resisted by the steel section. For this reason the recommendation to fill the gap between the decks is reasonable and has a significant influence on the beam behaviour.

5 Cost analysis

Due to the novelty of the flooring system, the initial investment will be higher compared to the traditional solution. A first cost assessment was performed by [13] including only the material costs. The cost analysis will be extended in this chapter by accounting for a wider range of inputs. In order to reduce the costs as much as possible, the shear connection will be optimized following the findings of the previous chapter. Due to the flexibility of formulation described in 2.8.1 it was adopted and implemented in Maple to carry out an extensive parametric study on composite beams using tapered beams and hot-rolled sections.

5.1 Problem definition

In the following sections two cases will be analysed. The first study aims to compare the costs of an office space constructed using demountable flooring systems with a traditional flooring. An extensive parametric study will be performed in order to obtain the additional costs required to construct a demountable composite flooring. The viability of two demountable steel-concrete composite flooring systems will be investigated.

The second case will provide a preliminary cost estimation for a demountable car park. An initial design performed by [36] focused on reducing the steel weight by using tapered beams and a uniform connector spacing. The main goal of this case study is to optimize the composite beam in terms of costs, by using tapered beams but in combination with a non-uniform connector arrangement. Through a sensitivity study it will be investigated if the cost inputs will influence the design of the composite beam.

Starting with the analytical model proposed by [37] described in 2.8.1, a design algorithm was built in order to serve the scope of the costs analysis. A sensitivity study must be performed on a large pool of data in order to see whether the cost inputs will influence the design of the composite cross-section. For this reason, the algorithm should be built such that it efficiently generates the solutions which satisfy the design requirements. The inputs were defined from industry enquiries, TU Delft market prices and literature. The research methodology of the cost assessment is presented in Figure 5.1.

Research questions:

- **Which are the most influential cost contributions to the final price of demountable composite floorings?**
- **To what extent a demountable flooring system will increase the initial cost per m^2 compared to a traditional solution?**

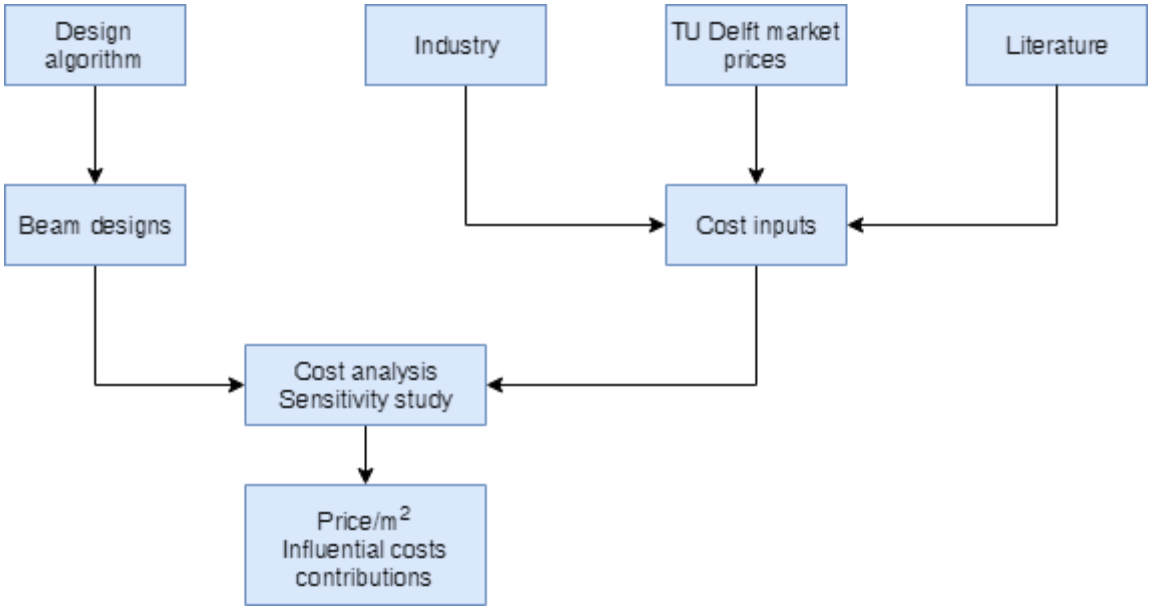

Figure 5.1 **Cost analysis methodology**

5.2 Design algorithm

The design algorithm structure is defined by the scope of the cost assessment and the analytical model. The algorithm should efficiently generate all the beam designs which satisfy the design requirements. For this reason, three types of algorithms were investigated.

Genetic algorithms [89] based on Charles Darwin's theory of natural evolution are commonly used in optimization problems. They significantly reduce calculation time when searching for the optimum out of a wide pool of possible solutions. However, for the present case, a genetic algorithm will not satisfy the scope of the cost analysis by not providing all the possible beam designs.

A second solution to reduce the number of iterations is to use a binary search algorithm [90]. However, due to nature of the relationship between beam stiffness and number of connectors (see Figure 4.26) a binary search algorithm would either lead to a bad performance or would need to be modified. For this reason it was not implemented

A simple approach is to use a brute-force search algorithm [91] to generate all possible beam designs for each set of parameters. However, this will require a large number of iterations to browse the entire domain of possible solutions. Moreover, in order to describe the beam behaviour, the analytical model needs to be solved numerically for each set of parameters. Solving numerically a large system of equations is computationally demanding especially for long span beams with a fine discretization. Coupling the disadvantages of the brute-force search with the computational demands of the analytical model will result in an inefficient algorithm. However, through engineering judgement,

the algorithm can be adapted in order to reduce the number of iterations. The structure of the algorithm is presented below in a simplified manner. The complete design algorithm is included in the appendix.

It was observed that out of roughly 544000 design possibilities for the two case studies only 15100 satisfy the requirements. In order to find these 15100 beam designs the code required only roughly 32700 incrementations due to the optimization. This translates in a reduced computation time by a factor of 16.

5.2.1. Design verifications

Variable loads are defined according to [83]. The uniformly distributed load is equal to q_k=2.5kN/m^2 for Category B and F buildings. An additional 0.5kN/m^2 was assumed to the variable loads. For office spaces another additional 0.3kN/m^2 was considered to account for flexible partitions. The self-weight of the beam is determined with the following densities $\gamma_{concrete}$=25kN/m^3 and γ_{steel}=78.5kN/m^3.

The resistance of the composite beam is verified according to [18, 23, 92] at ultimate limit state. However, composite beams are governed by stiffness requirements at serviceability limit state. The total beam deflection is limited by:

$$\delta_{tot} \leq L/250.$$

Where the total deflection is determined according to [36] as follows:

$$\delta_{tot} = \delta_{1(E_{steel}I_{steel},\, g_k)} + \delta_{21(EI_{composite\ at\ t_0},\, \psi_1 q_k)} + \delta_{22(EI_{composite\ at\ t_\infty},\ \ \psi_2 q_k)}.$$

To reduce computation time to half, δ_{22} was assumed in a conservative way as equal to 15% of δ_{21}. Factors for frequent and quasi-permanent combinations are defined by [93]. Reusable composite beams should not exceed the elastic range, and for this reason the end-slip must be limited to 1mm.

5.3 Cost inputs

Up to this moment, no demountable steel-concrete composite structure was built using the bolt coupler connector. For this reason, the costs are based on assumed material use and labour. The inputs were obtained from industry enquiries, TU Delft market prices and literature review. However, they are subjected to a high variability due to the novelty of the system, regional economic situation and country industry specific.

In the tables below, the cost inputs are defined in the following categories: materials, manufacturing, in-situ work and transportation. For traditional systems, the transportation and in-situ work are included in the manufacturing costs.

Materials			Source
Steel	/kg	2€	Industry
Hot dip galvanizing	/kg	0.25€	TU Delft
L120x120x10	/m	10€	TU Delft
Hole (punching)	/unit	2€	Industry
Concrete	/m^2	15€	Industry
Reinforcement mesh	/m^2	10€	Industry
Fire protection	/m^2	25€	Literature [94]
Profiled sheeting ComFlor75 0.9mm	/m^2	20€	Industry
Connectors			
M20 Injection bolt 8.8	/unit	3€	TU Delft
Coupler 10.8	/unit	3.1€	TU Delft
M20 bolt 8.8	/unit	0.75€	TU Delft
Washer	/unit	0.75€	TU Delft
Injected connector	**/unit**	**7.6€**	TU Delft
Non-injected connector	**/unit**	**5.35€**	TU Delft
Stud	**/unit**	**0.5€**	Industry

Table 5.1 **Material costs**

From Table 5.1, one can see that the price per demountable connector is higher by up to 15 times. This justifies the optimization of the shear connection as it reduces both material use and labour. The top flange, L-profile and profiled sheeting holes are assumed to costs roughly 2€, independent on the hole size. The top-flange and L-profile can be punched in an automatic process while the profiled sheeting can be either drilled or punched at the workshop or in-situ.

Manufacturing			**Source**
Casting and reinforcement installation	/m^2	15.00€	Industry
Decking for profiled sheeting slabs	/m^2	10.00€	Industry
Formwork, L-profile and anchors installation for prefabricated decks	/m^2	60.00€	Industry
Connectors installation before casting	/unit	1.00€	Industry
Stud welding	/unit	2.00€	Industry

Table 5.2 **Manufacturing costs**

The prefabricated decks require a labour intensive manufacturing to install the formwork, the welded L-profile, which protects the concrete edges, and the anchors. This translates in a high manufacturing cost.

In-situ work for the traditional profiled sheeting slabs was included in the manufacturing costs. During the experimental injection of the composite beams, a cost of 2.50€ was assumed to cover all the required material and labour. The price considers an injection time of 30 seconds per bolt if the resin mix preparation and injection is carried in parallel by two workers. A preliminary assessment indicates that a 70 ton crane [95] is sufficient for the installation of the prefabricated decks. The crane rental price is assumed based on [96] considering the average diesel price indicated by [97]. The installation of the decks requires one crane operator and two workers. Their assumed salary is 20€/hour.

In-situ work			**Source**
Resin injection • resin • consumable • release agent • labour	/unit	2.50€	TU Delft
Deck installation • crane 70t and fuel • 1 crane operator • 2 workers	/deck	185€	Literature [95-97]

Table 5.3 **In-situ costs**

The transportation costs were based on TU Delft market prices and literature review of [98-100]. For deck widths over 3.0m, there is a need of special transportation permit or the decks need to be transported vertically or inclined. This requirement will result in higher price for wider decks. Moreover, the length of the decks was limited to 10m. The transportation prices are influenced by many factors, so from project to project they can significantly change.

Transport			Source
Transport 3.6m wide deck	/unit	750€	TU Delft and literature [98-100]
Transport less than 3m wide deck	/unit	500€	

Table 5.4 **Transportation costs**

5.4 Office space case study

A first case study was performed to investigate the economic viability of two demountable steel-concrete composite flooring systems when compared to a traditional system. In order to satisfy the scopes of the case study, the following parameters were included in the design algorithm.

Flooring system	Parameters	Range
Traditional 1. profiled sheeting slab k_{sc}=80kN/mm **Demountable** 2. solid slab k_{sc}=55kN/mm 3. profiled sheeting slab k_{sc}=30kN/mm	Steel section	IPE, HEA, HEB
	Slab width	2.0m, 2.6m, 3.0m, 3.6m,
	Span	From 6 to 20m

Table 5.5 **Office space case study - parameters**

The thickness of the slabs is 120mm with the concrete class C30/37. The steel section is fabricated with S355 steel. The connector spacing for the solid slabs was set to 200mm while the geometry of the sheeting imposes a spacing of 300mm.

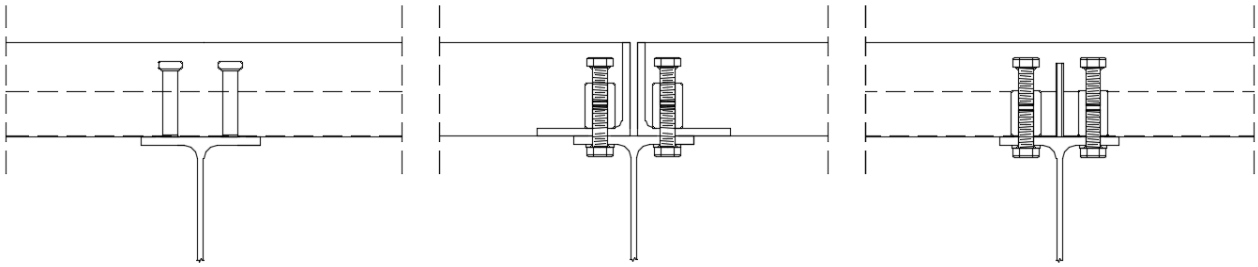

Figure 5.2 **Cross-section of composite beams (1 to 3 from left to right)**

5.4.1. Cost comparison

For the listed parameters, a number of roughly 13500 beams satisfy the design requirements out of approximately 400000 possible solutions. From Figure 5.3, it can be observed that there is a significant cost difference between the solid slab and profiled sheeting solution. This can be explained by the labour intensive manufacturing and the use of the angle profiles.

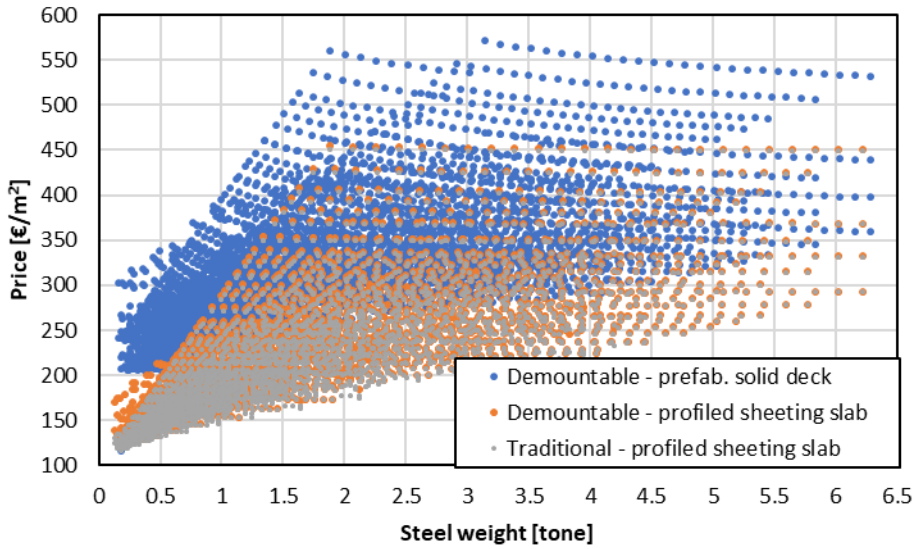

Figure 5.3 **Steel-weight against price - cost comparison**

From this point further, only the most economic design for a set of parameters will be presented.

Two clear trends can be observed when increasing the slab width and span (see Figure 5.4). For all three solutions the price per m^2 decreases while increasing the width of the slabs. However, as the span length increases, the price per m^2 rise.

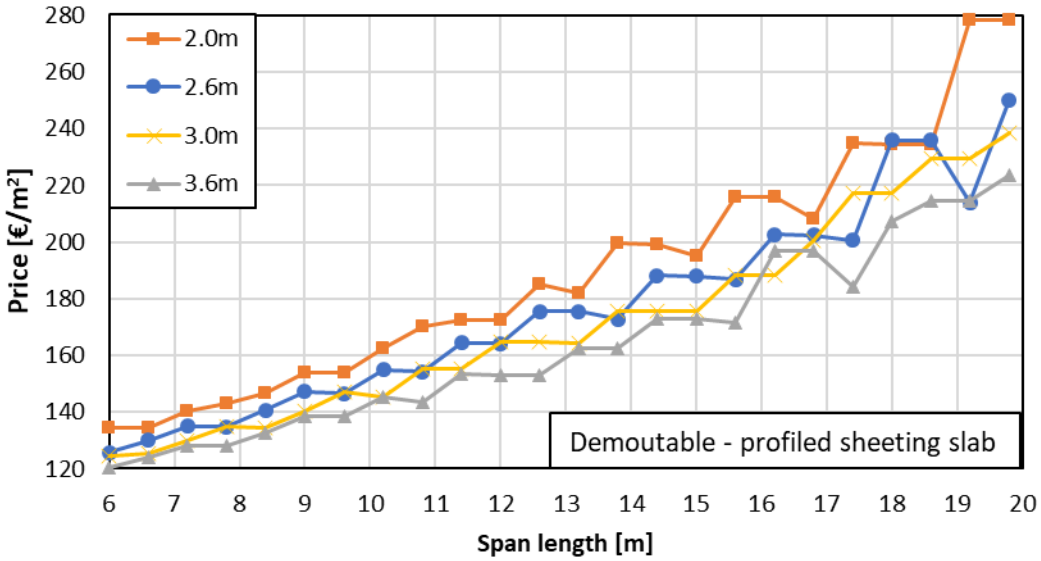

Figure 5.4 **Span length against price for demountable profiled sheeting slab - cost comparison**

Plotting the most economic solutions against the span length, the cost difference between the three systems can be observed (see Figure 5.5). As previously mentioned, the cost of the prefabricated solid decks is higher compared to the in-situ casted solutions. At a span of 10m the price of the solid slab solution significantly increases due to the imposed

transportation demands. A second change takes place at 16m due to the shift from slender IPE sections to stockier HEA. This is observed at 17.4m for the profiled sheeting slabs due to their reduced self-weight. The jump in prices of the demountable profiled sheeting between 15m and 18m is justified whether there is composite action (see Figure 5.7).

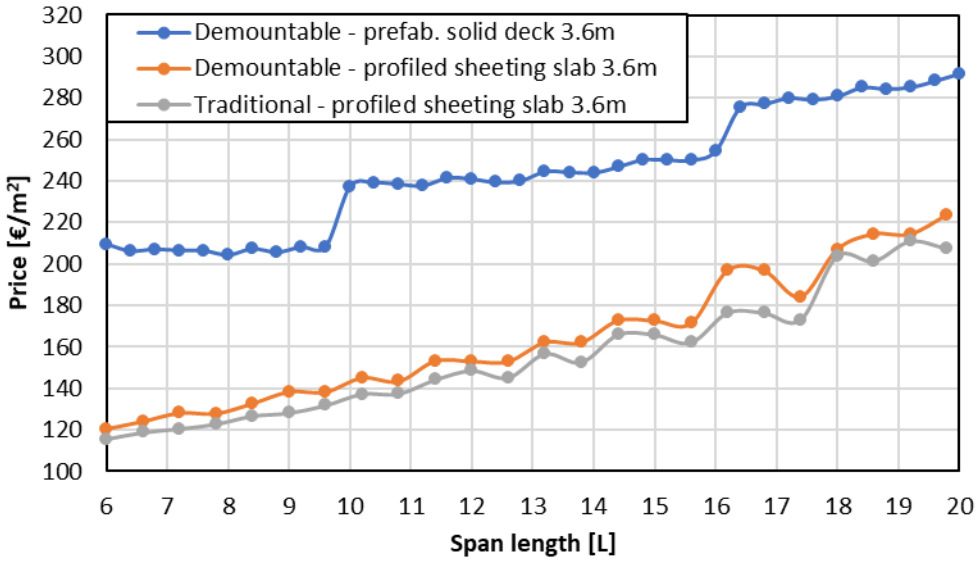

Figure 5.5 **Span length against price for 3.6m wide slabs - cost comparison**

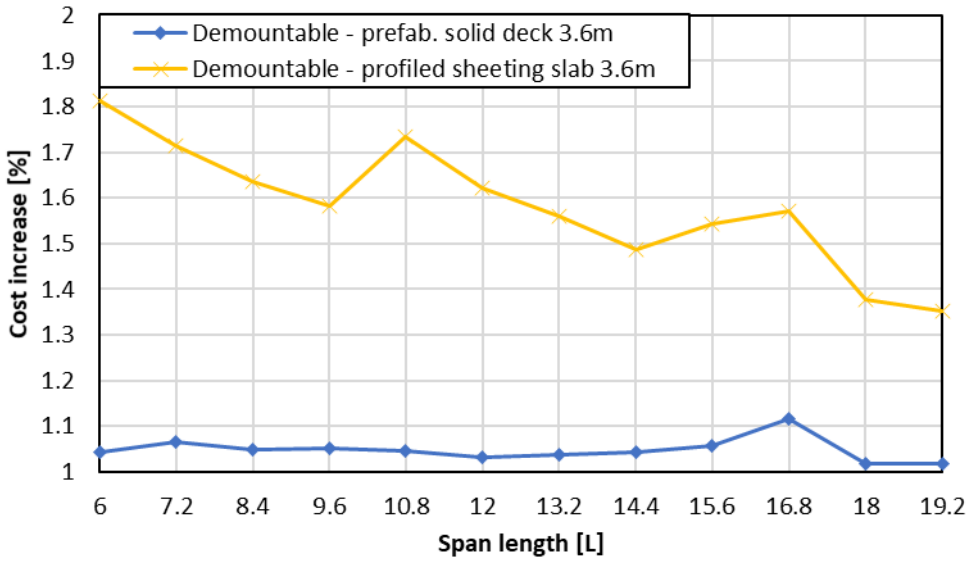

Figure 5.6 **Span length against cost increase for 3.6m wide slabs - cost comparison**

The cost increase of the demountable solutions is plotted at 1.2m intervals in Figure 5.6. For short spans, the cost increase of the prefabricated system is up to 80% and reduces to 35% for a span of 19.2m. On an average the cost increase for the prefabricated demountable system is 58% while it is 5% for the profiled sheeting. The profiled sheeting slab has a minor cost increase because it does not require a labour intensive manufacturing.

In Figure 5.7 the most economic solutions are presented by emphasizing whether the beam is composite or non-composite. Only 26% of the demountable profiled sheeting slabs are more economical as composite beams. This is explained by the low initial stiffness of 30kN/mm. For this reason, the economic viability of this system is at risk. On the other hand, using a shear connection will reduce the costs of the solid slab system in 86% of the cases. It was observed that the traditional system is always more economic as a composite beam.

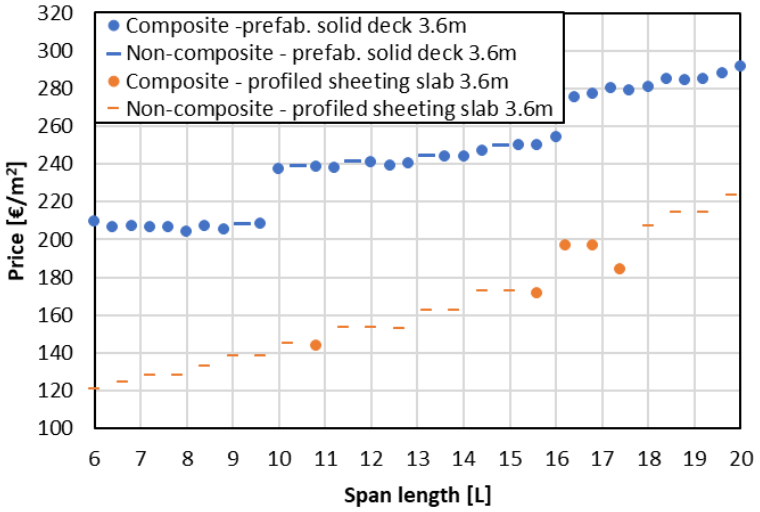

Figure 5.7 **Span length against price for composite and non-composite- cost comparison**

To further study whether the demountable profiled sheeting slab is a viable solution, a sensitivity study was carried out. The costs of the holes, connectors, injection and connector installation was reduced in two steps by 25% and 50%. In Table 5.6, the results of the sensitivity study are presented. A reduction of 50% to the costs attributed to connectors will increase the number of cases when composite action is justified. However, even for this significant cost reduction, the number of cases is limited to 42%. Future research on the bolt coupler connector in profiled sheeting slabs should focus on increasing the initial stiffness otherwise the system is not a competitive solution. The solid slab solution has a minor influence when the connector costs are reduced so an initial connector stiffness of 55kN/mm is reasonable to achieve an economic design.

Sensitivity study	Cases with composite action spans from 6m to 20m	
	Demountable - Prefab. solid deck	Demountable - profiled sheeting slab
0%	86%	26%
-25% of connector costs	89%	26%
-50% of connector costs	89%	42%

Table 5.6 **Connector costs influence on composite action**

5.5 Demountable car park optimization

Research and design verifications based on the car park layout from Figure 5.8 have been carried by [9, 36, 80, 101]. The cross-section of the composite beam and load-slip curve of the connector are presented in Figure 4.1 and Figure 2.45.

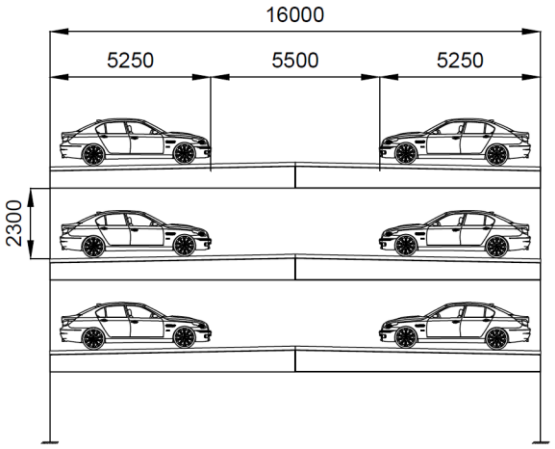

Figure 5.8 **Car park layout** [36]

A preliminary design has been performed by [36] however, without coupling the design with the construction costs. The taper slope was set to 1.9%, which translates in a 150mm increase of the mid-span height. Moreover, it was imposed by the manufacturer that the mid-span height of the steel section should not exceed 720mm. Since most of the deflection takes place during construction, the slab thickness is reduced to 120mm. To ensure proper support of the deck, the top flange width is kept at 300mm. The outcome of the design is presented in Figure 5.9. Considering the costs presented in the previous section, the final price per m^2 of flooring is equal to 208.2€. Based on this design, the composite beam will be optimized considering non-uniform connector arrangements and increased deck widths while accounting for the construction costs.

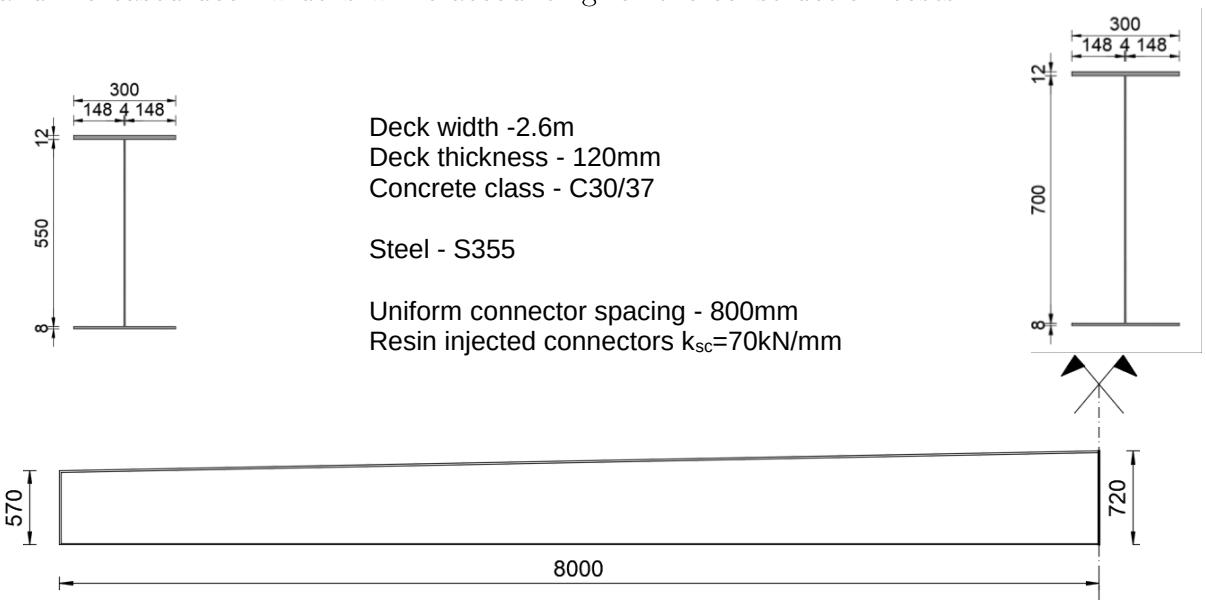

Figure 5.9 **Composite beam design according to** [36]

5.5.1. Cost analysis

According to the regulations of most European countries, car park structures with openings of equal or more than one third of the total surface area of outer walls do not have to fulfil any fire-resistance requirements [65]. For this reason, fire protection was not considered in the total cost of the structure. The remaining items listed in 5.3 were included.

In order to find the most economic beam design the following parameters were considered:

Parameter	Values
Deck width	2.6m, 3.0m and 3.6m
Section height at support	500mm up to 570mm
Top flange thickness	12mm up to 20mm
Bottom flange thickness	6mm up to 20mm
Web thickness	4mm and 5mm
Connector spacing	200mm

Table 5.7 **Car park optimization - parameters**

The top flange was designed so that it is classified as section class 3 in order to allow an elastic design. Because the shear connection is non-uniform, each deck will include two additional connectors at each quarter and mid-span to prevent uplift effects and to aid the construction process. It was confirmed that their number is sufficient to prevent vertical separation effects (see 4.7.2). These connectors will not be injected because of their minor contribution to the composite action. The initial stiffness of the connectors was reduced to 55kN/mm compared 70kN/mm used by [36] in their case study.

A total of 1550 beam designs which satisfy resistance and stiffness requirements were obtained using the design algorithm. The data set is presented in Figure 5.10 by plotting the steel weight of each beam section against the price per m^2. From the figure one can conclude that an increased deck width will reduce the price of the flooring. Moreover, the most economic design will not be the one having the lightest or heaviest steel section. This can be explained by the positive effect of composite interaction. As shown previously, an initial connector stiffness of 55kN/mm will yield an economic design as a composite beam.

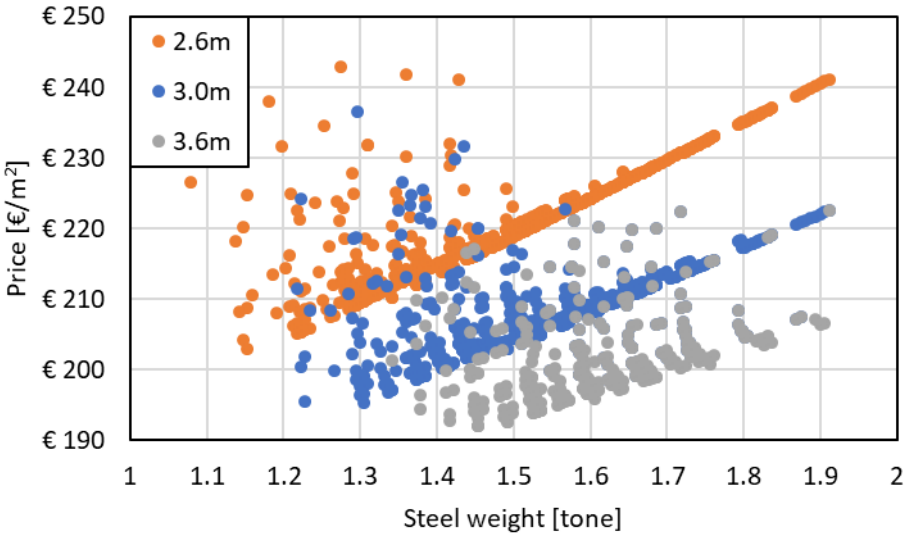

Figure 5.10 **Steel-weight against price - car park optimization**

From this point further, only the most economic design for a given set of parameters will be presented.

To further illustrate the beneficial effect of composite action, the number of connector pairs per half-span is plotted against the price in Figure 5.11. The cost decreases as connectors are added, however it increases if a certain number is exceeded. This can be explained by the exponential relation between number of connectors and beam stiffness (see Figure 4.26).

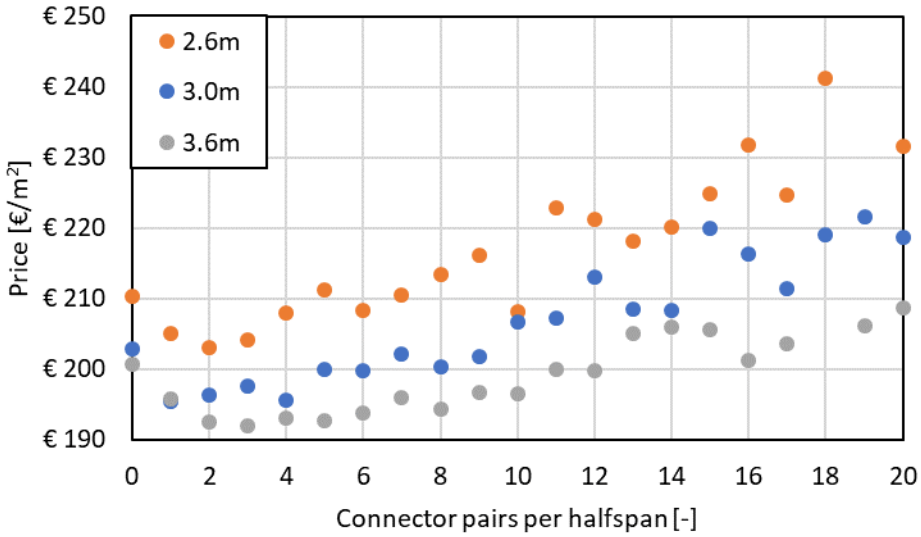

Figure 5.11 **Connector pairs against price - car park optimization**

The beneficial effect of increasing the deck width is presented in Figure 5.12. Increasing the deck width from 2.6m to 3.6m leads to a cost reduction of 5.4%.

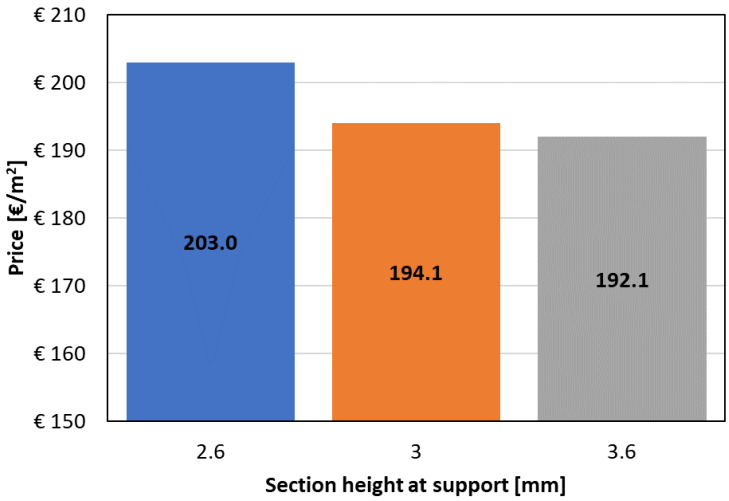

Figure 5.12 **Deck width against price - car park optimization**

Compared to the previous design of [36], the cost per m² reduced by 5.2€ for the same width or 16.1€ for a 3.6m wide deck. Therefore, using an optimized connector arrangement reduced the costs by 2.5%. Because the connector initial stiffness is lower by 22% compared to the case study of [36], the cost reduction was limited.

The lowest price per m² of demountable car park flooring is 192.1€. The top three solutions are presented in the table below. The most favourable solution is 1.c) as it uses the same thickness for the top and bottom flange. From a manufacturing point of view, this might further reduce the costs due to an easier steel supply. The number of connectors presented in the table represents only the ones which are injected.

Beam design	Section properties	Price
1.a)	t_{ft}= 12, t_{fb}= 18, t_w=4 h_0=570mm deck width=3.6m connectors/halfspan=6	192.1€
1.b)	t_{ft}= 14, t_{fb}= 16, t_w=4 h_0=570mm deck width=3.6m connectors/halfspan=6	
1.c)	**t_{ft}= 15, t_{fb}= 15, t_w=4** **h_0=570mm** **deck width=3.6m** **connectors/halfspan=6**	
2.a)	t_{ft}= 16, t_{fb}= 15, t_w=4 h_0=570mm deck width=3.6m connectors/halfspan=4	192.5€
2.b)	t_{ft}= 15, t_{fb}= 16, t_w=4 h_0=570mm deck width=3.6m	

	connectors/halfspan=4	
3.	t_{ft}= 14, t_{fb}= 15, t_w=4 h_0=570mm deck width=3.6m connectors/halfspan=10	192.7€

Table 5.8 **Top three most economic designs - car park optimization**

From Table 5.8, it can be concluded that an increased web thickness will not lead to a more economic design as expected.

Due to functionality or architectural constraints, it might be the case that the floor height is limited. In Figure 5.13 the flooring price was plotted against eight section depths considered. Reducing the steel height by 10mm will lead to a cost increase of 1%.

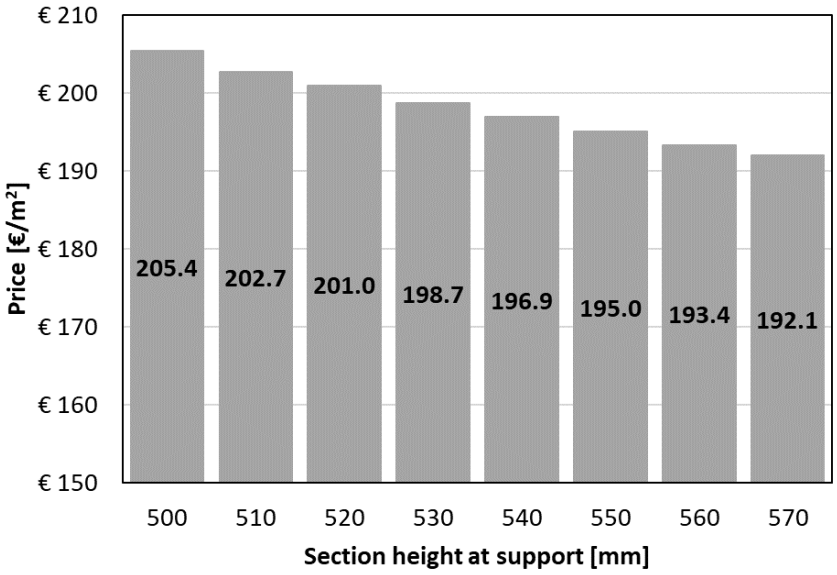

Figure 5.13 **Section height at support against price - car park optimization 3.6m width**

5.5.2. Sensitivity study

In order to carry out a sensitivity study the most influential cost contributions have to be identified. In Figure 5.14, the cost breakdown is presented for all three deck widths in three main categories. The most influential ones to the final cost are the material use (52% on average) followed by manufacturing (38% on average). The main categories are further broken down in Figure 5.15.

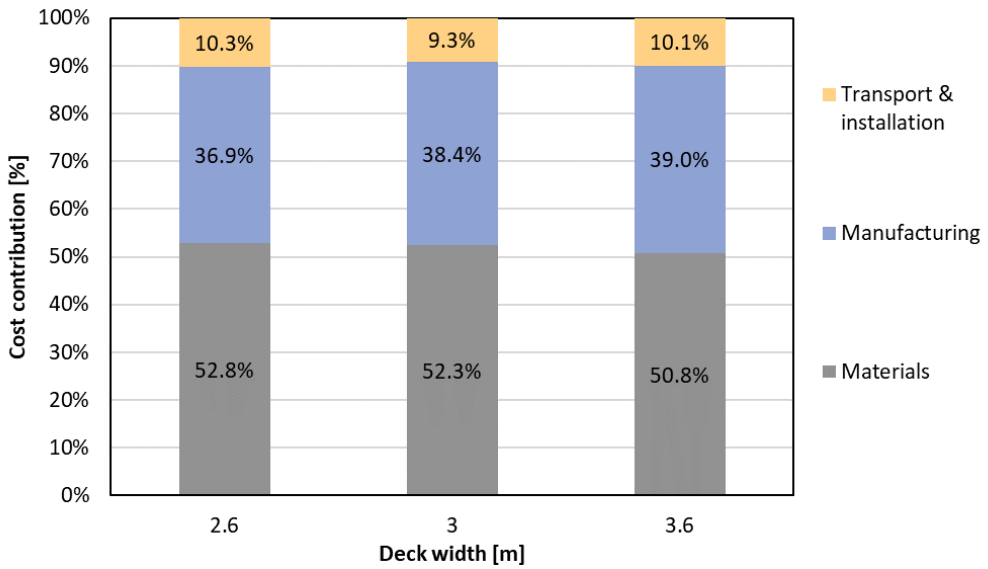

Figure 5.14 **Cost breakdown - car park optimization**

The steel beam has the highest cost contribution to the final cost (approximately 31% on an average). The design changed only at an unrealistic steel price of 1.25€ per kg. This can be explained by the low contribution of the connectors. Even though their unit price is very high, their contribution remains limited to 2.1%. Because of the high price per m^2 of the formwork, L-profile and anchor installation have a significant contribution to the final cost. Reducing or increasing this costs by 50% did not influence in any way the design. The final price of the demountable flooring system can be reduced by using smaller L-profiles. The material costs will decrease while the manufacturing would require less labour to install them.

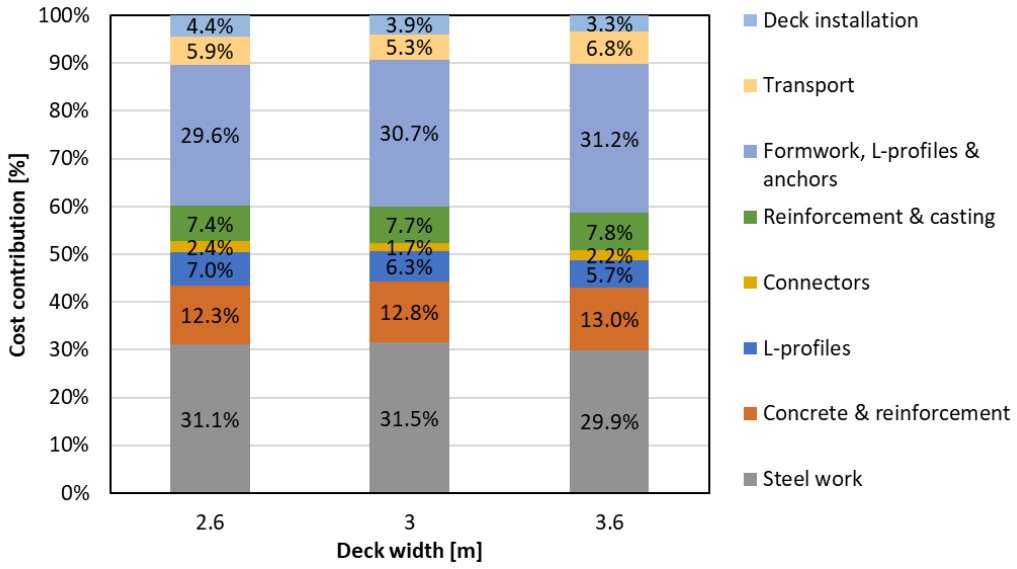

Figure 5.15 **Detailed cost-break down - car park optimization**

5.6 Conclusions

1. An extensive case study based on assumed cost inputs was performed using a design algorithm to generate 15500 beam solutions in order to study the economic viability of two demountable steel-concrete composite flooring systems. Using engineering reasoning to optimize the algorithm results in a reduced computational demand by a factor of 16.
2. The price of the demountable flooring constructed from large prefabricated decks increases compared to a non-demountable solution by 70% for spans ranging from 6m to 12m. For longer spans up to 20m the cost increase is 45%.
3. Demountable profiled sheeting slabs yield a minor average cost increase of roughly 5%. However, their suitability as composite beams is limited due to the low initial stiffness of the connector.
4. A sensitivity study varying the connector related costs, confirms the economic viability demountable composite flooring constructed with prefabricated concrete decks. On the other hand, even at a cost reduction of 50% for the connectors, having composite action in the case of demountable profiled sheeting slabs will result in the cheapest design for only 42% of the cases due to the low initial stiffness of the connector.
5. An optimized design of a demountable car park constructed in a combination of large demountable prefabricated decks and tapered beams yield a cost per m^2 of 192.1€. Using a non-uniform connector arrangement will reduce the costs up to 2.5%. Moreover, increasing the deck width by 1m from 2.6m will generate economic savings of up to 5.5%.
6. The highest influence on the final price of the demountable prefabricated flooring is given by the cost of the steel work (31%) followed by the labour intensive manufacturing (30.5%).
7. Out of the large number of beam designs, it was observed that most economical solution is not the one with the lightest or the heaviest steel section. This confirms that partial interaction can reduce the price of the flooring.
8. It was shown that only at an unrealistic steel price, the design of the composite beam will change. This is explained by the low cost contribution of the connectors of roughly 2%.

6 Conclusions and recommendations

In this section the main findings are presented and recommendations for future work are suggested based on the research carried throughout this thesis.

6.1 Conclusions

Experimental research confirms the construction and reusability of demountable composite flooring systems consisting of 2.6mx7.2m prefabricated decks is feasible. For the sake of reusability, the beam should be design within the elastic range. The disassembly of the system was successful even after the beam was plastically deformed.

The construction tolerances are achieved by using oversized holes. The hole clearance design is influenced by:

- Deformability of the beam during construction in the form of end slip,
- Imperfection of the beam and deck in longitudinal and transversal direction,
- Speed of execution and demounting.

The misalignment of the holes in longitudinal direction has the biggest influence on the hole size. In transversal direction, the installation of temporary bracing mitigated need for oversized holes. The used hole clearance of 12mm is justified by measurements and finite element results.

Resin injection of the large oversized holes allow for higher fabrication imperfections and reduced construction time while at the same time enables composite action of all the connectors under live loads. Experimental research confirms that overhead injection can be reliably and labour efficiently used for composite beams. The injection time can be significantly reduced to 30 seconds per bolt even at high ambient temperature by using a readily available manual caulking gun and a resin mix with a low viscosity.

Large lengthwise deviations of the decks require a mid-span gap in order to reduce the size of the hole clearance. It was shown by finite element analysis that if the gap is not filled before the live loads are applied, the actions will be resisted solely by the steel section.

The discontinuity of the decks at mid-span leads to differential displacement between the decks if only one side of the beam is loaded. Experimental research shows that a mid-span joint will reduce the differential displacement by up to 90% to 0.8mm at an axle load of 90kN.

The elastic and plastic beam behaviour is captured by finite element models based on push-out results of the demountable shear connector. The predicted deflection, stresses and curvature closely match experimental results. However, the interface slip is overpredicted which is in line with previous research of other authors. Extensive monitoring around the holes confirms that the concentrated load generated by the shear connector can be transferred to the top flange without local yielding.

The number of shear connectors is optimized by using a non-uniform arrangement to reduce construction costs. An extensive cost analysis of 15500 beam designs was performed by a design algorithm developed as part of this thesis. The cost efficiency of the bolt coupler connector in solid slabs was found in more than 85% of the studied cases when designing for composite action resulted in a more economical solution. The price of the demountable flooring constructed from large prefabricated decks increases compared to a non-demountable solution by 70% for spans ranging from 6m to 12m. For longer spans up to 20m the cost increase is 45%.

The demountable profiled sheeting slabs show a minor cost increase of 5% for spans ranging from 6m to 20m. However, due to the low initial stiffness of the connector, composite action gives an economic advantage only in a limited number of cases. Reducing the costs related to connectors to half resulted in 42% of the cases being more economical when designing the beam with composite action.

The optimized design of a demountable car park constructed in a combination of large demountable prefabricated decks and tapered beams is estimated to 192.1€/m^2 of floor surface. The highest influence on the final price of the demountable prefabricated flooring is the steel work (31%) followed by the labour intensive manufacturing (30.5%). The costs contribution of the connectors is approximately 2%.

6.2 Recommendations

1. **Feasibility of construction**

Current research could be extended to study the influence of deformations and imperfection of the columns on construction sequence.

The large out-of-straightness of the long angle profiles was measured during experiments. The position of the connectors is constrained by the L-profiles frames. The manufacturing process should be improved to reduce these deviations. A solution would be to use specially design formworks which would help in correcting the fabrication imperfections of the angle profile frame.

2. **Mechanical behaviour of composite beams**

The large deviation in terms of end-slip were recorded between experimental measurements and numerical analysis, in line with research of other authors [81, 82]. For this reason future research should focus on identifying the source of deviation and provide a reliable analytical model to predict the interface slip.

The researched mid-span span joint required a time consuming installation. A new design which can ensure a safe and easy assembly and disassembly should be investigated.

3. **Sustainability**

The thesis was limited only on assessing the economic viability of the demountable steel-concrete composite beams. Using the developed algorithm the composite beam should be designed having in mind both the cost and environmental inputs.

4. **Design algorithm**

The design algorithm can be further optimized by implementing a non-uniform segment discretization. Because the connectors are concentrated close to the supports the segment size can be increased towards the mid-span of the beam. This would significantly reduce computation time.

7 Bibliography

1. Nässén Jonas, Holmberg John, Wadeskog Anders, Nyman Madeleine, *Direct and indirect energy use and carbon emissions in the production phase of buildings: An input–output analysis.* Energy, 2007. **32**(9): p. 1593-1602.
2. Lizhen Huang, Guri Krigsvoll, Fred Johansen, Yongping Liu, Xiaoling Zhang, *Carbon emission of global construction sector.* Renewable and Sustainable Energy, 2018. **81**: p. 1906-1916.
3. https://ec.europa.eu/eurostat/statistics-explained/index.php/Waste_statistics%20. *Waste-statistics*. Accesed 25 September 2018.
4. (EEA), European Environmental Agency, *Review of Selected Waste Streams*, in *Waste Management & Research. Technical Report N.69*. 2002, European Environmental Agency, Copenhagen, Denmark.
5. C. K. Chau, W. K. Hui, W. Y. Ng, G. Powell, *Assessment of CO 2 emissions reduction in high-rise concrete office buildings using different material use options.* Resources, Conservation and Recycling, 2012. **61**: p. 22-34.
6. B. Addis, *Building with Reclaimed Components and Materials: A Design Handbook for Reuse and Recycling*. 2006: Earthscan.
7. Hopkinson P., Chen Han-Mei, Zhou Kan, Wang Yong, Lam Dennis, *Recovery and reuse of structural products from end-of-life buildings.* Proceedings of the Institution of Civil Engineers - Engineering Sustainability, 2018. **0**(0): p. 1-10.
8. Lu Aye, T. Ngo, R. Gammampila, P. Mendis, R. H. Crawford, *Life cycle greenhouse gas emissions and energy analysis of prefabricated reusable building modules.* Energy and Buildings, 2012. **47**: p. 159-168.
9. M. von Arnim, *Demountable composite steel-concrete flooring system for reuse*. 2017, Karlsruhe Institute of Technology: Karlsruhe.
10. R.P. JOHNSON, *Composite Structures of Steel and Concrete Beams, slabs, columns, and frames for buildings*. Third ed. 2004: Blackwell.
11. European Committee for Standardization, *EN1090-2: Execution of steel structures and aluminium structures - Part 2: Technical requirements for steel structures*. Brussels, Belgium: European Committee for Standardization (CEN), 2011.
12. L. Jaillon, C. S. Poon, Y. H. Chiang, *Quantifying the waste reduction potential of using prefabrication in building construction in Hong Kong.* Waste management, 2009. **29**(1): p. 309-320.
13. I.A. Gîrbacea, *Benefits of partial interaction. Cost of demountability*. 2018, Case study CIE4125, TU Delft.
14. Hayley Peterson, *A tsunami of store closings is about to hit the US — and it's expected to eclipse the retail carnage of 2017*, in *Business Insider*. 2018.

15. Kyle Arnold, *Retail apocalypse? Online competition drives store closings*, in *Orlando Sentinel*. 2017.
16. RICS, *Q2 2018: UK Commercial Property Market Survey, Punishing time for retail continues*. 2018.
17. Deric J. Oehlers, Mark A. Bradford, *COMPOSITE STEEL AND CONCRETE STRUCTURAL MEMBERS Fundamental Behaviour*. 1995: Pergamon.
18. European Committee for Standardization, *NEN-EN 1994-1-1. Eurocode 4: Design of composite steel and concrete structures - Part 1-1:General rules and rules for buildings.* . Brussels, Belgium: European Committee for Standardization (CEN), July 2005.
19. Deric J. Oehlers, Ninh T. Nguyen, Marfique Ahmed, Mark A. Bradford, *Partial interaction in composite steel and concrete beams with full shear connection.* Journal of Constructional Steel Research, 1997. **41**(2-3): p. 235-248.
20. Qing Quan Liang, *Analysis and Design of Steel and Composite Structures*. 2015: CRC Press.
21. K. S. Naraine, *"Slip and uplift effects in composite beams,"*. 1984, McMaster University,: Hamilton.
22. J.W.B. Stark, R. Abspoel, *CT4121 Steel Structures 3: Composite Constructions*. 2010: TU Delft.
23. European Committee for Standardization, *EN1993-1-1: Eurocode 3: Design of steel structures - Part 1-1: General rules and rules for buildings*. Brussels, Belgium: European Committee for Standardization (CEN), 2010.
24. Feldmann M., Heinemeyer C., Volling B, *Design Guide for Floor Vibrations*, L. ArcelorMittal, sections.arcelormittal.com, Editor.
25. European Committee for Standardization, *NEN-EN 1992-1-1. Eurocode 2: Design of concrete structures - Part 1-1: General rules and rules for buildings*. Standard, CEN, December 2004.
26. Normalisatie-instituut, Nederlands, *NEN-EN 1994-1-1+C1/NB. National annex to nen-en 1994-1-1+c1 Eurocode 4 design of composite steel and concrete structures – part 1-1: General rules and rules for buildings.* Nederlands Normalisatie-instituut, July 2012.
27. British Standards Institution, *British Standards Institution (1990), BS 5950: Structural Use of Steelwork in Buildings, Part 3 Design in Composite Construction. Section 3.1 Code of Practice for Design of Simple and Continuous Composite Beams including Amendments 2010*. British Standards Institution (1990)
28. American Institute of Steel Construction, *AISC 360-10, Specification for Structural Steel Buildings, Manual of Steel Construction*. American Institute of Steel Construction (2010).

29. Lawson R.M, Lam Dennis, Aggelopoulos E.S., Nellinger S.,, *Serviceability performance of steel-concrete composite beams.* Proceedings of the Institution of Civil Engineers - Structures and Buildings, 2017. **170**(2): p. 98-114.
30. Newmark N.M, Siess C. P and Viesst I.M, *Tests and Analysis of Composite Beams with Incomplete Shear Connection.* Proc. Soc. Experimental Stress Analysis 1951. **9**(1).
31. D. Lam, K. S. Elliott, D. A. Nethercot, , *Designing composite steel beams with precast concrete hollow-core slabs.* Proceedings of the Institution of Civil Engineers - Structures and Buildings, 2000. **140**(2): p. 139-149.
32. Ulf Arne Girhammar, Dan H.Pan, *Exact static analysis of partially composite beams and beam-columns.* International Journal of Mechanical Sciences, 2007. **49**(2): p. 239-255.
33. Jianguo Nie, C. S. Cai, *Steel–Concrete Composite Beams Considering Shear Slip Effects.* Journal of Structural Engineering, 2003. **129**(4).
34. Girhammar, Ulf Arne, *A simplified analysis method for composite beams with interlayer slip.* International Journal of Mechanical Sciences, 2009. **51**(7): p. 515-530.
35. Ulf Arne Girhammar, Vijaya K. A. Gopu, *Composite Beam-Columns with Interlayer Slip—Exact Analysis.* Journal of Structural Engineering, 1993. **119**(4).
36. M. P. Nijgh, M. Veljkovic, M. Pavlovic,, *Flexible shear connectors in a tapered composite beam optimized for reuse.* , in *Annual International Conference Proceedings 6th Annual International Conference on Architecture and Civil Engineering (ACE 2018)*, M.S.T. Anderson, Editor. 2018: Singapore : Global Science and Technology Forum.
37. Nijgh M., Veljkovic M., *Static and free vibration analysis of tapered composite beams optimised for reuse.* . Steel and Composite Structures, under review.
38. Braendstrup., C., *Conceptual design of a demountable, reusable composite flooring system. Structural behaviour and environmental advantages.* . 2017, Delft University of Technology.
39. Shim, Chang Su, *Experiments on limit state design of large stud shear connectors.* KSCE Journal of Civil Engineering, 2004. **8**(3): p. 313-318.
40. Jin-Hee Ahn, Chan-Goo Lee, Jeong-Hun Won, Sang-Hyo Kim, *Shear resistance of the perfobond-rib shear connector depending on concrete strength and rib arrangement.* Journal of Constructional Steel Research, 2010. **66**(10): p. 1295-1307.
41. Thi Hai Vinh Chu, Van Phuoc Nhan Le, Duy Kien Dao, Thanh Hai Nguyen,Duc Vinh Bui,, *Shear Resistance Behaviors of a Newly Puzzle Shape of Crestbond Rib Shear Connector: An Experimental Study.* Proceedings of the 4th Congrès International de Géotechnique - Ouvrages -Structures, 2017: p. 243-253.

42. Ali Shariati, N. H. Ramli Sulong, Meldi Suhatril, Mahdi Shariati, *Various types of shear connectors in composite structures: A review.* International Journal of Physical Sciences, 2012. **7**(22): p. 2876-2890.
43. *Hilti X-HVB system. Solutions for shear connections.* Hilti Corporation: Liechtenstein.
44. Michel Crisinel, *Partial-interaction analysis of composite beams with profiled sheeting and non-welded shear connectors.* Journal of Constructional Steel Research, 1990. **15**(1-2): p. 65-98.
45. Mahmood Md Tahir, Poi Ngian Shek, Cher Siang Tan, *Push-off tests on pin-connected shear studs with composite steel-concrete beams.* Construction and Building Materials 2009. **23** p. 3024-3033.
46. European Committee for Standardization, *EN1993-1-8: Eurocode 3: Design of steel structures - Part 1-8: Design of joints, Brussels,.* Belgium: European Committee for Standardization (CEN), 2010.
47. Jean-Pierre Jaspart, Klaus Weynand, *Design of joints in steel and composite structures.* 2016: ECCS - European Convetion for Constructional Steelwork.
48. Marko Pavlović, Milan Veljković, *Prefabricated demountable concrete and FRP decks in composite structures*
49. Marko Pavlović, Zlatko Markovića, Milan Veljković, Dragan Buđevaca, *Bolted shear connectors vs. headed studs behaviour in push-out tests.* Journal of Constructional Steel Research, 2013. **88**: p. 134-149.
50. Dallam LN, *High Strength Bolts Shear Connectors — Pushout Tests.* ACI J Proc, 1968. **9**: p. 767-9.
51. British Standard Institution, *BS 5400-5: Steel, concrete and composite bridges - Part 5: Code of practice for the design of composite bridges.* British Standard Institution, United Kingdom, 2005.
52. Xinpei Liu, Mark A. Bradford, Michael S. S. Lee, *Behavior of High-Strength Friction-Grip Bolted Shear Connectors in Sustainable Composite Beams.* Journal of Structural Engineering, 2015. **141**(6).
53. A. Kozma, C. Odenbreit, M. V. Braun, M. Veljkovic and M. P. Nijgh, , *Push-out tests on demountable shear connectors of steel-concrete composite structures* in *Proceedings of the 12th international conference on Advances in Steel-Concrete Composite Structures.* 2018: Valencia.
54. M.S. Pavlović, *Resistance of bolted shear connectors in prefabricated steel-concrete composite decks. PhD thesis, .* 2013, University of Belgrade.
55. X. H. Dai, D. Lam, and E. Saveri, *Effect of Concrete Strength and Stud Collar Size to Shear Capacity of Demountable Shear Connectors.* Journal of Structural Engineering, 2015. **141**(11).
56. N. Rehman, D. Lam, X. Dai, A.F. Ashour, *Experimental study on demountable shear connectors in composite slabs with profiled decking.* Journal of Constructional Steel Research, 2016. **122**: p. 178-189.

57. Dennis Lam, Xianghe Dai, Ashraf Ashour, Naveed Rehman, *Recent research on composite beams with demountable shear connectors.* Steel Construction, 2017. **10**(2): p. 125-134.
58. Naveed Rehman, Dennis Lam, Xianghe Dai, Ashraf Ashour, *Testing of composite beam with demountable shear connectors.* Proceedings of the Institution of Civil Engineers - Structures and Buildings, 2018. **171**(1): p. 3-16.
59. Dennis Lam, Xianghe Dai, *Demountable Shear Connectors for Sustainable Composite Construction* in *The 2013 World Congress on Advances in Structural Engineering and Mechanics (ASEM13).* 2013: Jeju, Korea.
60. Sarri, Alkioni, *Assessment of demountable steel-concrete composite shear connector system with injection bolts.* unpublished.
61. Nijgh M., Gîrbacea A., Veljkovic M. , *Elastic behaviour of a reusable tapered composite beam. Engineering Structures.* under review.
62. REUSE AND DEMOUNTABILITY USING STEEL STRUCTURES AND THE CIRCULAR ECONOMY, *Report on shear behaviour of demountable connectors in profiled composite slabs (Push tests).*
63. Alina Gritcenko, *Towards demountable composite steel-concrete flooring system.* unpublished.
64. Jacques Brozzetti, *Design development of steel-concrete composite bridges in France.* Journal of Constructional Steel Research, 2000. **55**(1-3): p. 229-243.
65. ArcelorMittal, *Car Parks in Steel.* 2014, ArcelorMittal - Commercial Sections, Esch-sur-Alzette.
66. *Techical Annex of REDUCE project (Reuse and Demountability using Steel Structures and the CircularEconomy).* 2016, RFCS proposal.
67. Nijgh, M., von Arnim, M., Pavlovic, M., & Veljkovic, M. , *Preliminary Assessment of a Composite Flooring System for Reuse*, in *8th International Conference on Composite Construction in Steel and Concrete.* 2017.
68. Nijgh, M. P., *New Materials for injected bolted connections: A feasibility study for demountable connections.* . 2017, Delft University of Technology.
69. Nijgh M., Xin H., & Veljkovic M.,, *Non-linear hybrid homogenization method for steel-reinforced resin.* Construction and Building Materials, 2018. **182**: p. 324-333.
70. Kolstein H., Li J., Koper A., Gard W., Nijgh M., & Veljkovic M.,, *Behaviour of double shear connections with injection bolts.* Steel Construction - Design and Research, 2017. **10**(4): p. 287-294.
71. Xin H., Nijgh M., Veljkovic M.,, *Computational homogenization method on steel reinforced resin used in the injected bolted connections*, in *13th World Congress in Computational Mechanics.* 2018.
72. VIBA. *RenGel© SW 404 / Ren© HY 2404 or HY 5159.* Accesed 11 September 2018; Available from:

https://www.viba.nl/media/files/resources/176099%2022172rengel-sw-404_hy-2404_hy-5159_eur_e1.pdf.

73. *RenGel SW404*. Accesed 11 September 2018; Available from: https://www.mouldlife.net/rengel--sw-404-1372-p.asp.
74. *REN HY 2404 Tube 50g - Samaro*. Accesed 11 September 2018; Available from: https://samaro.fr/fr/gel-coat/hu385-ren-hy-2404-pot-500-g-3819.html.
75. *Ren HY 5159*. Accesed 11 Septemeber 2018; Available from: https://shop.goessl-pfaff.de/art/6hy515901.
76. *acmos-82-aerosol*. Accesed 11 September 2018; Available from: https://www.formx.eu/sealer--release/acmos-82-aerosol---400gr.php.
77. *Makita XGC01Z 18V LXT 10-Ounce Caulk and Adhesive Gun*. Accesed 11 September 2018; Available from: https://www.amazon.com/Makita-XGC01Z-10-Ounce-Caulk-Adhesive/dp/B00OYVDOSG.
78. M. C. Moynihan, J. M. Allwood, *Viability and performance of demountable composite connectors.* Journal of Constructional Steel Research, 2014. **99**: p. 47-56.
79. L. Wang, M. D. Webster, J. F. Hajjar, , *Behavior of sustainable composite floor systems with deconstructable clamping connectors*, in *Proceedings of the 8th International Conference on Composite Construction in Steel and Concrete*. 2017: Jackon, WY.
80. G. Maheninggalih, *A demountable sturctural system of multi-storey building: Case study of car park building*. 2017, Delft University of Technology.
81. Gogoi, S., *Interaction phenomena in composite beams and plates*. 1964, Imperial College of Science and Technology.
82. G. Hanswille, M. Porsch and C. Ustundag, *Studies of the lifetime of cyclically loaded steel-concrete composite bridges.* Steel Construction, 2010. **3**(3): p. 140-148.
83. European Committee for Standardization, *NEN-EN 1991-1-1+C1. Eurocode 1: Actions on structures - Part 1-1: General actions - Densities, self-weight, imposed loads for buildings.* . CEN, December 2011.
84. T. M. Roberts, *Finite difference analysis of composite beams with partial interaction.* Computers & Structures, 1985. **21**(3): p. 469-473.
85. J. P. Lin, G. Wang, G. Bao and R. Xu,, *Stiffness matrix for the analysis and design of partial-interaction composite beams.* Construction and Building Materials, 2017. **159**: p. 761-772.
86. Sawade, R. Eligehausen and G., *A fracture mechanics based description of the pull-out behavior of headed studs embedded in concrete*.
87. Joshua M. Mouras, James P. Sutton, Karl H. Frank, Eric B. Williamson,, *The Tensile Capacity of Welded Shear Stud*. 2008.

88. Hirokazu Hiragi, Shigeyuki Matsui, Takashi Sato, Abubaker AL-Sakkaf, Shigeru Ishizaki, Yashuiro Ishihara, *Pull-out and shear strength equations for headed studs considering edge distance*. 2001.
89. *Genetic algorithm*. Accessed 10 October 2018; Available from: https://en.wikipedia.org/wiki/Genetic_algorithm.
90. *Binary search algorithm*. Accessed 10 October 2018; Available from: https://en.wikipedia.org/wiki/Binary_search_algorithm.
91. *Brute-force search*. Accessed 10 October 2018; Available from: https://en.wikipedia.org/wiki/Brute-force_search.
92. European Committee for Standardization, *NEN-EN 1993-1-5 Eurocode 3: Design of steel structures - Part 1-5: Plated structural elements*. CEN, October 2006.
93. European Committee for Standardization, *NEN-EN 1990 Eurocode - Basis of structural design*. CEN, december 2002.
94. Tata Steel, BCSA, *Steel construction cost*. 2015.
95. Liebherr, *Mobile crane - LTM 1070-4.2*.
96. Raimondi, *Rental survey 2017*.
97. *Netherlands Diesel prices*. Accessed 3 October 2018; Available from: https://www.globalpetrolprices.com/Netherlands/diesel_prices/.
98. Moiseenko, Ivan, *Economical feasibility of prefabricated solutions in healthcare design and construction industry*. 2017, TU Delft.
99. Lawson M., Ogden R., Goodier C.,, *Design in Modular Construction*. 2014, London: CRC Press.
100. TRANSPORT, EUROPEAN COMMISSION DIRECTORATE-GENERAL FOR ENERGY AND, *European Best Practice Guidelines for Abnormal Road Transports*.
101. Alina Gritsenko, *Structural design and construction simulation of a composite car park with demountable shear connectors. Case study CIE4125*. 2018, TU Delft.

8 Appendix - Additional measurements

In addition to the previously explained deviations, a set of two other measurements were performed. They have no influence on the feasibility of assembly and should only be regarded as informative.

8.1 Depth imperfection

The depth was measured at each stiffener and connector position. Since the flanges were welded continuously to the web only on one side, its influence must be quantified by measuring the left and right side of the section. The measurement was carried with regular measuring tape at the tip of the flange.

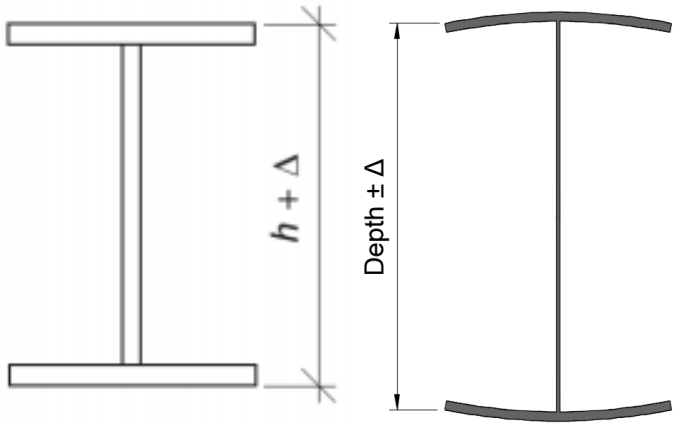

Figure 8.1 **Depth imperfection according to [11] and measuring procedure**

In the graphs below the depth deviation was plotted separately for the welded and unwelded side. The average value for the welded side is -2.85mm while for the unwelded is -6.21mm.

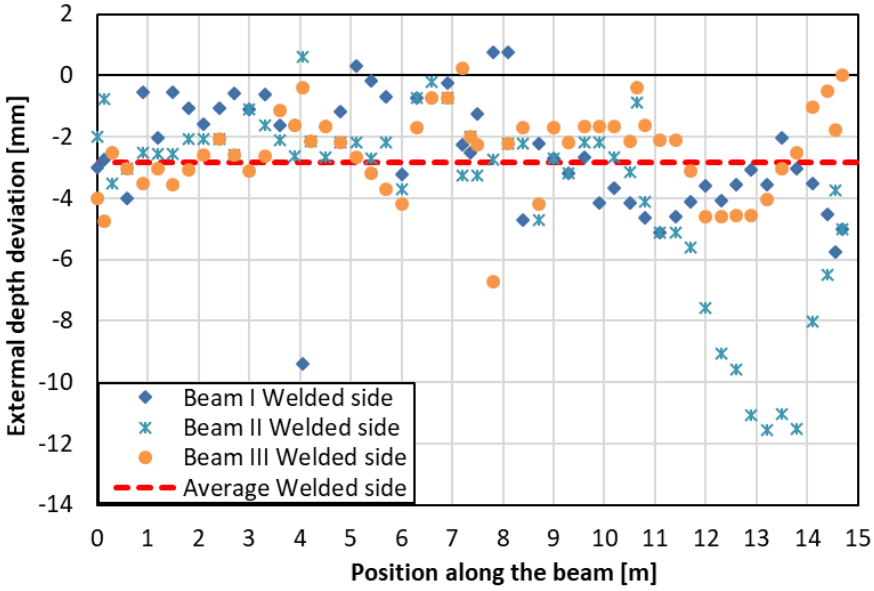

Figure 8.2 **Measurements external depth deviation - welded side**

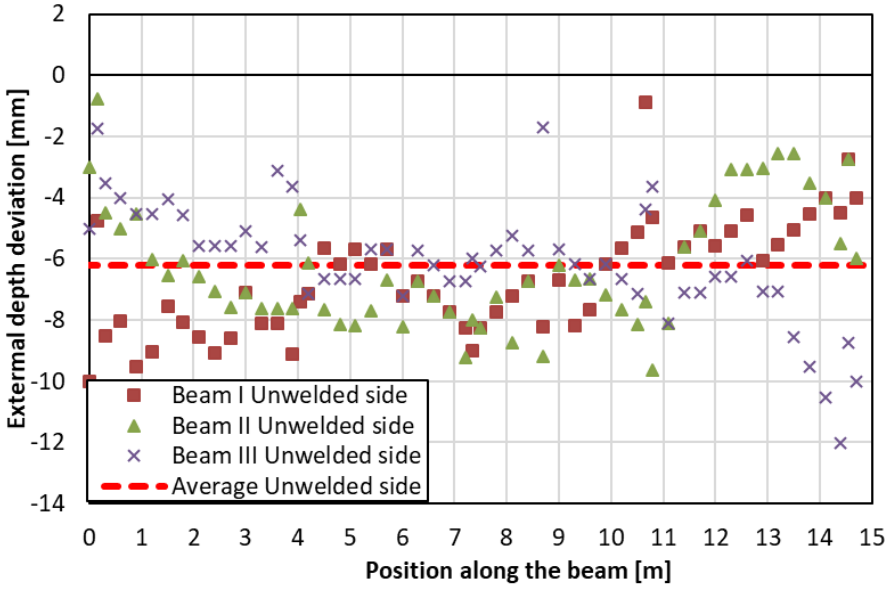

Figure 8.3 **Measurements external depth deviation - unwelded side**

8.2 Web eccentricity

The web eccentricity was measured at each stiffener and connector position on the unwelded side both at the top and bottom. The measurement was performed using regular measuring tape at the tip of the flange.

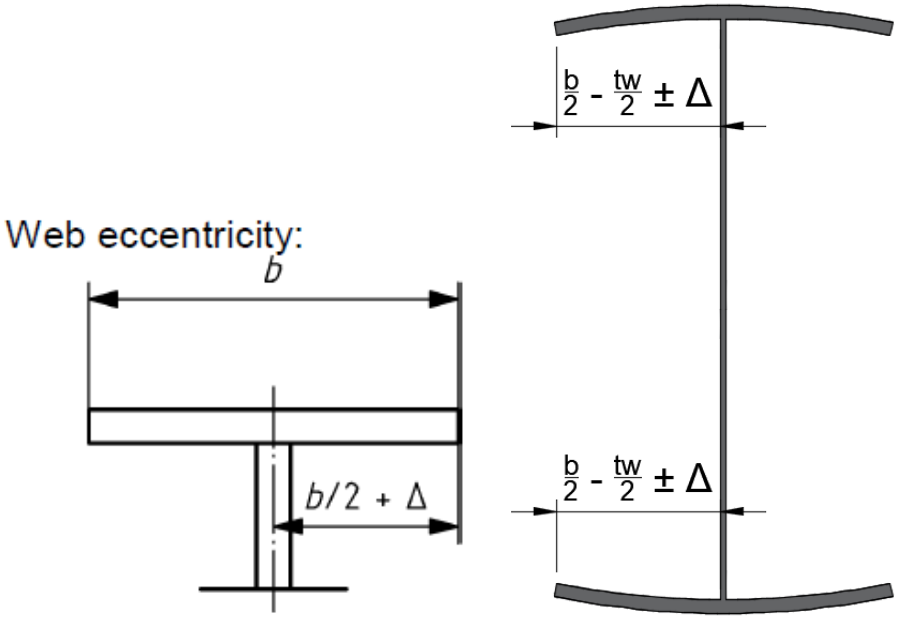

Figure 8.4 **Web eccentricity imperfection according [11] and measuring procedure**

The web exccentricity of the top flange is 0.85mm while the bottom 1.08mm.

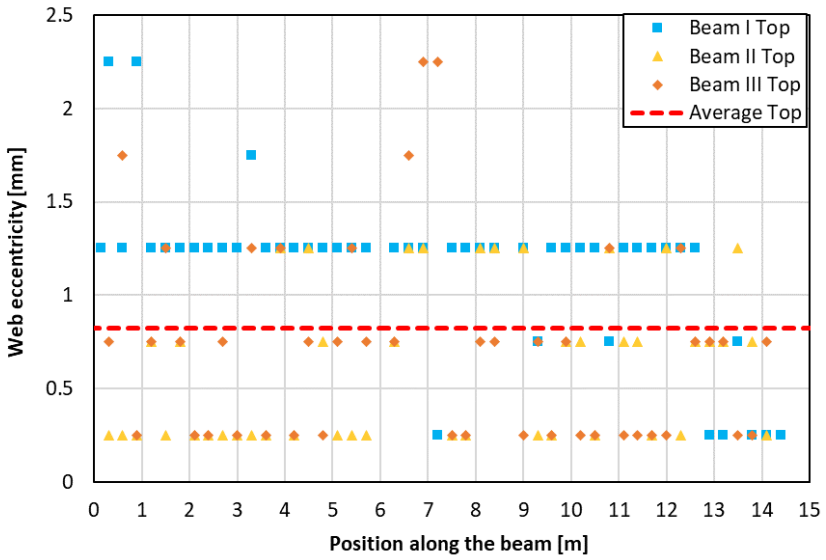

Figure 8.5 **Measured web eccentricity - top flange**

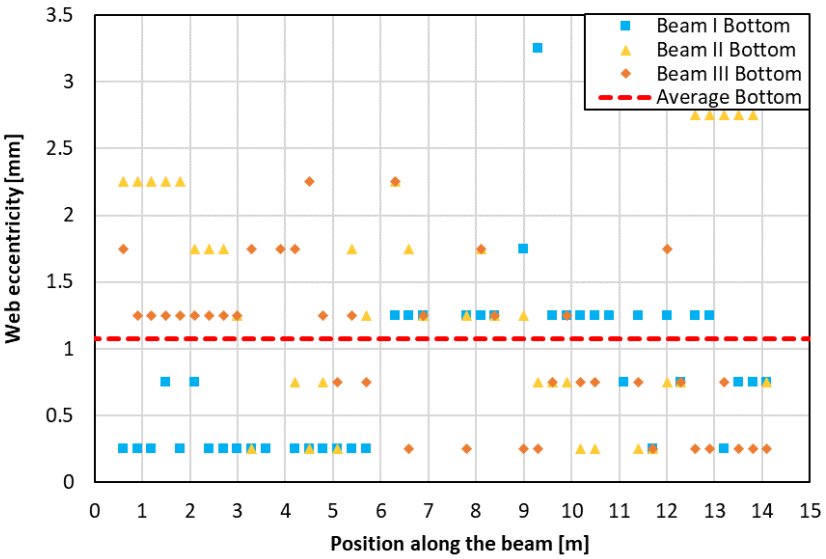

Figure 8.6 **Measured web eccentricity - bottom flange**

9 Appendix - experimental measuring equipment

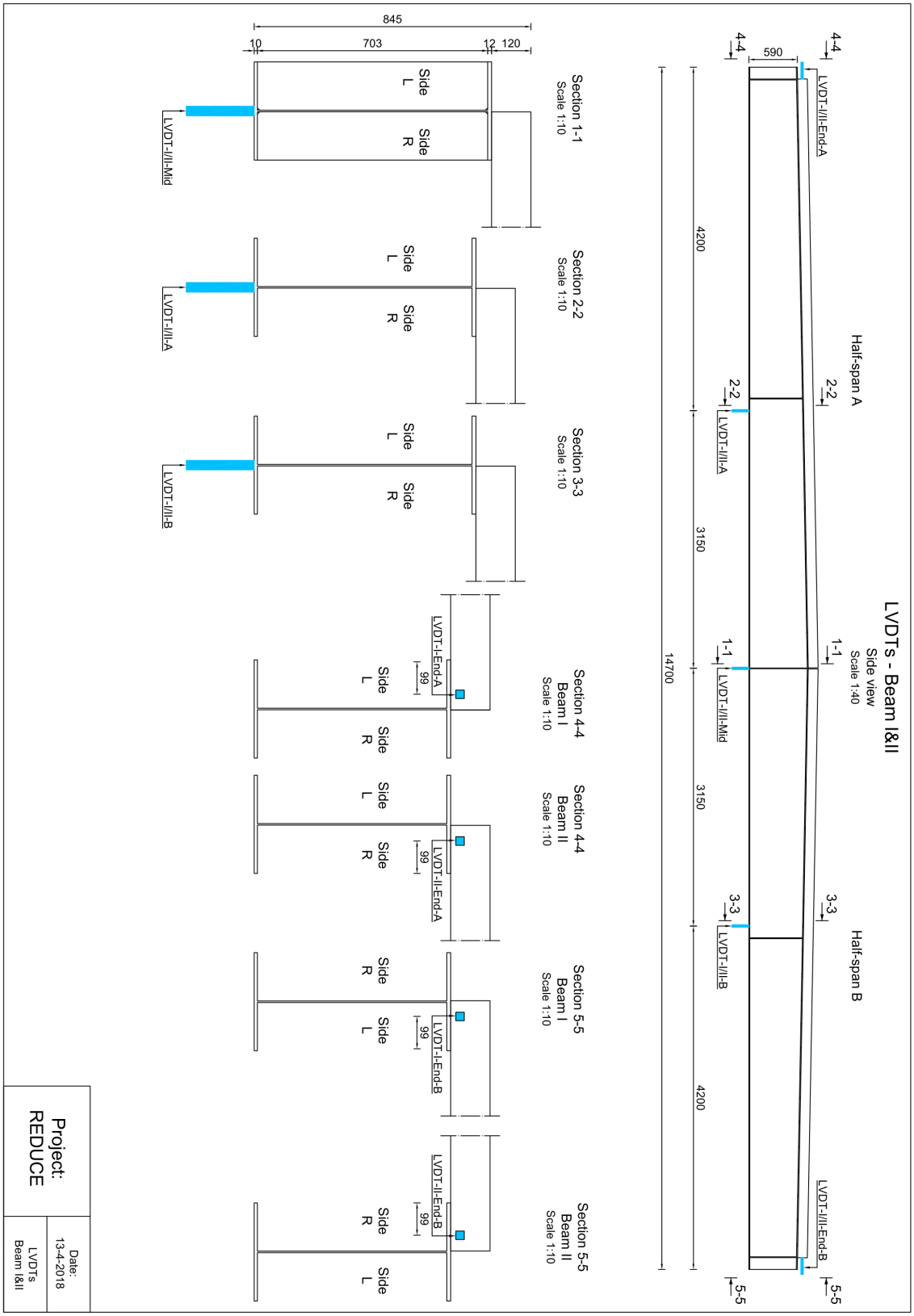
LVDTs - Beam I&II
Side view
Scale 1:40
Half-span A
Half-span B
4-4
590
LVDT-I/II-End-A
2-2
LVDT-I/II-A
1-1
LVDT-I/II-Mid
3-3
LVDT-I/II-B
LVDT-I/II-End-B
5-5
4200
3150
3150
4200
14700
Section 1-1
Scale 1:10
845
10
703
12
120
Side L
Side R
LVDT-I/II-Mid
Section 2-2
Scale 1:10
LVDT-I/II-A
Section 3-3
Scale 1:10
LVDT-I/II-B
Section 4-4
Beam I
Scale 1:10
LVDT-I-End-A
99
Section 4-4
Beam II
Scale 1:10
LVDT-II-End-A
Section 5-5
Beam I
Scale 1:10
LVDT-I-End-B
Section 5-5
Beam II
Scale 1:10
LVDT-II-End-B
Project:
REDUCE
Date:
13-4-2018
LVDTs
Beam I&II

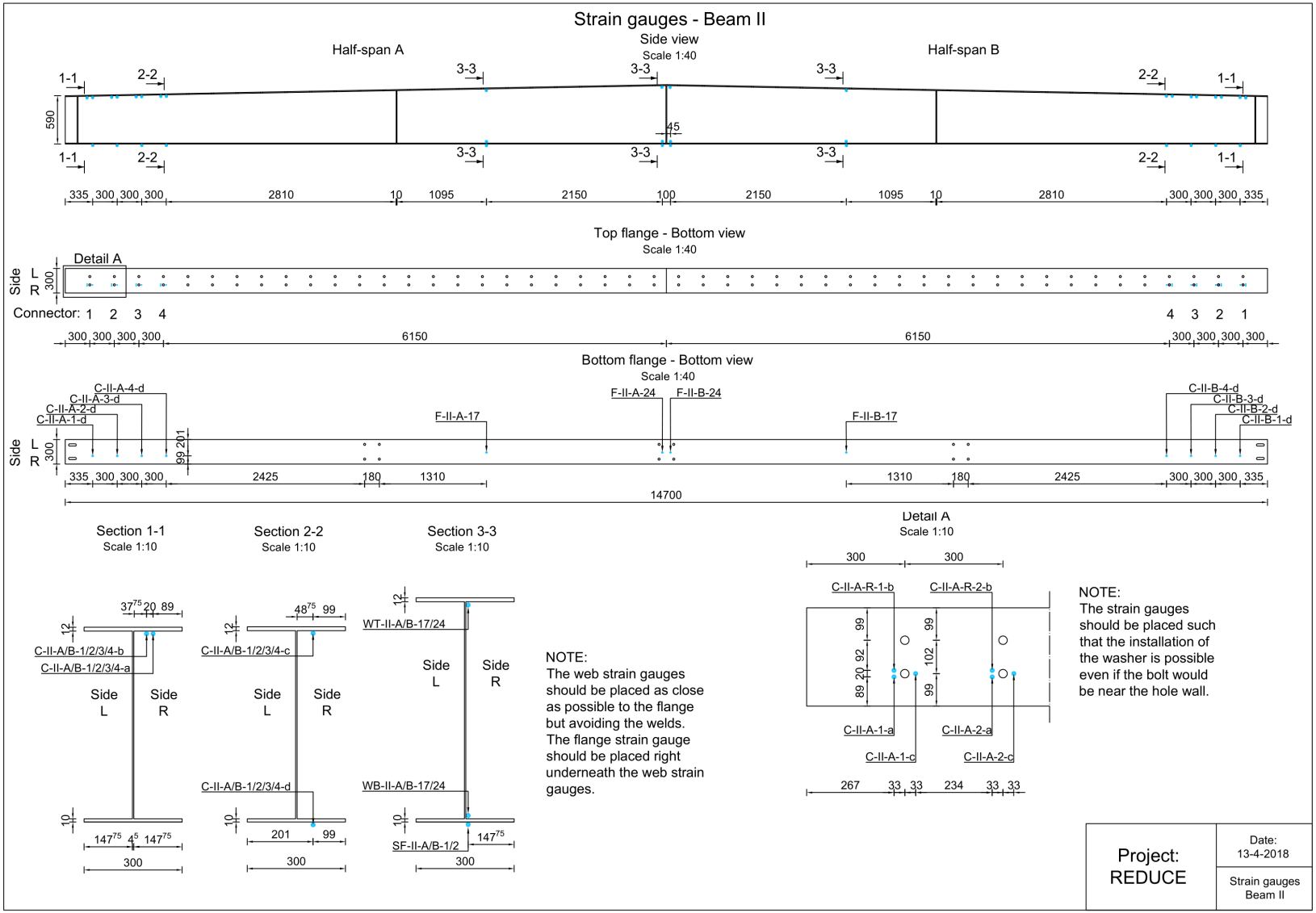
Strain gauges - Beam II
Side view
Scale 1:40
Half-span A
Half-span B
1-1
2-2
3-3
590
45
335 300 300 300 2810 10 1095 2150 100 2150 1095 10 2810 300 300 300 335
Top flange - Bottom view
Scale 1:40
Detail A
Side L R
300
Connector: 1 2 3 4 4 3 2 1
300 300 300 300 6150 6150 300 300 300 300
Bottom flange - Bottom view
Scale 1:40
C-II-A-4-d
C-II-A-3-d
C-II-A-2-d
C-II-A-1-d
F-II-A-24
F-II-B-24
F-II-A-17
F-II-B-17
C-II-B-4-d
C-II-B-3-d
C-II-B-2-d
C-II-B-1-d
99 201
335 300 300 300 2425 180 1310 1310 180 2425 300 300 300 335
14700
Section 1-1
Scale 1:10
Section 2-2
Scale 1:10
Section 3-3
Scale 1:10
37 75 20 89
48 75 99
12
10
C-II-A/B-1/2/3/4-b
C-II-A/B-1/2/3/4-a
C-II-A/B-1/2/3/4-c
C-II-A/B-1/2/3/4-d
WT-II-A/B-17/24
WB-II-A/B-17/24
SF-II-A/B-1/2
Side L
Side R
147 75 5 147 75
201 99
300
Detail A
Scale 1:10
C-II-A-R-1-b
C-II-A-R-2-b
C-II-A-1-a
C-II-A-2-a
C-II-A-1-c
C-II-A-2-c
99 92 20 89
102
267 33 33 234 33 33
NOTE:
The web strain gauges should be placed as close as possible to the flange but avoiding the welds. The flange strain gauge should be placed right underneath the web strain gauges.
NOTE:
The strain gauges should be placed such that the installation of the washer is possible even if the bolt would be near the hole wall.
Project:
REDUCE
Date:
13-4-2018
Strain gauges
Beam II

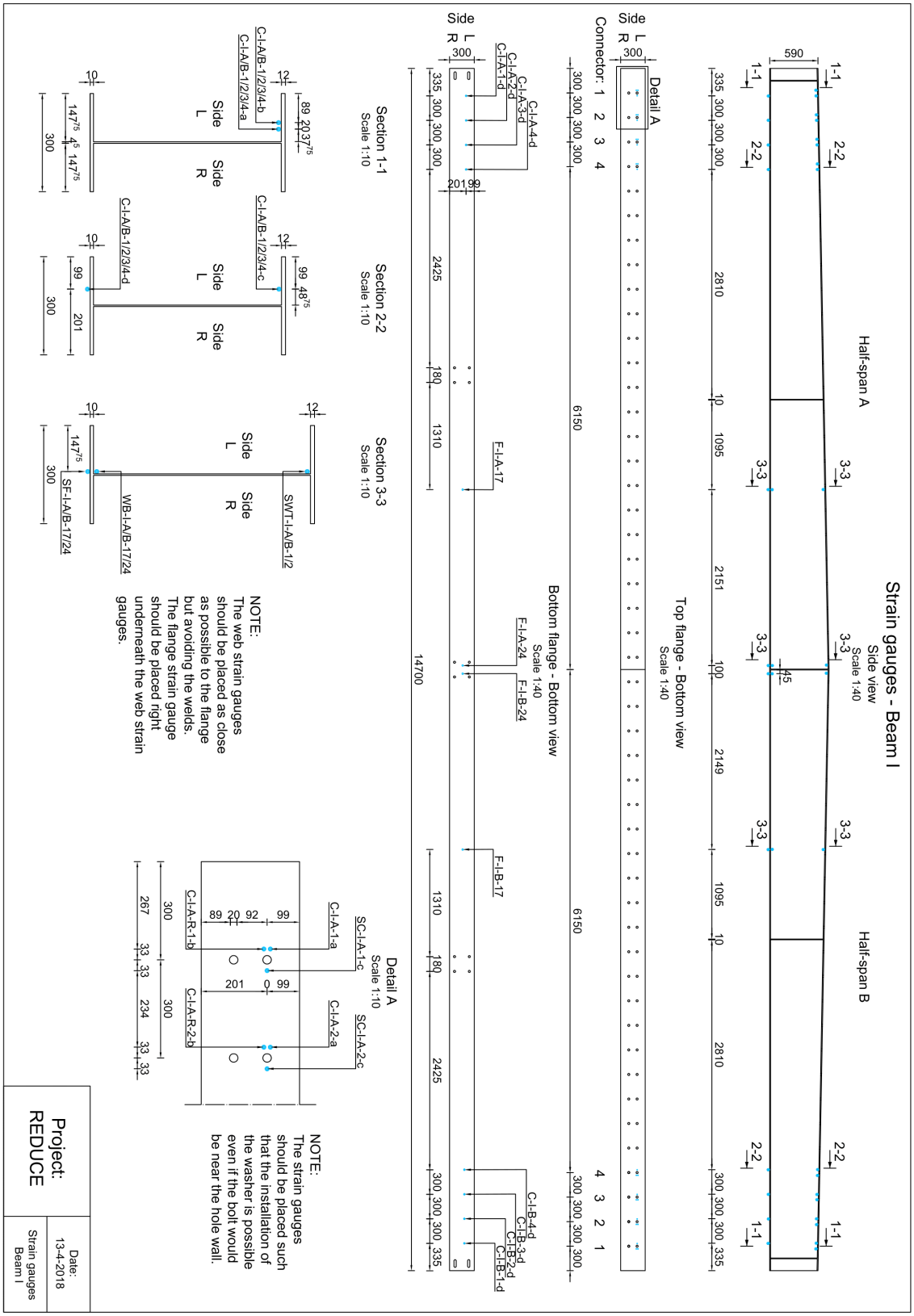
Strain gauges - Beam I
Side view
Scale 1:40
Half-span A
Half-span B
Top flange - Bottom view
Scale 1:40
Bottom flange - Bottom view
Scale 1:40
Connector: 1 2 3 4
4 3 2 1
Detail A
Scale 1:10
Section 1-1
Scale 1:10
Section 2-2
Scale 1:10
Section 3-3
Scale 1:10
NOTE:
The web strain gauges should be placed as close as possible to the flange but avoiding the welds. The flange strain gauge should be placed right underneath the web strain gauges.
NOTE:
The strain gauges should be placed such that the installation of the washer is possible even if the bolt would be near the hole wall.
Project:
REDUCE
Date:
13-4-2018
Strain gauges
Beam I

10 Appendix - design algorithm

```
#Ioan Andrei Gîrbacea - Composite beam  design algorithm
> restart:
#Rounding procedure
 Round := proc(x,n::integer:=1)
   parse~(sprintf~(cat("%.",n,"f"),x)):
 end proc:
> #Fixed input
L := 16000:
Ea := 210000:
Ec:=33000:
hc:=120:
Qk:=0.3e-2:
Gk:=0.3e-2+1/width:
bf:=300:
ksc:=55000:
> #Connector spacing and number of segments per half-span
space := 200:
numbseg:=L/2/space:
> #Maximum number of pairs per half-span
numberofpairs:=numbseg:
> #Design number (par) and the number of possible cases (counter)
par := 1:counter:=0:
> #Live monitoring of the code
[3, 40] Designed out c
0 Number of pairs
1.80 Utilization ratio
12 Top flange
6 Bottom flange
499.999 h0
> #Design algorithm.
#First five loops change the deck width, section height at support, top flange, bottom flange and web thickness
for width in [2600,3000,3600] do
 for hinitial from 499.999 by 10 to 569.999 do
  for topflange in [12,14,15,16,18,20] do
   for bottomflange in [6,8,10,12,14,15,16,18,20] do
    for web from 4 by 1 to 5 do

        #Local variables
        b1:=width:
        beff:= min((1/4)*L, b1):
        Ic := (1/12)*beff*hc^3:
        Ac := hc*beff:
        h0:=hinitial:
        hL:=h0+150:
        tft:=topflange:
        tfb:=bottomflange:
```

```
tw:=web:
q:=0.7*Qk*b1:

#Definition of the properties independent of number of connectors for each segment
for var1 from 1 to numbseg do
 var2 := var1-1:
 h1 := h0+(hL-h0)*var2*space/((1/2)*L):
 h2 := h0+(hL-h0)*var1*space/((1/2)*L):
 h := (h1+h2)*(1/2):
 ha[var1] := h:
 hw := h-tft-tfb:

 Aa[var1] := h*bf-(bf-tw)*hw:
 e1[var1] := (bf*tft*(h-(1/2)*tft)+hw*tw*((1/2)*hw+tfb)+
 (1/2)*(bf*tfb*tfb))/(bf*tfb+bf*tft+hw*tw):
 e2[var1] := h-e1[var1]:
 Ia[var1] := (1/12)*bf*tft^3+(1/12)*bf*tfb^3+(1/12)*tw*hw^3+bf*tft*
 (e2[var1]-(1/2)*tft)^2+bf*tfb*(e1[var1]-(1/2)*tfb)^2+hw*tw*
 ((1/2)*hw+tfb-e1  [var1])^2:

 r[var1] := e2[var1]+(1/2)*hc:
 EA0[var1]:=Ec*Ac+Ea*Aa[var1]:
 EAp[var1] := Ec*Ac*Ea*Aa[var1]:

 EI0[var1] := Ea*Ia[var1]+Ec*Ic:
 EIinf[var1] := EI0[var1]+EAp[var1]*r[var1]^2/EA0[var1]:
end do:

#Boolean variables required for the optimization of the code
check1:=0:check2:=0:

#Loop which increments the number of connector pairs
for pair from 0 by 1 to numberofpairs do


#Nested if for optimization of the code. Implemented in order to check first the cases of minimum and maximum interaction
if pair=1 then
 if check1=0 then
  pair:=numberofpairs:
  check1:=1:
 end if:
end if:


#Definition of all segments interface stiffness. This prevents division by zero
for var1 from 1 to numbseg do
 nsc[var1,par]:=1/10^3:
end do:
```

```
#Definition of the connector pairs
for var1 from 1 to pair do
 nsc[var1,par] := 2:
end do:

#Storing the number of the connectors for each design
connectors[par]:=2*pair:

#Definition of the properties dependent of number of connectors for each segment
for var1 from 1 to numbseg do
 K[var1,par] := nsc[var1,par]*ksc/space :
 alpha[var1,par] := sqrt(K[var1,par]*r[var1]^2/(EI0[var1]*(1-EI0[var1]/EIinf[var1]))):
end do:

#Definition of the deflection, axial force, bending moment, shear force and slip for each segment
for var1 to numbseg do
 var2 := var1-1:

 w[var1,par] := subs({_C1 = A[1+6*var2,par], _C2 = A[2+6*var2,par], _C3 = A[3+6*var2,par],
  _C4 = A[4+6*var2,par], _C5 = A[5+6*var2,par], _C6 = A[6+6*var2,par]},
  (1/2)*_C4*x^2+_C2*exp(alpha[var1,par]*x)/alpha[var1,par]^4+(1/6)*_C3*x^3+q*x^4/(24*EIinf[var1])+
  _C1*exp(-alpha[var1,par]*x)/alpha[var1,par]^4+_C5*x+_C6):

 N1[var1,par] := EIinf[var1]*(-(diff(w[var1, par], x, x, x, x))+
  alpha[var1, par]^2*(1-EI0[var1]/EIinf[var1])*(diff(w[var1, par], x, x))+
  q/EI0[var1])/(alpha[var1, par]^2*r[var1]):

 M[var1,par] :=(EIinf[var1]*(-(diff(w[var1, par], x, x, x, x))+
  alpha[var1, par]^2*(diff(w[var1, par], x, x))+q/EI0[var1])/alpha[var1, par]^2):

 V[var1,par] := diff(M[var1, par], x):

 s[var1,par] := (diff(N1[var1,par], x))/K[var1,par]:

end do:

#Definition of interface conditions
for var1 from 2 to numbseg do
 var2 := var1-1:

 IC[1+6*var2,par] := subs(x = space*var2, w[var2,par]) = subs(x = space*var2, w[var1,par]):
 IC[2+6*var2,par] := subs(x = space*var2, diff(w[var2,par], x)) =
                     subs(x = space*var2, diff(w[var1,par], x)):
```

```
        IC[3+6*var2,par] := subs(x = space*var2, M[var2,par]) = subs(x = space*var2,
M[var1,par]):
        IC[4+6*var2,par] := subs(x = space*var2, V[var2,par]) = subs(x = space*var2,
V[var1,par]):
        IC[5+6*var2,par] := subs(x = space*var2, N1[var2,par]) = subs(x = space*var2,
N1[var1,par]):
        IC[6+6*var2,par] := subs(x = space*var2, s[var2,par]) = subs(x = space*var2,
s[var1,par]):

    end do:

    #Definition of boundary conditions
    BC[1,par] := (subs(x = 0, w[1,par])) = 0:
    BC[2,par] := (subs(x = 0, diff(w[1,par], x$2))) = 0:
    BC[3,par] := (subs(x = 0, diff(s[1,par], x))) = 0:
    BC[4,par] := (subs(x = (1/2)*L, diff(w[numbseg,par], x))) = 0:
    BC[5,par] := (subs(x = (1/2)*L, diff(w[numbseg,par], x$3))) = 0:
    BC[6,par] := (subs(x = (1/2)*L, s[numbseg,par]))= 0:

    #Definition of boundary and interface condition list
    BConditions[par] := seq(BC[i,par], i = 1 .. 6):
    IConditions[par] := seq(IC[i,par], i = 7 .. 6*numbseg):
    Conditions[par]:={BConditions[par],IConditions[par]}:
    #Definition of constants list
    Constants[par] := {seq(A[i,par], i = 1 .. 6*numbseg)}:
    #Solving the linear system of equations
    aux[par]:=solve(Conditions[par],Constants[par]):
    assign(aux[par]):

    #Calculation of the deflection due to self-weight. Can be also obtained by setting the concrete
thickness and
    #elastic modulus to a very low value
    if pair=0 then
     h_s:=h0+(hL-h0)*x_s/(L/2):
     hw_s:=h_s-tft-tfb:
     e1_s:=(bf*tft*(h_s-
tft/2)+hw_s*tw*(hw_s/2+tfb)+bf*tfb*tfb/2)/(bf*tft+hw_s*tw+bf*tfb);
     e2_s:=h_s-e1_s:
     Ia_s:=(1/12*bf*tft^3+1/12*bf*tfb^3+1/12*tw*hw_s^3+bf*tft*(e2_s-tft/2)^2+
          bf*tfb*(e1_s-tfb/2)^2+hw_s*tw*(hw_s/2+tfb-e1_s)^2):

     deltaself:=Re(int((1/2*Gk*b1*x_s*(L-x_s))*x_s/(Ea*Ia_s),x_s=0..L/2)):
    end if:

    #Assigning the self-weight for each design case
    delta11[par]:=deltaself:

    #Calculation of the deflection under live loads for non-composite and composite section
    if pair=0 then delta21[par]:=0.7*Qk/Gk*delta11[par];
```

```
else delta21[par]:=(subs(x = (1/2)*L, w[numbseg,par])):
end if:

#Deflection due to creep - conservative approach to reduce calculation time
delta22[par]:=0.15*delta21[par]:

#Total mid-span deflection and end-slip
defl_mid[par]:=delta11[par]+delta21[par]+delta22[par]:
end_slip[par]:=-subs(x=0,s[1,par]):


#Utilization ratio
UR[par]:=Round(defl_mid[par]/(L/250),2):

#Condition to exit loop
if UR[par]<=1 then pair:=numberofpairs:
end if:

#Optimization of the algorithm by increasing the connector incrementation - based on the relation between
#number of connectors and beam stiffness
#The nested if was calibrated such that it never skips the beam design with the lowest utilization ratio
if pair>2 then
 if UR[par]>1.05 then pair:=pair+1:
 if UR[par]>1.1 then pair:=pair+1:
 if UR[par]>1.15 then pair:=pair+1:
 if UR[par]>1.2 then pair:=pair+1:
end if:end if:end if:end if:end if:

#If the number connector pairs exceeds the maximum allowed the code exits the loops (prevents infinite loops)
if pair>numberofpairs then pair:=numberofpairs:
end if:

#Nested if for optimization of the code. Implemented in order to check first the cases of minimum and maximum interaction
if check1=1 then
 if check2=0 then pairfull:=pair:parfull:=par:check2:=1:pair:=1: end if:
 if pairfull=numberofpairs then if UR[parfull]>1 then pair:=numberofpairs: end if:end if:
end if:


#Live monitoring tools
DocumentTools:-SetProperty("Label0", 'caption',
                    sprintf("%a Designed out of",[par,counter]), 'refresh'):
DocumentTools:-SetProperty("Label1", 'caption',
                    sprintf("%a Number of pairs",pair), 'refresh'):
DocumentTools:-SetProperty("Label2", 'caption',
```

```
                    sprintf("%a Utilization ratio",UR[par]), 'refresh'):
    DocumentTools:-SetProperty("Label3", 'caption',
                    sprintf("%a Top flange",topflange), 'refresh'):
    DocumentTools:-SetProperty("Label4", 'caption',
                    sprintf("%a Bottom flange",bottomflange), 'refresh'):
    DocumentTools:-SetProperty("Label5", 'caption',
                    sprintf("%a h0",hinitial), 'refresh'):

    #Steel weight
    weight[mat_steel,par]:=(tft*L*bf+tfb*L*bf+tw*h0*L+tw*(hL-h0)*L/2)/1000^3*7850:

    #Outputs
    tft_out[par]:=tft:
    tfb_out[par]:=tfb:
    tw_out[par]:=tw:
    b1_out[par]:=b1:
    h0_out[par]:=h0:

    #The design number is incremented
    par:=par+1:
    end do:

    #The number of possible cases is incremented
    counter:=counter+numberofpairs:

     end do:
    end do:
   end do:
  end do:
 end do:
#End of the design algorithm
> #Definition of the outputs
output := array(1..par-1,1..13):

for i  from 1  to par-1 do
 output[i,1]:=i:
 output[i,2] := (Round((defl_mid[i])/((L/(250))),2)):
 output[i,3] := Round(delta11[i],2):
 output[i,4] := Round(delta21[i],2):
 output[i,5]:=Round(delta22[i],2):
 output[i,6]:=Round(end_slip[i],2):
 output[i,7]:=tft_out[i]:
 output[i,8]:=tfb_out[i]:
 output[i,9]:=tw_out[i]:
 output[i,10]:=connectors[i]:
 output[i,11]:=Round((weight[mat_steel,i]),0):
 output[i,12]:=b1_out[i]:
 output[i,13]:=Round(h0_out[i],0):
end do:
```

```
#Show output
#print(output):
> #Write output to file
writedata(file,output):

> restart:
```

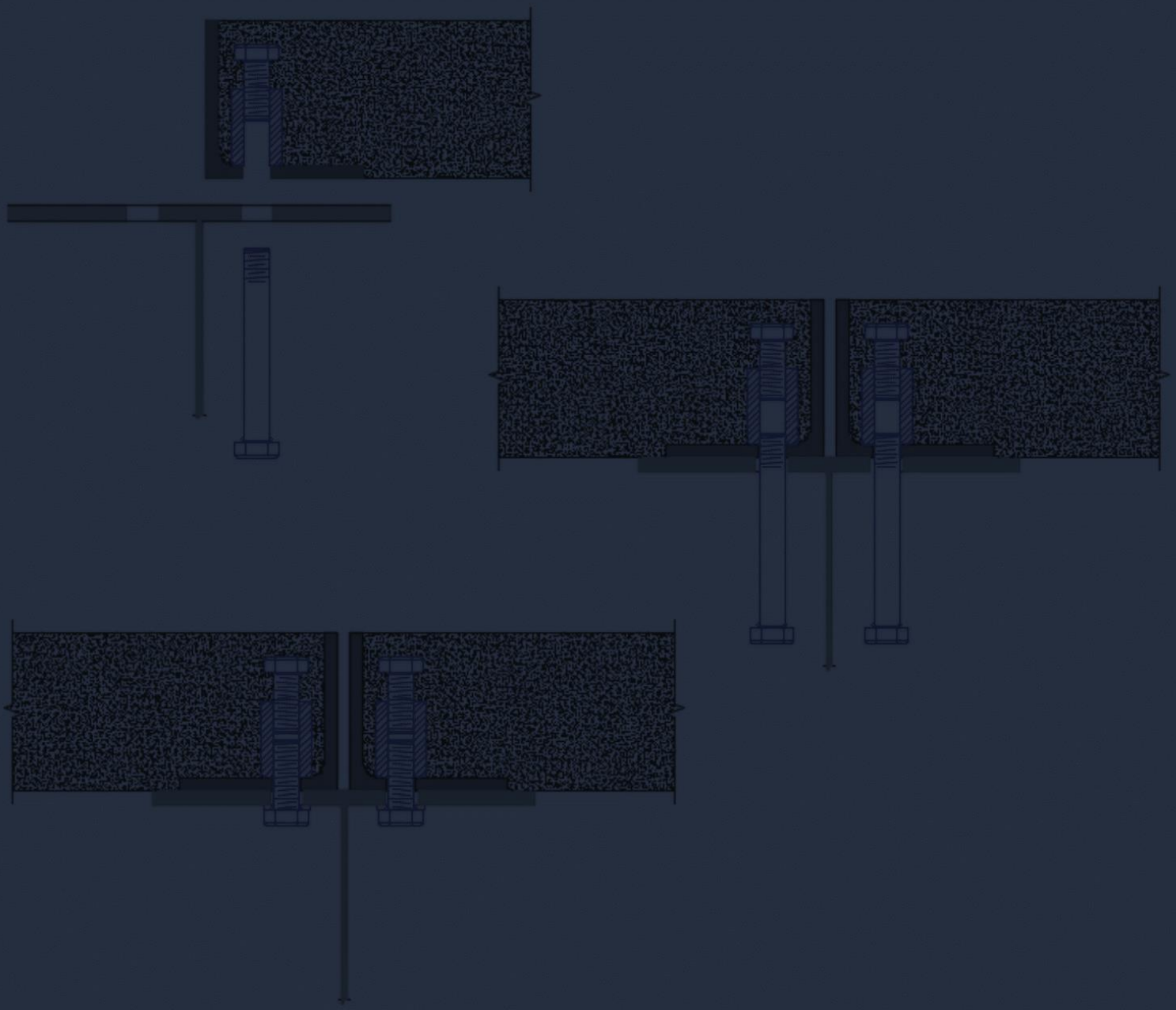

Master of Science in Civil Engineering

This thesis represents the final step of my master studies at Delft University of Technology. The thesis focused on covering three main aspects of demountable steel-concrete flooring systems aiming to confirm that demountable flooring systems can be a viable solution to current traditional floorings both in terms of construction, mechanical behaviour and economical aspects.

The research was carried at the Steel and Composite Structures department under the supervision of: prof. dr. M. Veljkovic, ir. M.P. Nijgh, dr. ir. R. Abspoel, ir. P. Lagendijk from Delft University of Technology and ir. M. Feijen from FMAX ISAAC. The experimental research took place at TU Delft's Stevin II lab as part of RFCS-project REDUCE (Reuse and Demountability using Steel Structures and the Circular Economy). I would like to thank all committee members for their professional guidance, especially to prof. dr. M. Veljkovic and ir. M.P. Nijgh for all their help and support. Moreover, I would like to express my gratitude to all the laboratory staff who made all the experiments possible.

Last but not least, I would like to thank my family, girlfriend and friends for their support throughout all my studies.